POLITECNICO
MILANO 1863

SCHOOL OF INDUSTRIAL AND INFORMATION ENGINEERING

Master of Science in Mechanical Engineering

Development of an innovative mechanistic-thermal model for studying the effect of MQL in peck drilling

Advisor:

Prof. Paolo Albertelli

Co-advisor:

Eng. Luca Bernini

Candidate:

Alessandro Moramarco

ID Number:

10519754

Academic year: 2023/2024

Abstract

This dissertation initially presents the state of art of Minimum Quantity Lubrication (MQL), exploring the application and impact of this type of cooling technique in modern machining practices. The study critically examines various aspects related to MQL, including its formulation development, configurations, and effectiveness in reducing environmental impact and tool wear, while enhancing cutting performances.

Indeed, in this thesis, the influence of MQL on a specific machining process, peck drilling process is investigated: theoretical models for predicting cutting forces and temperatures reached in the workpiece are reviewed and extended to include the concept of oblique cutting theory. The dissertation discusses the application of the predictive machining theories developed to analysing cutting mechanics and thermal dynamics under various machining parameters and lubrication conditions.

The conceived mechanistic cutting model exploits the Oxley's theory extended to Johnson-Cook material flow stress formulation, extending it further to the oblique cutting concept characterization.

When dealing with thermal model, in this work, an extension to the partial differential solution for heat conduction is provided to analyse the temperature rise in the workpiece caused by the peck drilling strategy.

The conceived models are applied to understand from a phenomenological point of view, the effects of adopting MQL on the chip formation mechanism and heat generation and propagation.

In conclusion, this dissertation highlights the critical role of MQL in drilling process. MQL oil flowrate affects the mechanics of cutting decreasing the friction coefficient. This reduces the heat generated, reducing the workpiece temperature. MQL air flowrate doesn't have any effect on mechanics of cutting but helps to decrease temperature of workpiece increasing convective refrigeration. By integrating experimental findings with theoretical models, the study contributes to advancing the understanding of this particular lubrication technique, providing the relations between the machining process dynamics and the cooling parameters used in the process.

Key-words: Minimum Quantity Lubrication (MQL), peck drilling, workpiece temperature, oblique cutting forces.

Abstract in italiano

Questa tesi presenta inizialmente lo stato dell'arte della Lubrificazione a Minima Quantità (MQL), esplorando l'applicazione e l'impatto di questa tecnica di raffreddamento nelle pratiche di lavorazione moderne. Lo studio esamina in modo critico vari aspetti relativi alla MQL, inclusi lo sviluppo delle sue formulazioni, le configurazioni e l'efficacia nella riduzione dell'impatto ambientale e dell'usura degli utensili, migliorando al contempo le prestazioni di taglio.

Infatti, in questa tesi viene indagata l'influenza della MQL su un processo di lavorazione specifico, il processo di foratura a intervalli (peck drilling): vengono rivisti ed estesi i modelli teorici per la previsione delle forze di taglio e delle temperature raggiunte nel pezzo, includendo il concetto di teoria del taglio obliquo. La tesi discute l'applicazione delle teorie di lavorazione predittiva sviluppate per analizzare la meccanica del taglio e la dinamica termica sotto vari parametri di lavorazione e condizioni di lubrificazione.

Il modello di taglio meccanicistico sviluppato sfrutta la teoria di Oxley estesa alla formulazione del flusso di stress del materiale di Johnson-Cook, estendendolo ulteriormente alla caratterizzazione del concetto di taglio obliquo.

Per quanto riguarda il modello termico, in questo lavoro, viene fornita un'estensione della soluzione differenziale parziale per la conduzione del calore per analizzare l'aumento di temperatura nel pezzo causato dalla strategia di foratura a intervalli.

I modelli concepiti vengono applicati per comprendere, da un punto di vista fenomenologico, gli effetti dell'adozione della MQL sul meccanismo di formazione del truciolo e sulla generazione e propagazione del calore.

In conclusione, questa tesi evidenzia il ruolo critico della MQL nel processo di foratura. Il flusso d'olio del MQL influenza la meccanica del taglio riducendo il coefficiente di attrito. Questo riduce il calore generato, abbassando la temperatura del pezzo. Il flusso d'aria MQL non ha alcun effetto sulla meccanica del taglio, ma aiuta a diminuire la temperatura del pezzo aumentando la refrigerazione convettiva. Integrando i risultati sperimentali con i modelli teorici, lo studio contribuisce ad avanzare la comprensione e l'applicazione di questa particolare tecnica di lubrificazione, fornendo le relazioni tra le dinamiche del processo di lavorazione e i parametri di raffreddamento utilizzati nel processo.

Parole chiave: Lubrificazione a Quantità Minima (MQL), foratura a intervalli, temperatura del materiale, forze di taglio obliquo.

Contents

List of Figures

List of Tables

1 Introduction

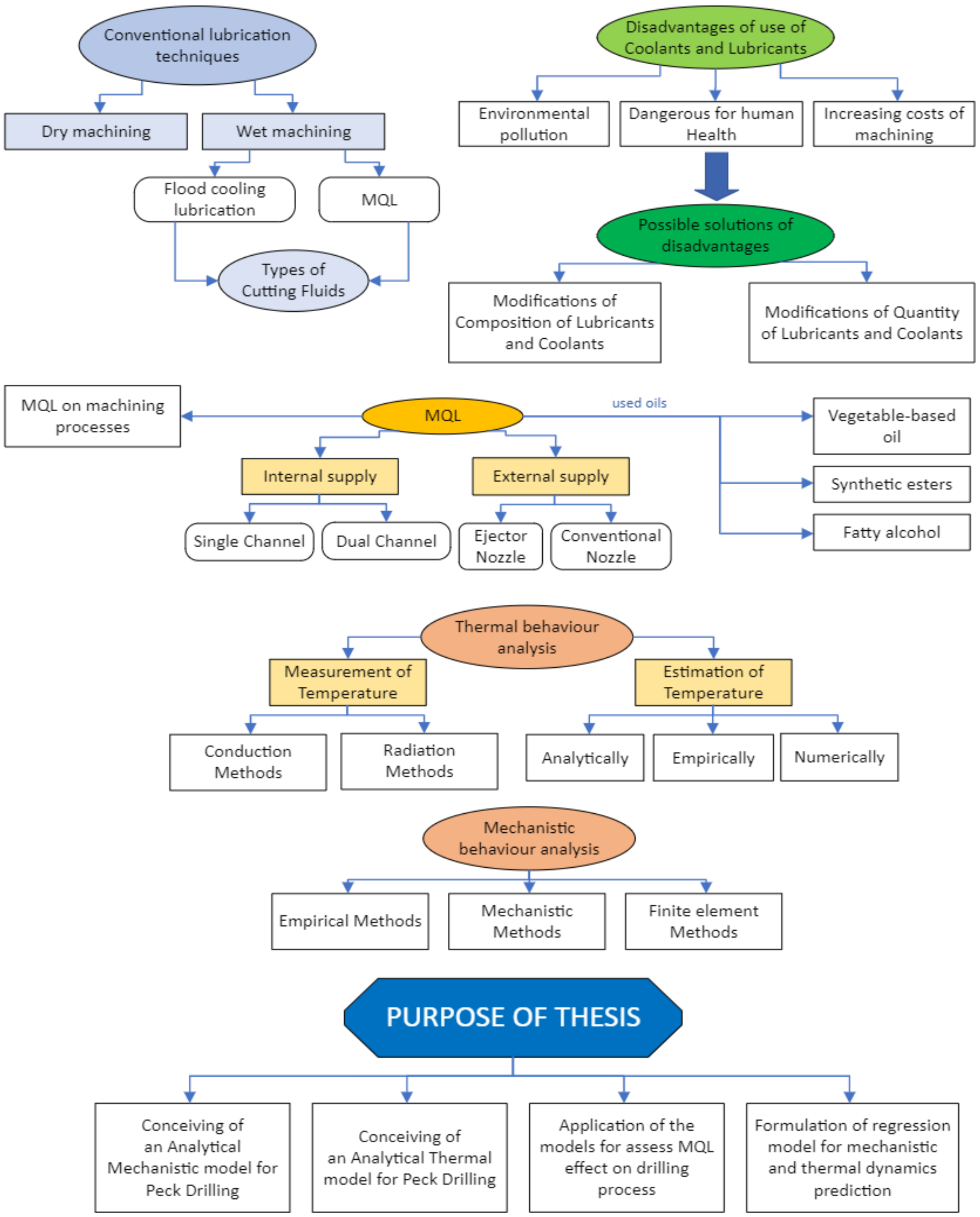

1.1. Conventional cooling lubrication techniques

When optimizing a machining operation, the primary objective of any machining operation is to reduce overall costs and enhance both quality and productivity. Depending on the workpiece, the production structure, and the production location the costs related to the use of cooling lubricants ranges from 7 - 17% of the total costs of the manufactured workpiece. [1]

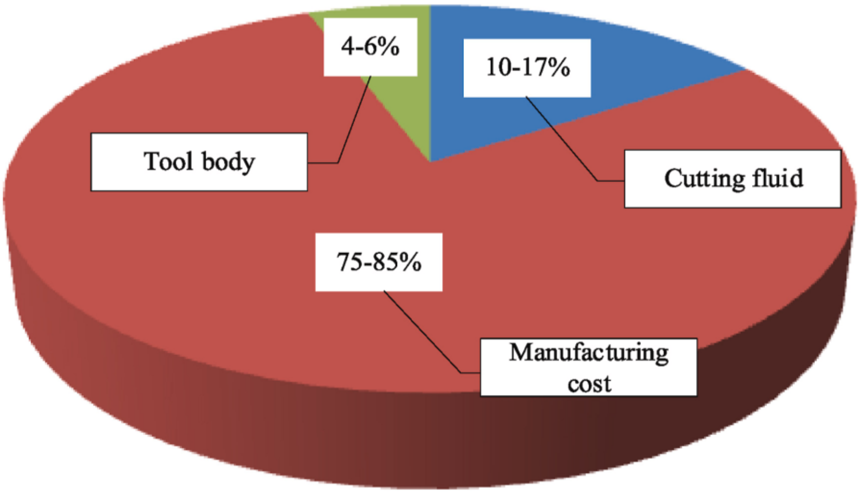

Figure 1: Numerical portions of total production cost. [2]

Achieving this goal involves operating at the highest possible cutting parameters, maximizing the MRR, while also extending tool life. Additionally, minimizing part rejections and reducing downtime are key priorities in machining operations. Especially in the last few years, besides the reduction of costs, another particularly crucial aspect to consider during machining is the impact that the machining operation will have on the environment. All these aspects require a meticulous study on the type of cutting fluid and how this fluid is fed on the working zone.

During machining, heat is generated at the *primary deformation zone* due to shear and elasto-plastic deformation (heat is mainly generated in this zone), at *secondary deformation zone* (chip–tool interface) due to rubbing and/or shear, and at *tertiary deformation zone* (workpiece–tool interface) due to rubbing between tool and machined surface. These heat sources all have a significant influence on the cutting forces, tool life, and chip formation mode. [3]

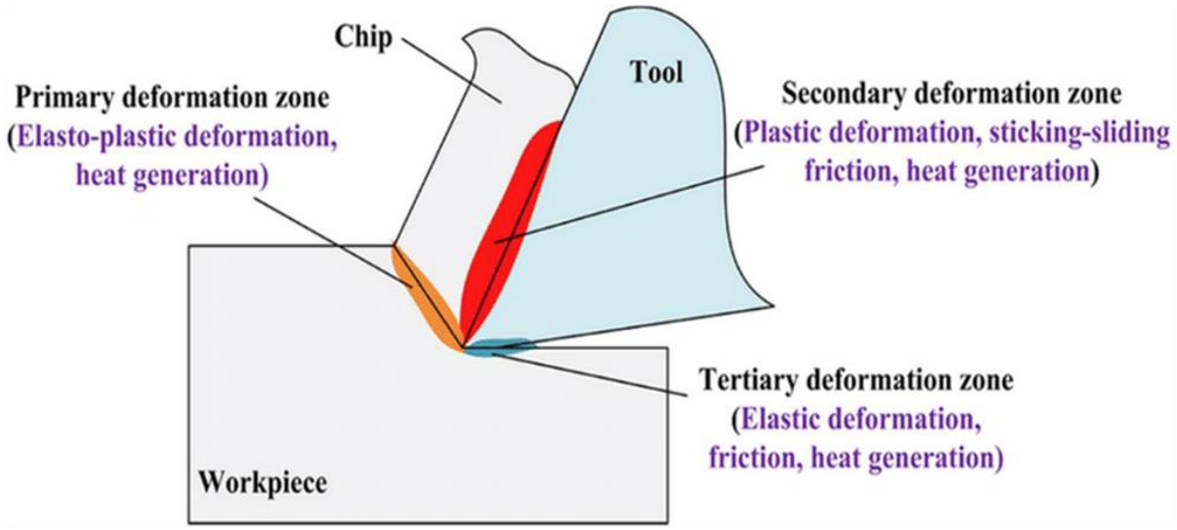

Figure 2: Different zones where heat is generated during orthogonal cutting [4]

Machining process can be primarily classified based on their usage of cutting fluids:

- *Dry machining*: the process is performed without the usage of any cooling lubricant, with just air blowing towards cutting area. Since the high temperature and tool wear generated in this type of process, most of all for the machining of hard-to-cut material (e.g. titanium alloy), some techniques have been studied to overcome this problem such as the use of particular coating tools.

  Another solution recently studied are the textured tools. This type of tool is featured by grooves and dimples obtained on the surface of tool. Siju et al.[5] analysed this solution proving a reduction of the cutting and thrust forces on turning by 31.2% and 16.2%, respectively, with respect to non-textured tools, allowing to reduce also heat generation. Moreover, a reduction of friction of about 13%–26% has been registered. However, the total absence of cooling lubricant is not practicable in some cases, especially when processing steel and aluminium, due to the risk of sticking of working material on the tool surface.

- *Wet machining*: the process is performed with the addiction of cooling lubricant applied to the workpiece and cutting tool, capable to decrease the friction in the tool-workpiece interface, to reduce the heat generation and to increase the heat rejection.
  This technique is widely used in various machining processes, such as milling, turning, and drilling, to improve efficiency, tool life, and surface finish.

Different types of cutting fluids, such as oils, emulsions, and synthetics, are used based on the specific requirements of the machining process and the materials involved. Usually, the delivery of the lubricant is performed with a stream of lubricant with a relatively high flow rate to facilitate the access to the cutting zone. This technique is called 'flood cooling lubrication'.

Conventional cutting fluids cannot cool down and lubricate effectively as expected and become more ineffective as the cutting speeds increase, owing to reduction in chip-tool contact length. Moreover, the high amount of cutting fluid used in this technique represents a predominant part of the costs of production as well as representing a high risk for the environment.
To try to solve this problem the use of particular vegetable-based and biodegradable fluids can represent a solution to mitigate the environmental impact of cutting fluids, as well as the usage of different delivery techniques for the lubricant cooling, as *MQL*.

1.2. Cutting fluids

The environmental impact of cutting fluids has become a growing concern in recent years due to their potential toxicity. The overarching goal of the ISO 14000 family of standards is to safeguard the environment while simultaneously considering and harmonizing with socioeconomic needs and demands. Industries that adhere to these standards, will be required to measure and demonstrate reductions in the five primary components: harmful air emissions, water pollution, waste management, soil contamination, and the preservation of natural resources and raw materials [4]. To reach and respect these goals, the cutting fluids choice and usage have predominant importance in the industrial field, where they are indispensable. In fact, cutting fluids allow to [3]:

- reduce the coefficient of friction, consequently minimizing heat generation and aiding in heat dissipation. Moreover, this may cause less built-up edge (BUE) on the tool and provide better surface finish [4];
- remove the chips from the rake surface and transport them away;
- cleaning tools, workpieces, and fixtures from residues of cutting material;
- maintain a consistent temperature throughout the workpiece and machine tool, which is essential for meeting the specified tolerances.

1.2.1. Types of cutting fluids

Different types of cutting fluids exist, mainly concerning about their nature and composition.

Cutting fluids can be classified into four main categories [5]:

- cutting oil,
- soluble oils (emulsified oils, emulsions),
- synthetic (chemical) fluids,
- semi-synthetic (semi-chemical) fluids.

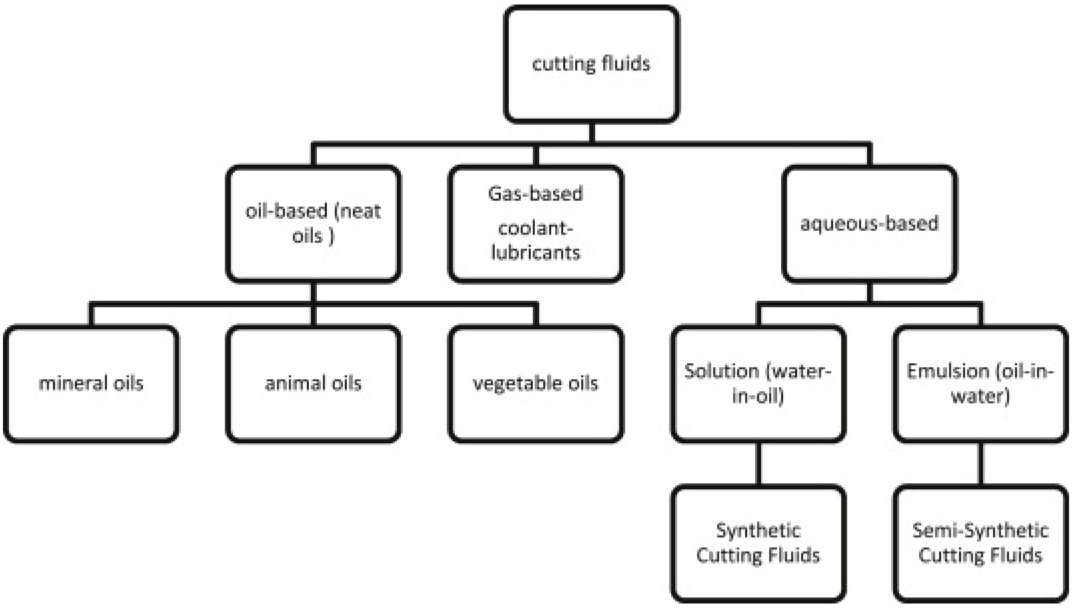

Figure 3: Types of cutting fluids [6]

Oil-based lubricants, also known as neat oils, are derived from a variety of sources, including mineral, animal, vegetable, and synthetic oils. Among these, mineral oils (which are petroleum-based) are the most common type due to their favourable lubricating properties. These cutting fluids typically incorporate additives to improve their performance. For example, the properties of naphthenic mineral oils and paraffinic mineral oils are often enhanced through the inclusion of fatty lubricants, extreme pressure additives, odorants, viscosity modifiers, and polar additives[7]. Their main disadvantage is the high flammability as they are good in lubrication but poor in cooling, as a result, their characteristics become poor when machining in higher load and temperatures, resulting in mist and smoke [7].

When an *aqueous-based* product is mixed with water, the "emulsifiable" type forms an emulsion, whereas the "soluble" type creates a solution. The presence of water in emulsions enhances their cooling properties, while the inclusion of oil helps mitigate the potential for water to induce oxidation [7].

Additionally, extreme pressure additives are incorporated into this cutting fluid for usage under high-pressure conditions. Emulsions are generally recommended for high-speed and low-pressure machining operations where there is a significant increase in temperature. Infestation by micro-organisms such as bacteria, yeasts, and fungi represent the weakness of emulsions due to the high amount of water. The presence of bacteria causes separation in the emulsions [6].

Synthetic cutting fluid, which is made of chemicals with additives and diluted in water, is free from mineral oil. Synthetic cutting fluid is a good coolant, but it provides insufficient lubrication compared to other cutting fluids due to lack of oiliness [7]. Consequently, these fluids are especially employed for machining operations with low cutting forces, where effective cooling is a fundamental necessity.

Semi-synthetic fluids are essentially chemical emulsions that consist of mineral oil diluted in water, with the addition of certain additives aimed at reducing the size of oil particles, thereby enhancing their effectiveness as lubricants [7].

Type of cutting fluids	Advantages	Disadvantages
Straight oils	Excellent lubricity and rust control	Low cooling, fire hazard, create mist or smoke, limited to low-speed and heavy cutting operations
Soluble oils	Good lubricity and cooling	Rust control problems, bacterial growth, evaporation losses
Semi-synthetics	Good cooling, rust control and microbial control	Foam easily, stability is affected by water hardness, and easily contaminated by other machine fluids
Synthetics	Excellent cooling, microbial control, non-flammable, non smoking, good corrosion control, reduced misting and foaming problems	Poor lubricity and easily contaminated by other machine fluids

Figure 4: Advantages and disadvantages of different cutting fluids [6]

1.2.2. Environmental and human issues regarding cutting fluids

It is reported that around 80% of all occupational infections of the operators were due to skin contact with cutting fluids [8]. This is due to the complexity in the composition of cutting fluids that may be irritant or allergenic, even if the raw materials are safe. The International Agency for Research on Cancer (IARC) reported that petroleum-based cutting fluids containing heterocyclic and polyaromatic rings is carcinogenic and exposure to it could result in occupational skin cancer [9]. The presence of these harmful substances in cutting fluids, which are both toxic and less biodegradable, has led to significant technological and environmental issues. Additionally, they pose serious health risks, including lung cancer, respiratory diseases, dermatological problems, and genetic disorders [6].

Cutting fluids that contain chlorinated paraffin, especially in extreme pressure conditions, can transform into dioxins under the influence of heat and pressure. This transformation process could potentially result in chlorine acne. Moreover, the disposal of cutting fluids containing chlorinated compounds is restricted; they can only be burned in specialized incineration facilities due to the toxic nature of dioxins, which can be released during uncontrolled burning. Consequently, these cutting fluids are classified as hazardous waste, posing significant risks to both human life and the environment [6].

Figure 5: Potential disadvantages of cutting fluids. [10]

Additionally, in machining operations, cutting fluids can vaporize and atomize under high pressure and temperature, leading to the formation of cutting fluid mist. This mist, along with fumes, smoke, and odours produced by cutting fluids containing chemical additives like sulphur, chlorine, phosphorus, hydrocarbons, and biocides, can cause skin reactions and respiratory problems. Exposure to these mist and fumes poses significant health risks to workers in machining environments [6].

Mainly for soluble cutting fluid, where a high portion of water is present, health issues often stem from the growth of bacteria and fungi. The presence of bacteria can diminish the lubricating properties and alter the pH of the cutting fluid, reducing its service life and potentially posing health risks to operators. To control bacterial growth, various bactericides, humectants, and germicides are used in metalworking fluids. However, these chemical additives are recognized as hazardous substances, posing risks to both the environment and the health of workers.

For those reasons, vegetable-based cutting fluids that are eco-friendly, renewable, less poisonous, and high biodegradable are extremely attractive to replace petroleum-based cutting fluid. Those biodegradable cutting fluids accomplish the lowest amount of environmental contamination and provide high reliability and satisfactory economic conditions. Moreover, the output of bio-based cutting fluid is cleaner and generates less mist in the air minimizing the occupational health risks [6].

To reduce the risks linked with humans and environment highlighted above, and to reduce the costs of manufacturing, besides the development of vegetable-based or synthetic cutting fluids, some techniques to reduce the amount of lubricant used in the processes are under analysis.

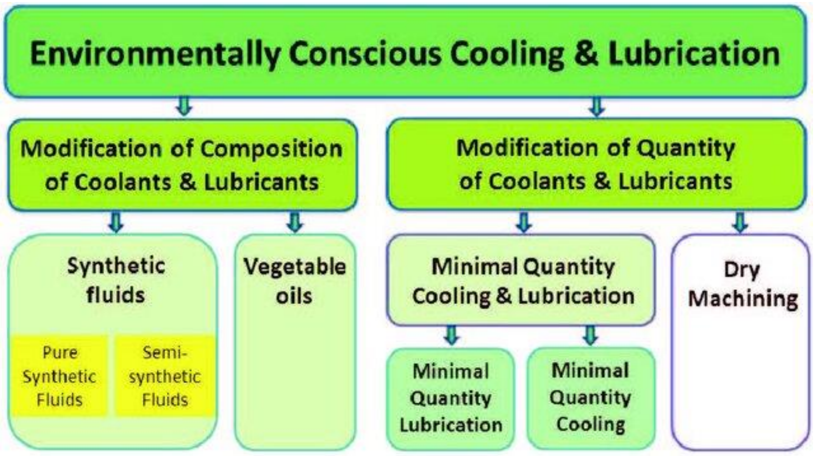

Figure 6: Possible solutions to environmental problem related to cutting fluids. [10]

In this thesis, the efficiency of MQL, Minimum Quantity Lubrication, will be taken under analysis after a discussion about the state of art of this particular lubrication and cooling technique.

1.3. MQCL - state of art

As previous highlighted, the choices about cutting fluids represent a crucial aspect affecting manufacturing cost, productivity and environmental impact. Due to the ecological problem, besides the eco-friendly nature on cutting fluid, a drastic reduction of the amount of these fluids, for example respect of the conventional usage of flood cooling, is therefore necessary.

One of the most recent studied solutions is the implementation of Minimum Quantity Cooling Lubrication (MQCL) technology. MQCL technology has gained global attention due to its minimal oil consumption and its ability to provide excellent machining performance, often better with respect to traditional flood cooling [1]

Three important properties are required for the MQL fluids:

- Biodegradability
- High lubrication effect
- High stability

These properties guarantee the respect of sustainability and allows a low oil consumption [3].

The main types of lubricant used in MQL are vegetable-based oils, synthetic esters and fatty alcohols (long-chained alcohols made from natural raw materials or from mineral oils) [11].

In the table below the principal characteristics and properties of these lubricants are highlighted.

Lubricant	Properties
Vegetable-based oils	Dense, homogeneous, and strong lubricating film to absorb pressure and reduce heat generation High flash point (reduced smoke formation and fire hazard) and high boiling point (low vaporization and misting) Non-toxic to the environment Biologically inert
Synthetic esters	Good biodegradability and toxicologically harmless High flash and boiling point Low viscosity Good corrosion resistance Very good lubrication properties but low cooling properties.
Fatty alcohol	Good biodegradability and toxicologically harmless, Low flash and boiling point Comparatively high viscosity, Poor lubrication properties but high heat removal capability due to the high evaporation heat.

Table 1: Properties of main fluids used in MQL [11].

In machining operations, vegetable-based oils and synthetic esters are often employed, especially when the primary goal is to minimize friction and adhesion between the tool, workpiece, and/or chips. These lubricants are typically used in operations such as drilling, fine-boring, tapping, and thread-forming. In contrast, fatty alcohols find common usage in machining processes where cooling is prioritized over lubrication. This is particularly evident in operations like sawing, turning, and milling of grey cast iron, as well as in the machining of cast aluminium alloys. Different lubricants are chosen based on the specific requirements of each machining operation.

The majority of authors in literature, observed that the performance of MQL machining is better than that of wet machining. MQL enabled a substantial reduction in cutting temperature improving the dimensional accuracy. Moreover, it enhanced the chip-tool interaction while maintaining the sharpness of the cutting edges because MQL tends to reduce wear and damage on the tool tip [12]. In fact, it has been demonstrated that flood cooling, while highly effective at lower cutting speeds, becomes less efficient at higher speeds due to the increased heat generation. At these elevated speeds, the coolant may struggle to reach the critical areas, such as the tool-workpiece interface, resulting in inadequate cooling of this zone [13].

In MQCL machining processes, the cooling lubricant is delivered to the tool-workpiece interface as an aerosol, comprising a blend of oil and air. Depending on the composition and primary purpose of this aerosol, it's possible to categorize it into two distinct types: Minimum Quantity Lubrication (MQL) and Minimum Quantity Cooling (MQC)[1].

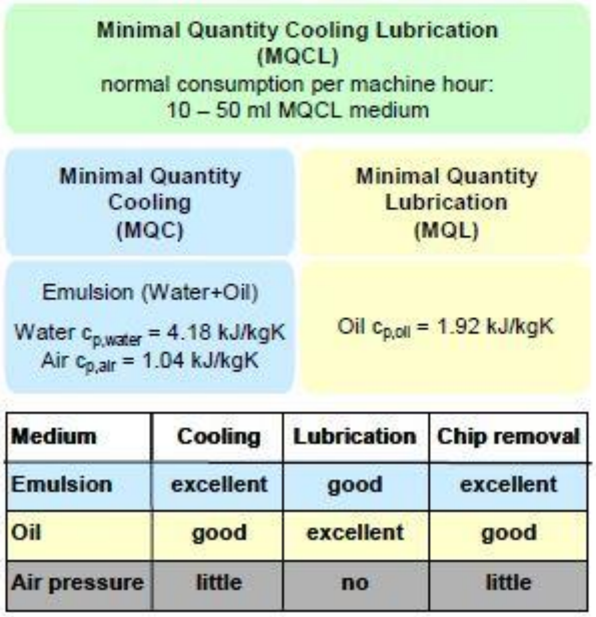

Figure 7: Characteristics of MQL and MQC [1]

<u>*MQL:*</u>

In Minimum Quantity Lubrication (MQL) machining, oils are used as the fluid medium, and the primary function of the lubricant is to diminish *friction* and prevent *adhesion* between the workpiece, chip and tool, with the objective of reducing heat generation. As a result, both the tool and workpiece experience lower levels of heat when compared to completely dry machining. In this scenario, the direct cooling effect of the aerosol has a relatively minor impact due to the restricted thermal capacity of oil and air, as well as the small amount of the medium used in the machining operation [14].

It has a better reachability as a result of the high pressure, the required air pressure varies from 2 to 6 bar [11]. The flow rate can vary from 50 to 500 mL/hour which is about three to four orders of magnitude lower than the amount commonly used in flood cooling condition [12].

<u>MQC</u>:

In MQC machining operations, emulsions and water are employed as the fluid medium, and the primary objective of the lubricant is the *cooling* of the tool or workpiece more effectively than what can be achieved with oil alone.

In MQC application, heat transfer is predominantly in the evaporative mode, which is more efficient than the convective heat transfer prevalent in conventional wet machining. [15]

In MQC operations, emulsions provide considerably less lubrication compared to oil but more than water and air, which provide no lubrication at all. However, emulsions offer a significantly greater direct cooling effect due to their higher thermal capacity compared to oil and air. Up to this point, MQC remains a relatively unexplored technique, despite its potential to substantially address thermal issues affecting the tool and/or workpiece in dry machining operations.

1.3.1. Delivery of the lubricant for MQL

There are two main delivery methods used in MQL technology.

- <u>Internal supply</u>: in the internal delivery system, a blend of compressed air and oil is introduced into the cutting zone through the machine tool's spindle. This setup is commonly referred to as a through-tool application in Minimum Quantity Lubrication (MQL). There are two distinct configurations of this system available for use [11]:
    - *<u>Single channel</u>*: the oil and compressed air are mixed before being supplied through the cutting tool to the workpiece/tool zone.
    - *<u>Dual channel</u>*: the oil and compressed air are delivered in different channels and are only mixed before the holder of the cutting tool.

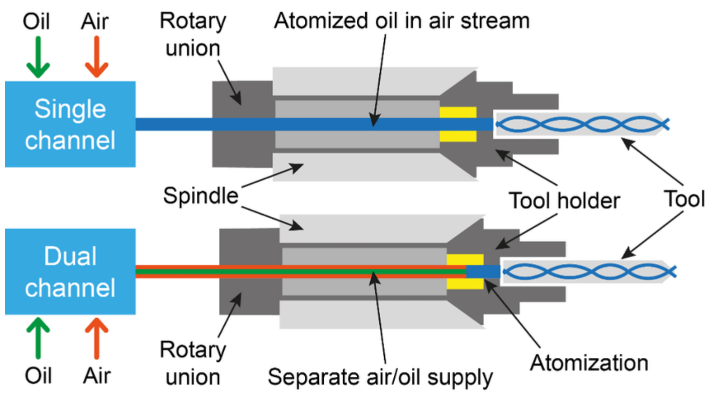

Figure 8: Single and Dual channel configurations for MQL internal supply [16]

- External supply: In this scenario, the aerosol is sprayed onto the tool from the outside using one or more nozzles. It's crucial to emphasize that the quantity and orientation of these nozzles significantly impact the quality of the workpiece. Typically, this technique is applied in operations such as sawing, end milling, face milling, and turning.

  Two possible techniques can be adopted: [11]

  - using *ejector nozzles*: the compressed air and oil are supplied to the ejector separately, and mixing occurs just after the nozzle.
  - using *conventional nozzles*: the aerosol is prepared in an external atomizer and then transported to a conventional nozzle.

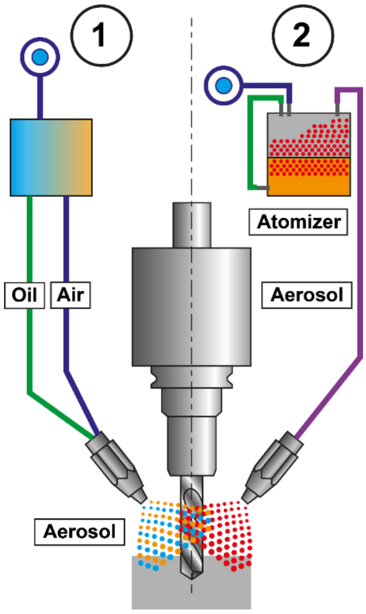

Figure 9: Ejector nozzle (1) and conventional nozzle (2) configurations for MQL [16]

1.3.2. MQCL on machining processes

In literature, most of the research conducted was aimed to study and demonstrate the improvement on roughness, tool life and on the severity of cutting forces, that MQL can provide during machining, so considering mostly the lubrication effects. Less research is focused on the reason for temperature reduction usually registered during machining with MQL, most of all for milling, in which the intermittent cutting makes difficult the measurement of temperature directly.

Below a list of documents analysing the behaviour of MQL and how it affects the major parameters related to different machining processes is presented.

Turning

Dhar et al. [17] demonstrated the improvement reachable with MQL during turning of a 125 mm diameter and 760 mm long rod of AISI-1040 steel of common use in a powerful and rigid lathe (USA, 15hp) at different cutting velocities and feeds. The cutting forces results on about 5–15% reduction, reduced flank wear allowing improving surface finish and dimensional accuracy. Moreover, sizeable reduction in the cutting zone temperature consequently has been registered by tool-workpiece thermocouple technique, reducing friction, BUE formation, thermal distortion of the work and wear of the cutting tool.

Vasu et al. [3] conducted experiments on Inconel 600 alloy using MQL with different percentage of Al_2O_3 and dry machining. Compared to dry machining, using MQL resulted in a reduction of the average tool tip interface temperature of about 12 to 20%, a reduction of surface roughness and tool wear. A standard K-type thermocouple, mounted at the site of the tool–workpiece junction, was used to monitor directly the tool tip interface temperature. The results on the main process parameters, function of the different types on lubricant can be seen in the picture below.

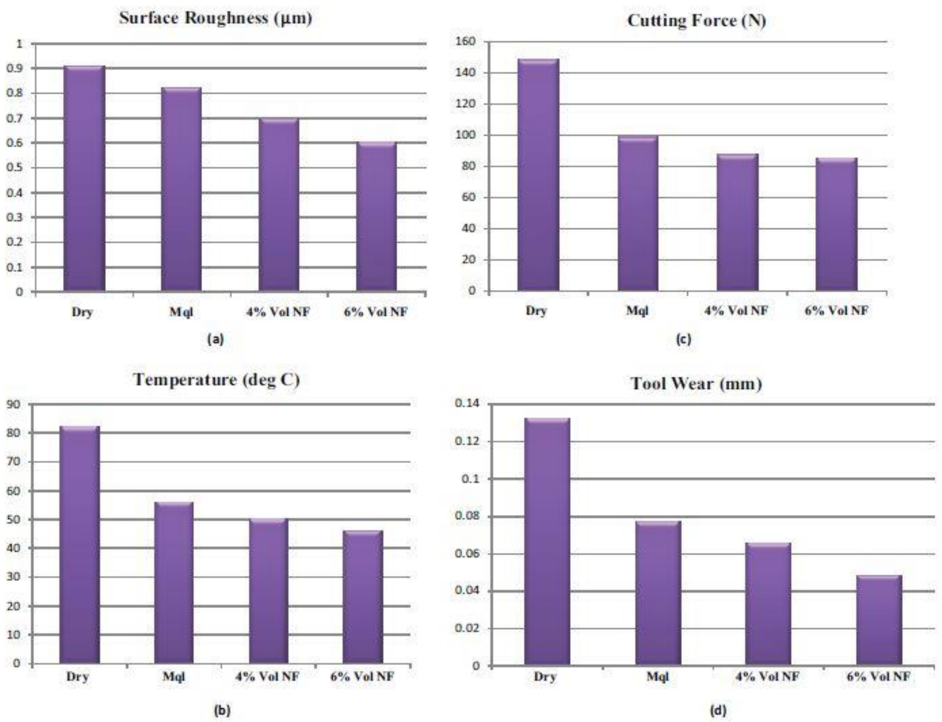

Figure 10: Surface roughness, cutting force, temperature and tool wear for Dry, MQL and MQL with 4% vol. and 6% vol. of $Al2O3$ [3]

Thakur et al. [18] conducted experiments on turning Inconel 718, demonstrating that MQL could be effectively utilized for machining these super alloys, also determining the optimal cutting parameters. They also provided correlations and conducted confirmation tests for flank wear.

Ali et al. [19] performed tests carried out by straight turning of medium carbon steel on a lathe (7.5 kW) by a standard uncoated carbide insert with ISO designation-SNMG 120408 at different speed-feed combinations. They demonstrated a reduction in friction at the chip-tool interface, chip thickness ratio, built-up-edge formation and wear at the cutting edges, allowing to improve the surface finishing. By means of a direct measurement of temperature on tool-work interface, using tool-workpiece thermocouple technique, they showed a reduction in cutting temperature in MQL respect to Dry machining.

Gupta et al. [20] performed experimental analysis on a turning process of hardened steel using biodegradable olive-oil based MQL spray. Tool flank wear, chip morphology, surface, roughness and chip-tool interface temperature (using a calibrated tool-workpiece thermocouple system) have been analysed to assess the coming improvements due to MQL usage. Experiments resulted on reductions in Ra, Rq, and cutting temperature of about 23.4%, 23.8%, and 24% respectively in terms of mean values showing the advantages of using MQL and the possible solution of using olive oil-base lubricant regarding the environmental problems previously highlighted.

Milling

Liu et al. [21] operated an end-milling machining on titanium alloy (Ti–6Al–4V) to investigate the effects of MQL on the cutting forces, measured by means of a dynamometer, and on cutting temperature using a semi-manual thermocouple. They noticed that lower cutting forces and cutting temperatures are achieved with an increase in air pressure of MQL, maintaining constant the other process parameters. After about 0.5 MPa, an increasing trend has been noticed. The same result was obtained up to a distance of 25 mm from cutting zone. A more constant behaviour was noticed changing the spray angle. They result on an average decrease in cutting temperature by 13.3% and cutting force by 14.28%.

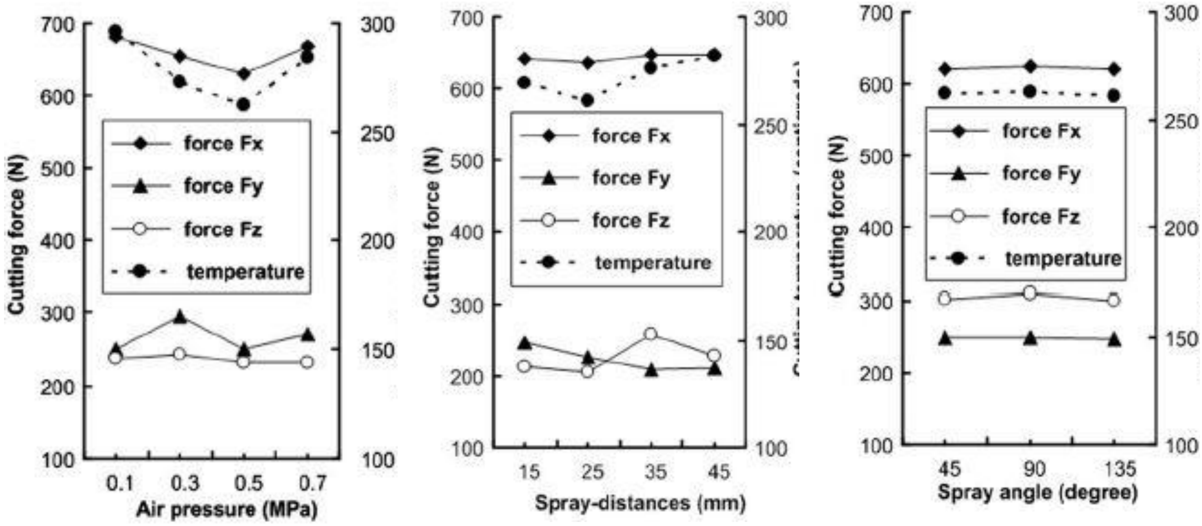

Figure 11: Cutting forces and temperature as a function of air pressure, spray distance and spray angle [21]

Yan et al. [22] carried out some machining tests on 50CrMnMo forged steel using a milling machine. Their analysis was focused mainly on the characterization of tool wear and surface finishing comparing the results obtained considering dry cooling, flood cooling and MQL. The tool lives obtained from conventional wet cutting and MQL conditions are 36.1 min and 62.1 min, respectively. It shows that the application of MQL technique has increased the tool life by 2.03 times as compared to dry cutting and 1.72 times compared to conventional flood cutting fluid supply cutting.

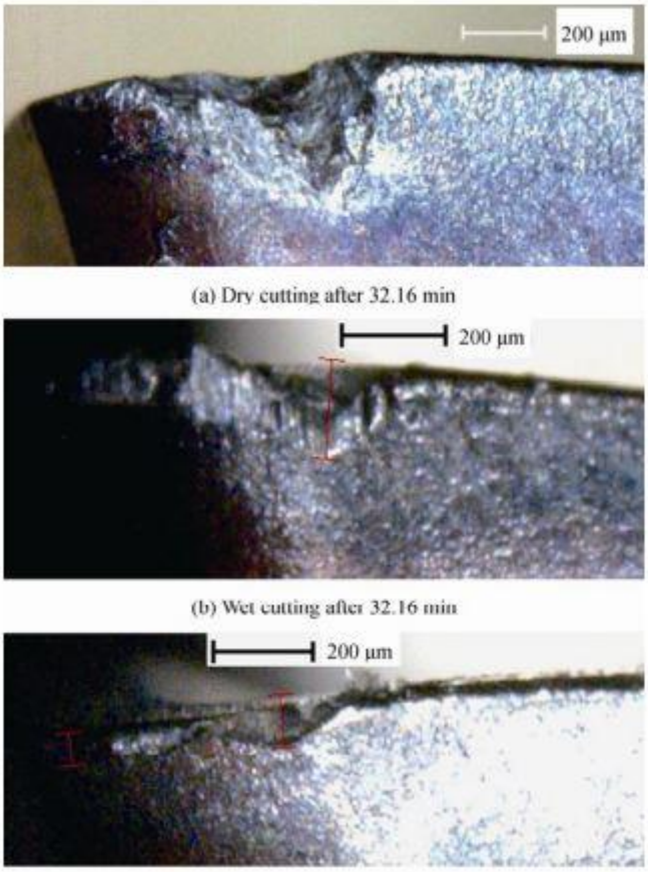

Figure 12: Flank wear for dry, wet and MQL machining after 32.16 min. [22]

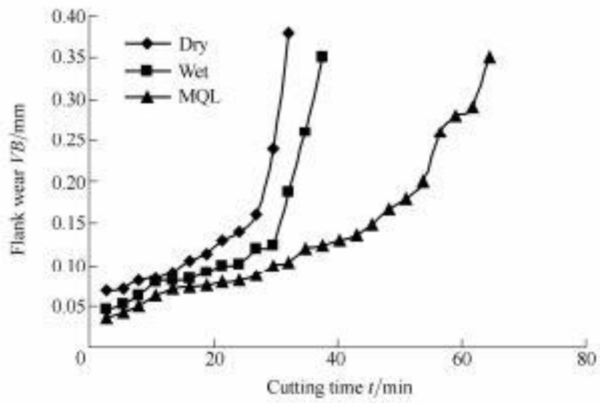

Figure 13: Trend of tool flank wear as a function of time for dry, wet and MQL machining. [22]

Drilling

Zeilmann et al. [23] performed a drilling test on plates of alpha–beta Ti6Al4V alloy (tensile strength Rm = 970 N/mm2 and hardness 300 HB) with dimensions 200 mm × 150 mm × 20 mm. Holes were drilled with 8.5 mm diameter drills through the smallest dimension using a vertical machining centre. To verify the temperature in the piece for different depths, three k-thermocouples have been installed as in the figure below to determine the gradient temperature along the drilled holes. The experiments were conducted in dry condition, flood condition and MQL delivered internally and externally with respect to the tool.

In the obtained results, it is interesting to notice how the MQL delivered internally allows a reduction of temperature of about 50% respect to the one delivered externally.

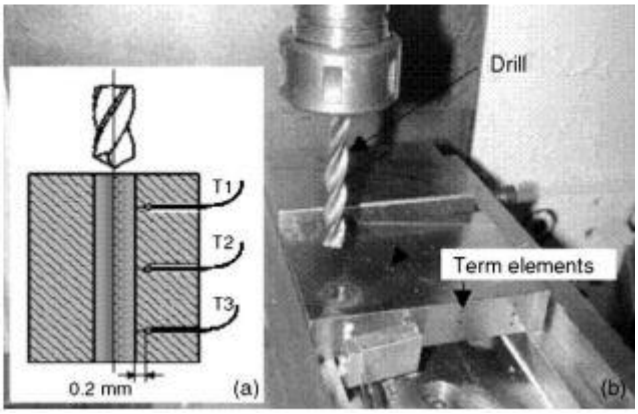

Figure 14: Configuration of thermocouples in experimental setup. [23]

The study of Rahim et al. [24] discusses the outcomes of an investigation into the impact of using different Minimum Quantity Lubrication (MQL) lubricants, namely synthetic ester and palm oil, in the drilling of Ti6Al4V. For comparative analysis, dry cutting was also carried out. The study revealed that drilling under dry conditions led to the shortest tool life, primarily due to severe chipping. The application of MQL proved to be advantageous in various measured aspects such as tool life, thrust force (measured by dynamometer), torque, and temperature (measured by K-thermocouple).

It's particularly interesting to notice how MQL with palm oil allowed better cutting performances, with respect to MQL with ester oil, in all the four parameters considered in the analysis, as demonstrated in the results shown below.

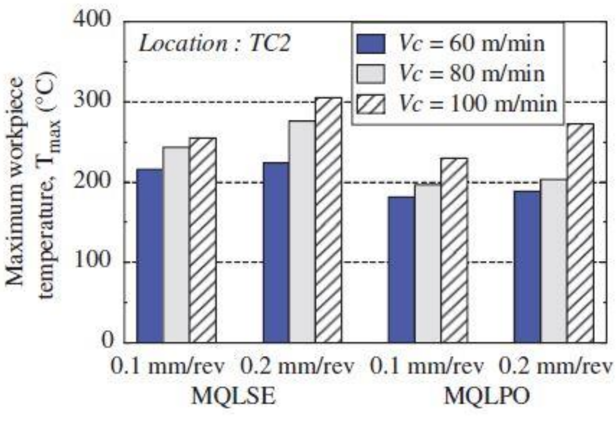

Figure 15: Thrust force, torque and maximum workpiece temperature

for MQLSE and MQLPO [24]

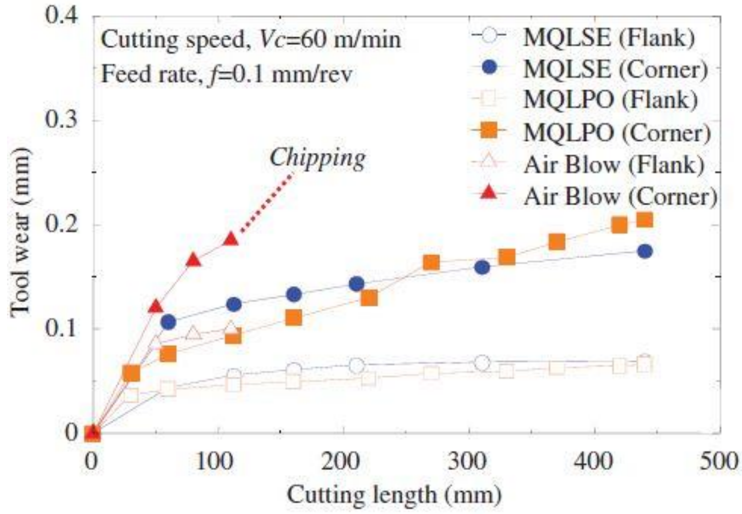

Figure 16: Tool wear as a function of different cutting lengths for MQLSE, MQLPO and Air Blow. [24]

1.4. Thermal behaviour analysis – state of art

The estimation of temperature, with measurements or prediction techniques, is crucial for any machining process because excessive high temperature of machining can lead to different problematics that will decrease the accuracy of the workpiece but also its economic effectiveness.

During the process of metal cutting, a significant amount of heat is generated due to the friction between the cutting tool and the workpiece, as well as the metal undergoing plastic deformation in the form of chips. This heat causes the cutting tool to lose its hardness, reducing its resistance to wear, and altering its size. Moreover, the heat also impacts the dimensions of the machined surfaces. These thermal changes in both the tool and workpiece result in decreased precision in machining. Additionally, higher temperatures lead to increased wear of the cutting tool. Therefore, studying the maximum temperature and its distribution during metal cutting is a crucial aspect of determining appropriate cutting parameters.

Below, a list of unwanted consequences related to high temperature on the cutting zone is presented [25].

Effect of cutting temperature on tool:

- Rapid tool wear (i.e. reduced tool life).

- Plastic deformation of the cutting edges if the tool is not enough hot-hard and hot-strong.
- Thermal flaking and fracturing of the cutting edges due to thermal shocks.
- Built-up-Edge (BUE) formation.

Effect of cutting temperature on workpiece:

- Dimensional inaccuracy due to thermal distortion and expansion-contraction during and after machining.
- Surface damaging by oxidation, rapid corrosion, burning.
- Induction of tensile residual stress and micro cracks at the surface or subsurface.

The temperature is influenced by different aspect of the process, e.g. materials of tool and workpiece (low conductive materials increase more heat generation), tool geometry, cutting parameters, types and delivery methods of cutting fluid. Indeed, the cutting temperature can be controlled or reduced acting on these characteristics of the machining process. Different techniques have been developed and used in literature to measure and estimate the value of temperature in different region of the machining process, in relation to the problem to be studied and analysed.

1.4.1. Temperature measurement

Different methods and instrumentations can be found used in literature to measure the temperature for a cutting process. A primary classification can be related to the physical phenomena of heat transmission used by the measuring instrument: Conduction and Irradiation [26]

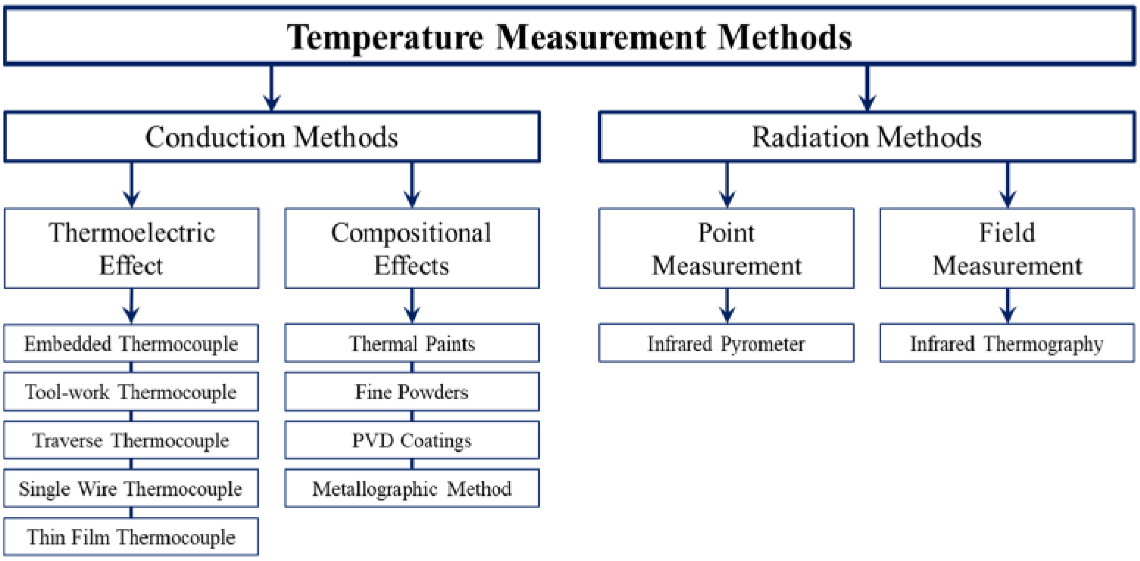

Figure 17: Temperature measurements methods.[26]

1.4.1.1. Conduction methods

Thermoelectric effect

Thermocouples represent the most used instrument to measure the temperature. The temperature measurement using a thermocouple relies on the Seebeck effect, which means that a minor thermoelectric current, known as electromotive force (emf), is produced when two different metals, alloys, or nonmetals are connected at one end, called the hot junction. At the opposite end, referred to as the cold junction, the Seebeck voltage or open circuit voltage is gauged. This voltage is determined by the temperature disparity between the hot and cold junctions, as well as the Seebeck coefficients of the materials employed. Thermocouples classification is based on their material composition and is designated by the type letter, such as platinum and platinum–rhodium combinations (types B, R, and S) which are called noble metal thermocouples, whereas the rest (types E, J, K, N, and T) are called base metal thermocouples [27]

- Embedded thermocouple. This technique utilizes thermocouples inserted into drilled holes in either the cutting tool or workpiece to measure temperatures at specific points. Accurate placement near the surface of interest is crucial due to steep temperature gradients near the cutting zone. Challenges include precise placement due to these gradients and the potential impact of the holes on tool strength and heat conduction. Innovations like rotating collectors and wireless (Bluetooth) data acquisition devices aim to address these challenges in rotating and intermittent machining processes such as milling and drilling [28], [29].

- Tool-workpiece thermocouple technique. This method of temperature measurement in machining is based on using the difference in materials between the cutting tool and the workpiece. The hot junction forms at their contact region during machining, while the tool or workpiece acts as the cold junction. This setup creates an electromotive force due to the temperature gradient between the cutting zone and the surroundings, allowing temperature measurement. However, it has limitations: both the tool and workpiece must be conductive, and readings reflect an average temperature at the tool-workpiece interface, not accounting for localized spikes. Issues like built-up edge formation can lead to inaccurate readings, and slight thermocouple positioning changes can significantly affect measurements.

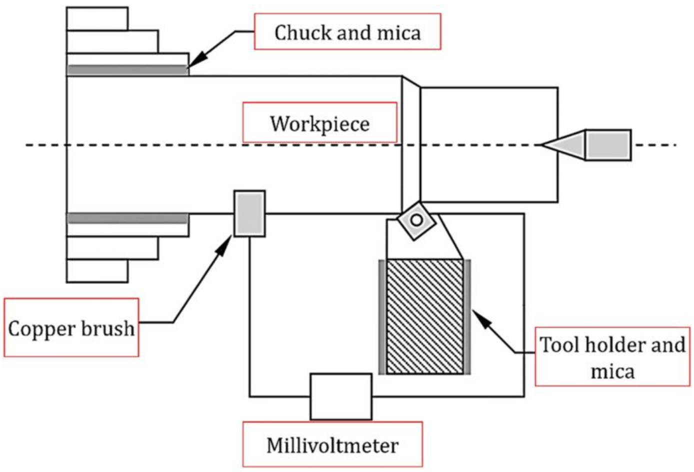

Figure 18: Example of tool-workpiece thermocouple technique for turning process [20]

- Traverse thermocouple. Arndt and Brown [30] developed the traverse thermocouple technique to analyze temperature variations across different points and surfaces of a tool during machining of AISI 1011 steel. This method involves creating a thermoelectric junction between the tool and a fine probe made from a different material, such as high-speed steel and cemented carbide. The probe is systematically moved along the tool's surface, recording temperatures at each position. This approach allows for a detailed and continuous temperature distribution relative to a specific edge of the tool to be mapped. However, despite its effectiveness, the technique is complex to set up and has inherent limitations.

- Single wire thermocouple. Hirao [31] introduced the single wire thermocouple method as a variation of the embedded thermocouple technique. This method measures the temperature on the flank face of the cutting tool by inserting a thin insulated wire into a hole in the workpiece. During machining, when the wire is severed, it forms a thermocouple junction with the cutting tool, generating an electromotive force that correlates with the temperature. The single wire thermocouple method is appreciated for its simplicity in both use and calibration, and it allows for the use of electrically insulating tool materials. However, it has limitations. It may not always capture the maximum temperature at the tool-chip interface, and the temperatures recorded are generally lower than those obtained with the tool-workpiece thermocouple technique. Additionally, experimental errors can arise from variations in the wire's position along the cutting zone, impacting the accuracy of temperature measurements.

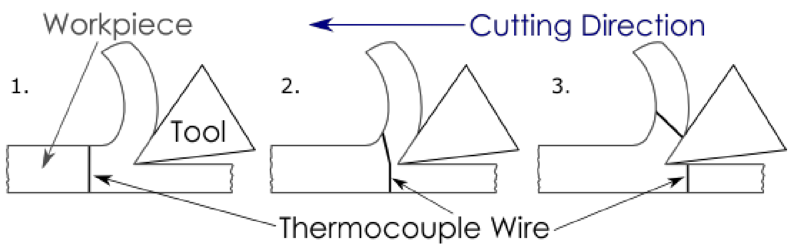

Figure 19: Single wire technique illustration. [32]

- Thin film thermocouple. Unlike traditional approaches like tool-work thermocouples and embedded thermocouples, TFTCs are applied directly onto the surface of cutting tools, they are typically created through thin film deposition or lithography processes, leading to minimal adverse effects, enhanced measurement precision, and rapid response times. This is due to their exceptionally small size, which results in minimized volume. The introduction of thin film thermocouples (TFTCs) in cutting temperature measurement has partially mitigated the drawbacks associated with the methods mentioned earlier.

Compositional effect

Using materials with different compositions the respond in different way to the temperature reached in the cutting zone, a temperature measurement can be performed. In general, these are methods with a not so high accuracy in the measurement and they are used to validate or together to the thermocouple techniques exposed above.

- Thermal-sensitive paints. Despite its applicability is typically restricted to controlled heating environments and the results obtained using this method need to be validated using other temperature measurement techniques, the utilization of thermal sensitive paints, capable of changing colour based on temperature variations, represents one of the most straightforward and cost-effective techniques for measuring the surface temperature of cutting tools or workpieces during machining operations. In this approach, the boundary between the two colours of the paint indicates the isotherm corresponding to the temperature at which the colour change occurs.
- Fine powders. This method is employed to analyse the temperature distribution on the rake face of cutting tools. It involves using fine powders with a consistent melting point. The estimation of temperature distribution can be performed observing the boundary line that distinguishes the regions of melted and unmelted powder scattered on the tool surface. This boundary line represents the equi-temperature line at the melting point of the powder being used.

  The primary advantages of this temperature measurement method include the absence of calibration requirements, as the powders used have consistent melting points, and the capability to acquire temperature distributions. However, there are notable limitations associated with this approach. The powder used takes a long time to melt entirely, leading to delays in obtaining accurate temperature readings. Additionally, the method exhibits poor thermal response [33]. To compensate for these limitations, experiments often need to be repeated multiple times using different powders with varying melting points, adding complexity to the process.
- PVD coating. In contrast to the method involving fine powders with constant melting points, this approach offers superior responsiveness to temperature changes. Additionally, it eliminates the necessity for specialized calibration, does not disrupt the inherent temperature field being measured, and can be applied to various types of tool materials. This includes high-speed steel, cemented carbide, ceramics, and CBN, regardless of their conductivity. Moreover, this method is suitable for almost any

temperature range, including extremely high temperatures, small areas, and high temperature gradients.

- Metallographic. By observing the microstructural changes and/or by measuring the microhardness of the heat-affected zone within the cutting tool after a machining operation, the temperature can be determined.

  The main limitation of this method of temperature estimation is that it can be used only within the range of cutting conditions suitable for high-speed steel and when relatively high temperatures are generated.

1.4.1.2. Radiation methods

Recent advancements in temperature measurement during machining have focused on noncontact radiation methods, specifically infrared (IR) detection techniques. These methods gauge the surface temperature of an object by detecting the thermal energy it emits. They offer several advantages: rapid response times, minimal interference with temperatures or materials, and are particularly beneficial for brittle and electrically resistant materials like ceramic cutting tools. However, noncontact radiation methods come with limitations. They are typically more expensive to deploy compared to contact-type sensors such as embedded thermocouples. The accuracy of IR techniques can vary based on the emissivity of the surface being measured, which differs across materials and surface conditions. Moreover, obstacles like machining chips can obstruct the IR sensor's view, potentially compromising the precision of temperature measurements. [25]

Point measurement

- Infra-red pyrometer. Noncontact radiation methods provide the advantage of easily capturing the temperature distribution during machining processes. However, they require dry cutting conditions for optimal operation. Accurate temperature measurement hinges on selecting appropriate measurement locations, as chip obstruction can significantly impact readings. Additionally, understanding and accounting for surface emissivity is crucial, as it varies based on surface characteristics like roughness, cleanliness, and oxidation state. These variations introduce uncertainties in temperature measurements, complicating the task of obtaining precise and reliable results in machining operations. [26]

Field measurement

- Infra-red thermography. Infrared thermography, akin to infrared radiation pyrometry, employs an infrared or CCD camera to map temperature distributions across an object's surface using color-coded representations. This visual approach facilitates easy interpretation and analysis of temperature data by displaying different colours for varying temperature levels. Operating without physical contact ensures no disturbance to the temperature field, allowing direct visualization of isotherm distributions. However, challenges include longer exposure times (10-15 seconds), variable emissivity, and constraints with lubricant use, alongside high setup costs. Despite these drawbacks, its non-contact nature and real-time temperature visualization make infrared thermography invaluable in manufacturing, research, and maintenance, with ongoing efforts to improve accuracy and usability. [26]

1.4.2. Temperature estimation

Usually the temperature to be measured is localized in zone where physical instrument cannot be mounted due to problem related to too high temperature, for example in combustion chamber where a thermocouple will be destroyed, or where instrument with irradiation method cannot reach directly the measuring zone due to obstacles. In this cases the temperature will be estimated indirectly, measuring temperature or other parameters linked with it, through the use of mathematical models, or simulation software. The estimation of temperature reached in the interface between tool and chip during metal cutting can considered as example of this kind. In literature, different methods to estimate the temperature reached in a determined area can be found. Specifically, cutting temperature can be estimated:

- Analytically. Analytical models developed to calculate temperature reached in the cutting zone from the cutting parameters used for the process or other measurements conducted on different zones of the working area (e.g. zone of workpiece, chip, etc.). To address certain limitations associated with numerical methods, researchers have developed a diverse range of analytical techniques capable of predicting temperatures in machining processes with comparable accuracy while offering significantly improved computational efficiency. However, these methods also come with their own set of drawbacks, including intricate input requirements and high mathematical complexity. Additionally, simplifying assumptions are often necessary to streamline the problem, so they always introduced an error to be considered during estimation. [26]
- Empirically. These techniques involve performing a series of experiments to study the impact of independent variables such as depth of cut, tool geometry, feed, and cutting speed on output parameters like surface roughness, cutting temperature, force, and tool wear. The goal is to create empirical models that

establish relationships and predict values of responses between input and output process parameters. While these methods have provided acceptable solutions in certain applications, their usage is restricted due to constraints, assumptions, and limitations inherent in the modelling technique [26].

- Numerically. Usage of thermal simulation on FEM software represent a good instrument to the estimation of temperature being able to represent the entire thermal field associated to the cutting process. It is associated to the specific cutting process under analysis, so usually it is used to validate the analytical model developed to characterize the temperature estimation. Examples of numerical methods that have been effectively utilized to model machining processes and determine temperature distributions in the workpiece, chip, and tool, including the shear zone and tool rake face temperatures are the finite element method, finite difference method, and boundary element method. These methods can also predict steady-state temperatures and transient temperature variations. The key benefit of these methods is the reduction in simplifying assumptions compared to analytical approaches. However, their usage comes with drawbacks, including low computational efficiency, high computational costs, and the need for a substantial number of input parameters. These parameters must be determined through extensive experimental work and mechanical property tests, making real-time prediction and optimization challenging in the context of process parameter planning [26].

Method	Major merits	Major demerits	Remarks
Numerical methods	Reduction of simplifying assumptions Sufficient prediction capability and accuracy	Low computational efficiency High computational costs	Large number of input parameters need to be experimentally determined
Analytical methods	High computational efficiency	Complex input requirements High mathematical complexity	Need simplifying assumptions
Empirical methods	Very effective for simple problems	Experimental data may be overfitted Model predictions can be erroneous in some parts of the domain	Large number of experimental tests need to be performed Assumptions are needed

Table 2: Properties of the different methods of temperature estimation. [26]

With this paradigms, Patne et. al [34] performed a temperature estimation on a drilling process of a titanium alloy combining the overmentioned techniques. After the application of an analytical approach to compute the different heat partitions between tool, chip, and workpiece, they provided the results to a FEM simulation to compute the temperature field in the workpiece and tool. Then, they validated the simulation results thanks to IR camera measurements on the workpiece and with temperature behaviour, measured with thermocouple embedded in the drill bit, for the tool temperature.

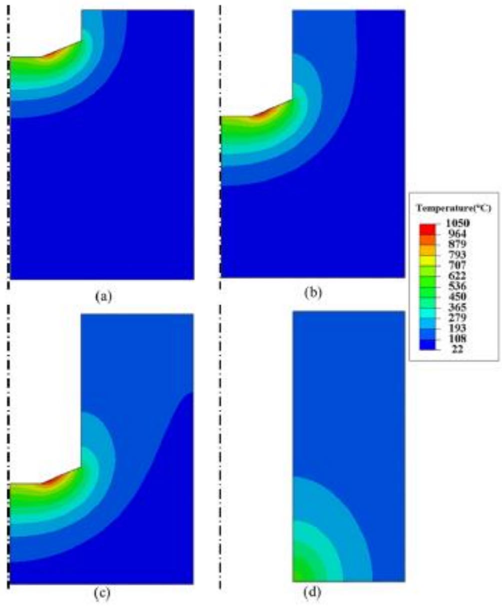

Figure 20: Temperature distribution in the work piece at various drilling depths for cutting speed of 1600 rpm and feed rate of 0.051 mm/rev [34]

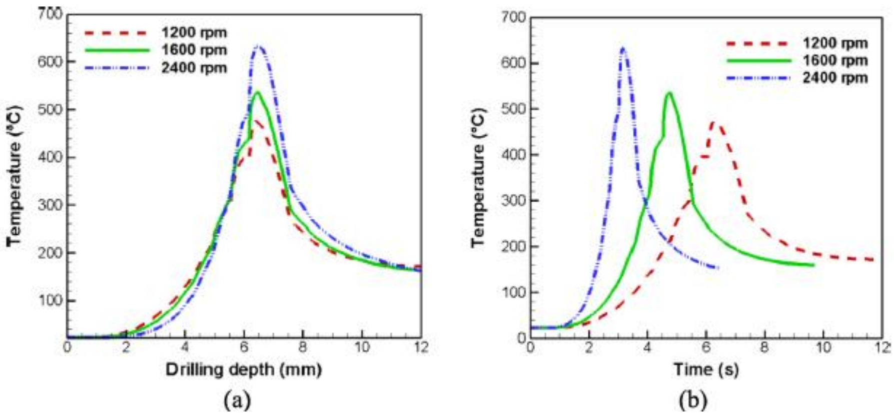

Figure 21: Temperature distribution at contact point between drill and work piece at depth of 5.5 mm for feed rate of 0.051 mm/rev as a function of (a) drilling depth and (b) time [34]

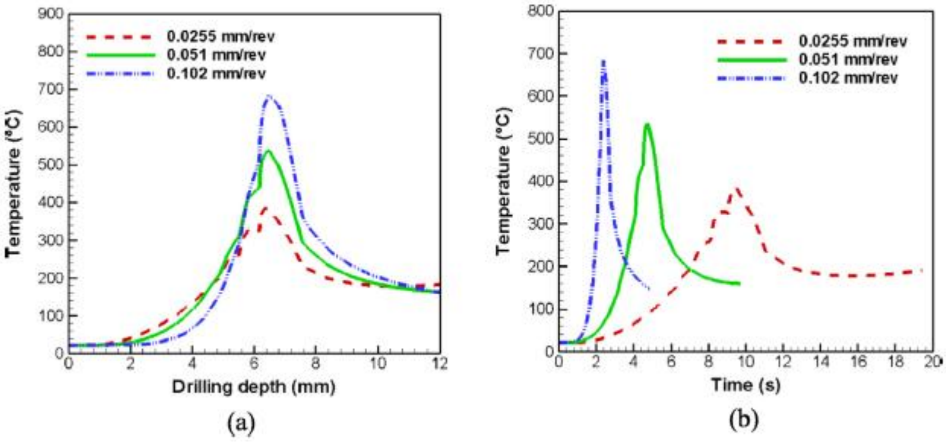

Figure 22: Temperature distribution at contact point between drill and work piece at depth of 5.5 mm for cutting speed of 1600 rpm as a function of (a) drilling depth and (b) time [34]

The finite element model produced in the mentioned work, was used to predict the temperature distribution at a contact point between the drill and workpiece, for given processing conditions. Fig. 21 shows the temperature distribution at the contact between the drill and the work piece, at a depth of 5.5 mm from the top surface of the work-piece for varying cutting speed. From the figure, an increase of the temperature inside the work-piece can be related to an increasing of the cutting speed.

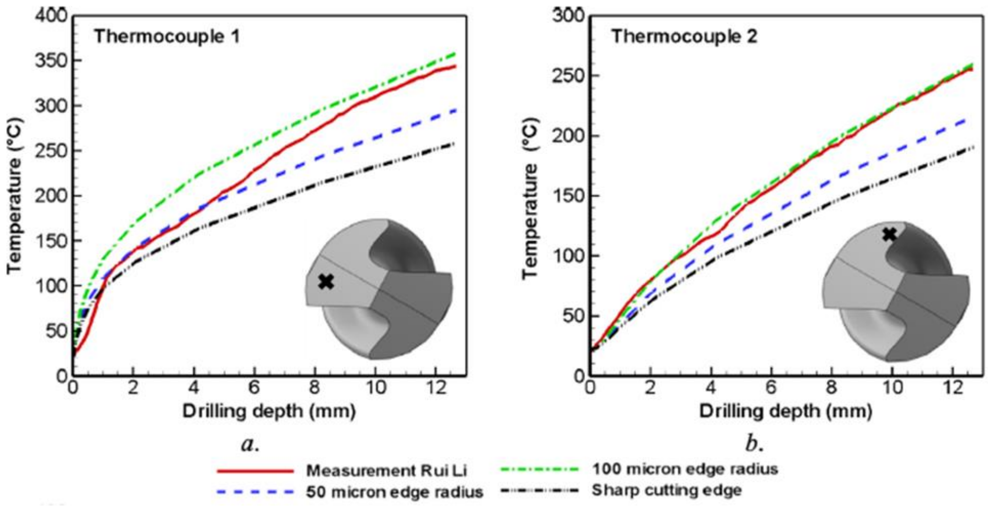

Figure 23: Comparative study of measured and modeled temperature for 2 thermocouple locations. [34]

Fig. 22 shows the temperature distribution at the same location of the previous mentioned figure, for varying feed rates. It is concluded from the figure that as the feed rate increases an increase in temperature of the workpiece can be noticed.

To validate the results obtained for the tool temperature behaviour, Patne et. al compared their results with the ones obtained by Li et al. [35] with different edge radius values. From their results shown in Fig. 22 with an higher edge radius, the partition of heat generated on flank surface going into the tool is higher with respect to the one with lower edge radius, leading to an increase in temperature of the flank surface.

The aim of the research of Segurajauregui et al. [23] is to determine the amount and ratio of heat generated during drilling operations and to quantify the heat transferred to the workpiece based on cutting speed and feed rate. In fact, as a consequence of the trend of eliminating lubrication, or at least reduce the amount of oil involved in the process, the workpieces experienced an increase in temperature. This higher heating can lead to distortion that can be predicted using the finite-element method (FEM), if the heat input to the workpiece during machining is known.

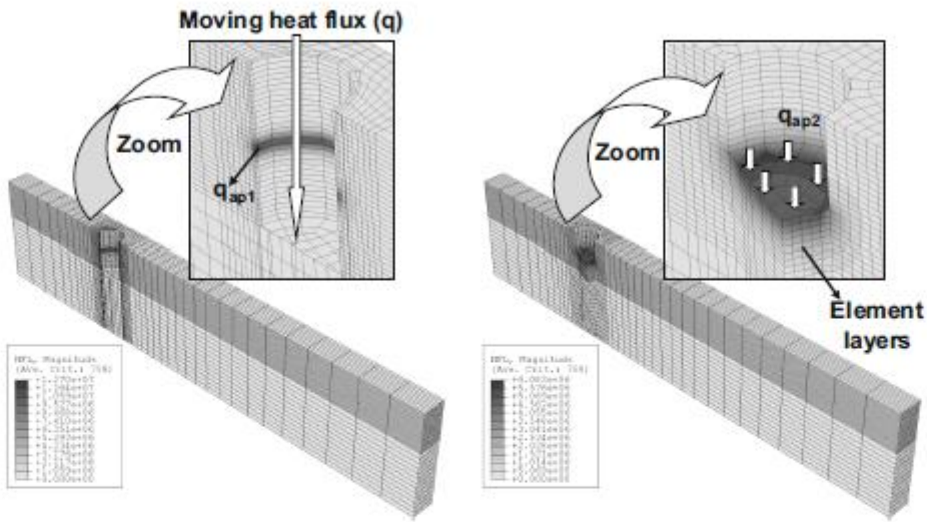

Figure 24: Numerical model without element deletion (left) and with element deletion (right). [36]

Some experiments were conducted on aluminum (Al2017) samples during drilling operations with MQL, and torque and workpiece temperature were measured. Temperature was measured using infrared methods, and drilling torque was measured with a piezoelectric dynamometer. Once the temperature measurements have been performed, an inverse simulation approach, based on minimization of error between numerical and experimental results on temperature, was used to calculate the heat input to the workpiece for each machining condition.

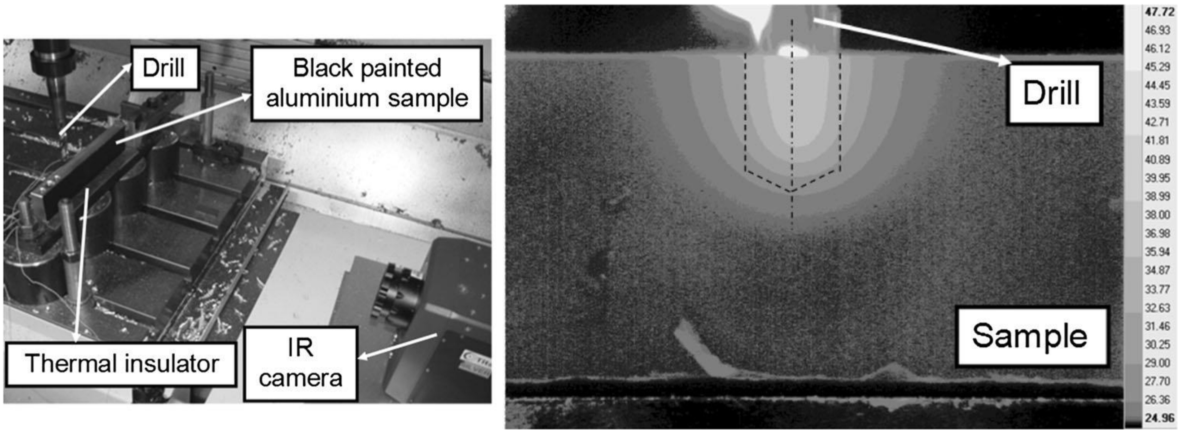

Figure 25: Experimental setup (left) and IR measurement for one test (right).[36]

The total amount of heat produced during the process was calculated as:

$$Q_{tot} = 2\,\pi\,M\,\frac{n}{60}\,t_c$$

where:

- M = measured torque
- n = spindle speed of the drill in r.p.m.
- t_c = cutting time

Then, after the prediction of heat flux due to minimization of errors between experimental and numerical temperatures, the percentage of heat going into the workpiece in relation with the cutting parameters, Vc and f, has been plotted.

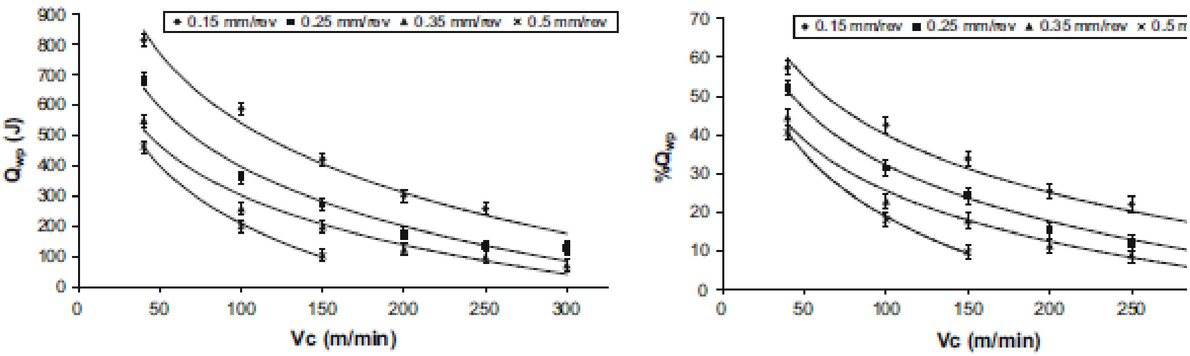

Figure 26: Q and %Q for different cutting conditions. [36]

From the analysis of results, the following conclusion were drawn [36]:

- The amount of heat transferred to the part decreases for higher cutting speeds (Fig. 26) . In fact, increasing the Vc by approximately six times reduces the Q_{wp} value by about eight times, as can be seen for f = 0.35 mm/rev.
- The effect of feed rate is also very clear: more heat is transferred to the workpiece when the feed rate is lower. A threefold increase in the f value can decrease Q_{wp} by almost four times (for Vc = 150 m/min).
- With low cutting parameters the percentage of the total heat transferred to the workpiece is very high in comparison with that transferred under higher cutting parameters.
- The coefficient of total heat going into the workpiece $\%Q_{wp}$ varies between 6 and 53 % of the overall cutting energy depending on Vc and f values. The MQL effect could be noted in the minimum $\%Q_{wp}$ value (6 % with MQL vs. 10 % in dry drilling).

Fleischer et al. [33] work dealt with the development of a mathematical model as a function of the cutting parameters and tool geometry to predict the heat flux input to simulate distortion using a FEM simulator. The thermal response of a component during metal cutting with MQL is analyzed by examining the correlation between the heat generated and factors such as drill type, drill hole diameter, and other drilling parameters. This analysis aimed to predict whether part tolerances could be maintained under these conditions. From an extened analysis of the literature they noticed that the input in the workpiece during machining present high fluctuations according to small differences of tool geometri or cutting parameters. They proposed ranges for the distribution of thermal power generated during cutting, taken from literature anaysis, shown in Fig. 27 . They reported that, since the wide parameter ranges, no regularities could be established in bibliographical references. Furthermore, most of the experimental data were made in orthogonal cutting [33].

	Drilling	Turning	Milling
Tool	5-15 %	2,1-18 %	5,3–10 %
Work piece	**10-35 %**	**1,1-20 %**	**1,3-25 %**
Chip	55-75 %	74,6-96,3 %	65-74,6 %

Figure 27: Distribution of the cutting energy from literature analysis. [37]

Simulation programs like ABAQUS require an input value that is independent of machining time and the machined surface. Therefore, the total quantity of heat generated cannot be directly used. Instead, the quantity of heat is related to the surface machined within one second. This resultant value is referred to as the surface heat flux. The formula used in the work described was:

$$\dot{q} = \frac{c_p \cdot m}{A \cdot dt} dT$$

To determine the temperature needed in the heat flux computation they set an experimental campaign where different holes have been drilled in an aluminum block. Drills with diameters from 6 mm to 17.5 mm are employed. A Kistler rotational dynamometer, which determines torque and feed force, was used for the force measurement. The temperature was measured with NiCr-Ni-thermocouples that were fixed on the sample. One of the thermocouples was placed 0.1 mm away from the drill wall and the other two thermocouples were placed on the corners of the sample 5 mm away from the edges of the probe.

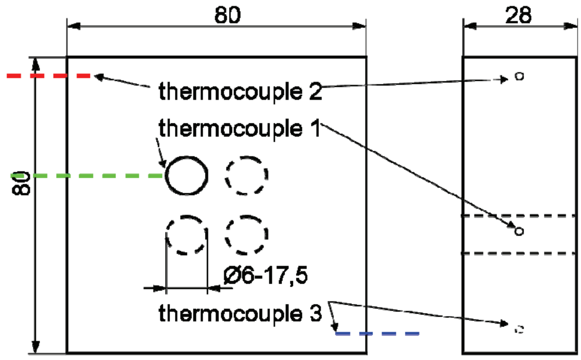

Figure 28: Experimental setup and Thermocouple arrangement. [37]

The influence of feed rate and cutting speed on heat input was analyzed using a drill with a radial cutting edge and a diameter of 14 mm. The results showed that the dependency of surface heat flux on cutting speed at a constant feed rate per tooth is linear. Meanwhile, the relationship between feed rate per tooth at a constant cutting speed can be modeled using a second-degree polynomial or an exponential function. The effect of drill diameter on heat flux is also linear. Although theoretically, drill geometry should influence heat flux, this was not confirmed in the conducted experiments. experiments also demonstrated that heat generation is highly dependent on the state of the tool's wear.

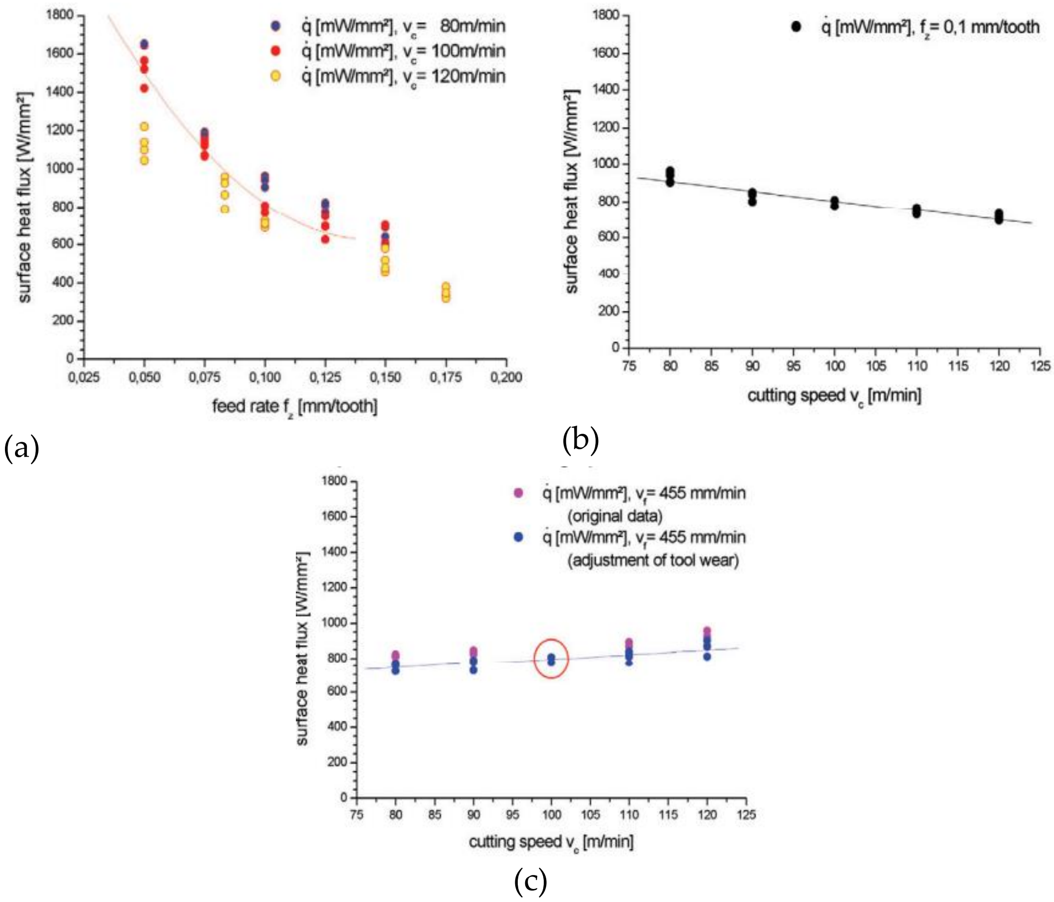

Figure 29: Surface heat flux at: (a) constant Vc in dependence on fz, (b) constant fz in dependence on Vc, (c) constant Vf in dependence on Vc. [37]

1.5. Mechanistic behaviour analysis - state of art

In literature, the predicition of forces related to machining of parts, have been performed utilizing empirical, mechanistic, and finite element methods. All this techniques are based on the predictive model developed by Oxley [38]. Initially, empirical models were created to investigate the relationships between thrust force, torque, and various drilling parameters and they were usually succeeded by a mechanistic approach, which offers a more precise depiction of the process kinematics. The finite element method (FEM) is the most detailed of these approaches, employing advanced mathematical models of metal plasticity and requiring fewer experiments [39].

The mechanistic modeling approach is an improvement over the empirical approach, as it incorporates more detailed process knowledge rather than relying solely on empirical fitting of equations through multivariate regression. It requires a thorough understanding of process kinematics and operates on the assumption that cutting forces are proportional to the uncut chip area or chip load. Calibration constants derived from experimental data account for material characteristics. This approach necessitates fewer calibration experiments and is more likely to maintain accuracy outside the tested range due to its better grasp of process physics [39]. An example present in literature where a mechanisitic approach was used to predict the dynamics of drilling process is shown below.

In Chandrasekharan et al. [40], a mechanistic approach was used to develop cutting force models and predict the thrust and the torque in drilling. They further applied the developed model to predict the cutting dynamics of Fiber-Reinforced Composite Materials (FRCM). This approach exploited a different set of fundamentals of the process including chip load, chip thickness, cutting angles that remain the same whether machining metals or FRCM. They initially determined the variation of the specific angles introduced in oblique cutting along the lip of the drill as functions of the normalized radial coordinate. Then, they developed a model for the lips of the drill considering oblique cutting computing the torque and thrust force considering in the formulas the different specific cutting pressures along the direction of the forces involved during drilling process.

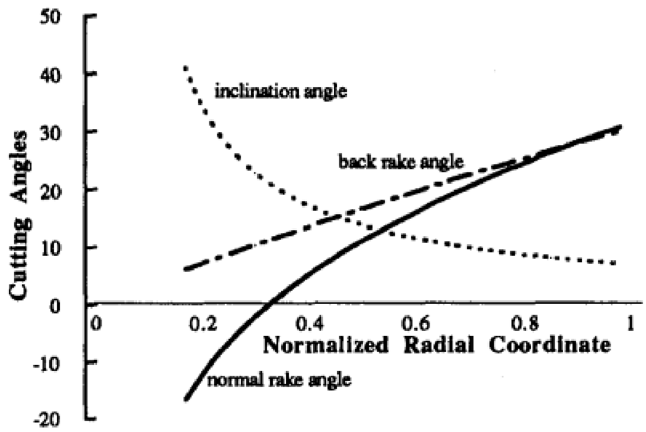

Figure 30: Variation of the cutting angles with the normalized radial distance for a conical point drill (118 deg. point angle, 33 deg. helix angle, 0.144 deg. web thickness-to-diameter ratio). [40]

Concerning the chisel behaviour, in literature two strategy are usually choiced: Consider the chisel action only as indentation mechanism or divide the chisel in two regions, considering a part acting with an indentation mechanism and a part with the orthogonal cutting one. Chandrasekharan et al. considered the chisel action as indentation and orthogonal cutting. Whereas for the higher brittleness of FRCM they considered for the entire length of chisel the ortogonal cutting mechanism. In this case, they considered the specific cutting pressure to compute thrust force and torque involved in the process, too.

To calibrate and then validate the model, the authors performed drilling experiments on an OKUMA (MC-4VAE) CNC Machining Center and measured thrust and torque forces by means of a Kistler (9273 A) four-channel dynamometer. They calibrated and validated the model for drilling metals (gray cast iron) and FRCM (AMOCO T300/934 unidirectional carbon fiber/epoxy matrix) with carbide drills, without any use of coolant.

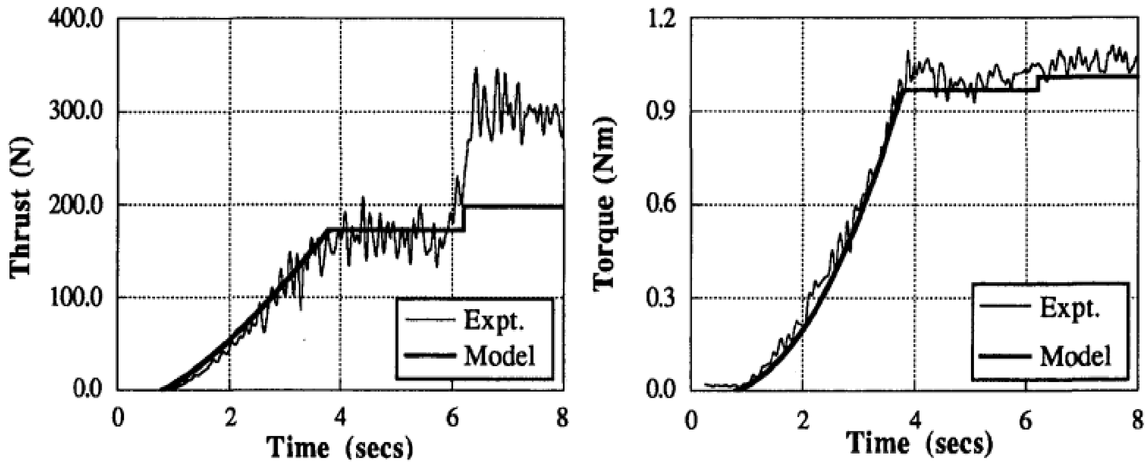

Figure 31: Thrust and torque for 15.875 mm diameter, 118 deg. point angle, 33 deg. helix angle, pilot hole diameter 3.175 mm, speed 800 rpm, feed 0.102 mm/rev. [40]

In the figure above an example of the results obtained in the work of Chandrasekharan et al. was shown, confirming the reliability of the model developed from researchers.

The finite element method (FEM) is the most advanced approach, involving comprehensive modeling of parameters such as ambient temperature, friction factors, and heat transfer coefficients, as well as relationships like constitutive laws, failure criteria, and contact models. While the simulation execution can be extremely time-consuming—often taking significantly longer than mechanistic models—FEM generally requires experiments only for validation purposes. Despite its complexity and time demands, FEM offers detailed insights into drilling force modeling with minimal experimental validation [39]. An example present in literature where a mechanisitic approach has been used to predict the dynamics of drilling process is shown below.

In the work of Strenkowski et al. [41] the development of a finite element drilling model involves representing the drill cutting lips geometry as a series of oblique sections. Initially, an analytical model for oblique cutting is used to analyze a single section in the cutting lip region of the drill by following the scheme of Fig. 32. At each oblique cutting section, the three-dimensional cutting forces are calculated and then combined to determine the drilling thrust force and torque for various operating conditions

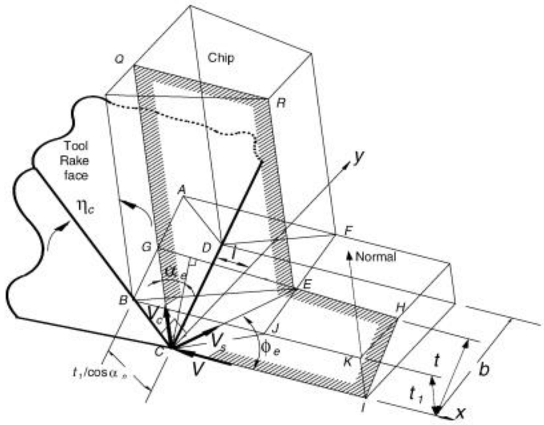

Figure 32: Model of oblique cutting. [41]

The model is verified by comparing its predicted thrust force and torque with both measured and published data. Initially they validated the two models, for oblique and orthogonal cutting on lathe of tube, resulting in high match between measured and modelled forces. Then they performed drilling tests on a Bridgeport milling machine using a high-speed steel twist drill with a 3.2 mm web thickness, 30° helix angle, and 118° point angle. The workpiece was an AISI 1020 steel block. Three drills with 6.35, 9.53, and 12.5 mm diameters were used for three feed rates of 0.051, 0.076, and 0.102 mm/rev.

The results on thrust force are shown below confirming the reliability of the model developed in the prediction of cutting force. They also compared the results on torque with published measured data on other experiments confirming the results on thrust force.

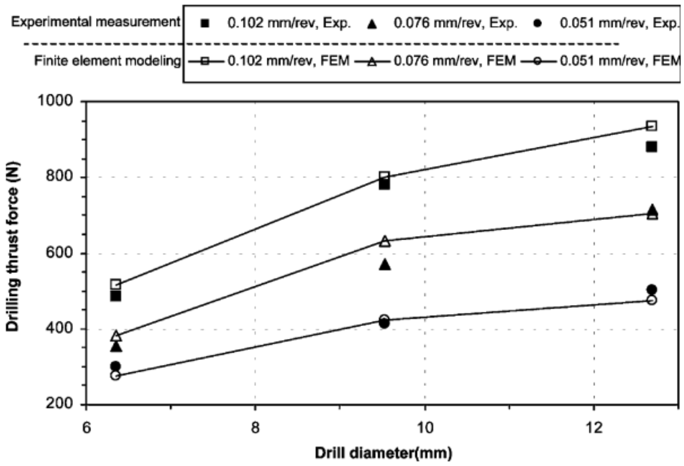

Figure 33: Comparison of finite element predicted and measured thrust force in nine drilling tests. [41]

1.6. Purpose of thesis

According to the information obtained from the study of the state of art, in literature a gap on analytical modelling for predicting torque, forces and angles involved during the drilling operation, especially in peck drilling process, was identified. Peck drilling is a machining process where the drill bit is periodically retracted to remove chips and allow cooling, crucial for preventing tool breakage and maintaining hole quality. It is especially important in deep hole drilling and machining tough materials, ensuring effective chip evacuation and temperature management.

Moreover, the majority of the studies concerned the estimation of temperature reached by the workpiece and the relative heat partition coefficient. Such studies implemented a FEM simulation of the process, requiring high computational and time costs. Furthermore, the FEM simulation required a specific formulation for each case studied.

Furthermore, just few publications dealt with the capability of MQL lubrication to affect process related quantities and the temperature of the parts involved in the process. Despite the knowledge of the reduction of the generated cutting forces, torque and temperature, learned thanks to the observations performed with several experimental campaign conducted about the use of different lubrication strategy, a lack on the characterization of the parameters affected by the use of MQL and their phenomenological effect on force and temperature involved in the process is present.

For these reasons, this work is articulated in achieving the following objectives:

- Conceiving of an analytical model to study the mechanistic parameters of the oblique cutting, to be applied to a peck drilling operation analysis.

- Conceiving of an analytical model for the prediction of temperature reached in the workpiece during peck drilling process.

- Application of the models to experimental data to assess the relations between the change of temperatures, forces and torque with the use of MQL under different lubrication conditions and different process parameters.

- Formulation of regression models, from the observation of the experimental results, able to predict a priori the mechanistic and thermal dynamics involved into the process.

List of symbols

Variable	Description
α_r	Orthogonal cutting rake angle
α_t	Diffusivity of tool material
α_w	Diffusivity of workpiece
β	Angle of conical surface
γ_d	Dynamic rake angle of oblique cutting
γ_{AB}	Shear strain along AB shear line
$\dot{\gamma}_{AB}$	Shear strain rate along AB shear line
$\dot{\gamma}_{int}$	Shear strain rate at tool-chip interface
δ_r	Helix angle at specific radius
δ	Helix angle at diameter
ε	Reference angle
ε_{AB}	Equivalent strain al AB shear line
$\dot{\varepsilon}_{AB}$	Equivalent strain rate along AB shear line
$\dot{\varepsilon}_{int}$	Equivalent strain rate at tool-chip interface
θ	Angle between R resultant force and AB shear line
λ	Friction angle
ρ	Density of workpiece material
σ_N	Normal stress at tool-chip interface calculated from resultant force R
σ_N'	Normal stress at point B using stress boundary condition
ω	Web angle at specific radius
τ_{int}	Shear stress at tool-chip interface
ϕ	Shear angle
ψ_c	Chisel edge angle
κ_t	Half-point angle
A	Yield strength in J-C flow stress model
A_{ch}	Instantaneous indentation area of chisel edge
B	Strain coefficient in J-C flow stress model
C	Strain rate constant in J-C flow stress model
C_0	Ratio of shear plane length and thickness of primary shear zone
c_p	Specific heat of workpiece

D	Drill bit diameter
f	Feed rate
Fs	Shear force
Fc	Cutting force
Ft	Transverse force
Fr	Radial force
F_f	Friction force
Fz	Thrust force
F	Friction force at tool chip interface
h	Tool chip interface length
H_b	Brinell hardness of tool material
i	Inclination angle
k	Conductivity of workpiece
l	Shear plane length
m_{chip}	Mass of chip per unit time
$\dot{m}_{air}$	MQL air flowrate
$\dot{m}_{oil}$	MQL oil flowrate
Mt	Cutting torque
N	Normal force at tool-chip interface
n_{eq}	Generalized train hardening exponent
P	Power
r	Radial distance
R	Radial coordinate of infinitesimal area of cone
R_T	Adimensional thermal number
t_p	Half web thickness before splitting point
t_1	Uncut chip thickness
t_2	Chip thickness
T_{ab}	Shear plane temperature
T_{int}	Tool-chip interface temperature
T_s	Temperature on shear plane
T_w	Ambient temperature
ΔT_{sz}	Temperature increase in shear zone
V_c	Cutting velocity
V_{chip}	Chip velocity
V_s	Component of velocity along shear plane
w	Chip width

2 Mechanistic models for peck drilling

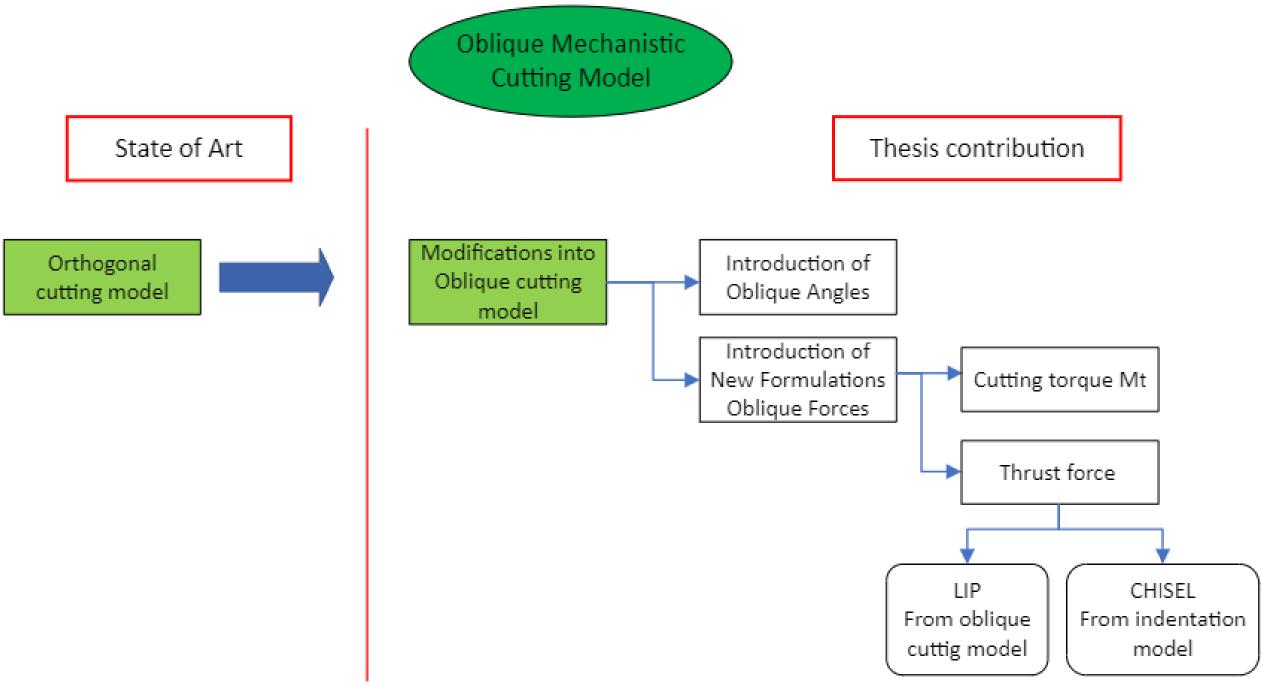

In this section the development of the mechanistic model for the computation of the oblique cutting parameters is discussed. The development starts from the study of the orthogonal model described in the work of Lalwani et al. [42], and then continues with the enhancement implementation of the model, transforming it into a model suitable for the study of the dynamics of oblique cutting.

2.1. Orthogonal cutting model

Lalwani et al. [42] extended the Oxley's predictive analytical model, outlined in his work [38] in 1989, that provides a detailed analytical framework for chip formation, incorporating assumptions about the shear zones, strain rates, and the effects of temperature on Johnson and Cook flow stress material model. A summary of the key components and assumptions of Oxley's theory [38] is shown:

Chip Formation and Plastic Zone:

The chip is formed in a plastic zone, extending from the tool cutting edge to the layer of chip adjacent to the tool-chip interface.

Assumptions in Oxley's Theory

1. Plane-Strain and Steady State Conditions:
   - Assumes plane-strain conditions and a steady-state process with a sharp tool.
2. Shear Zones:
   - The primary shear zone is assumed to be parallel-sided.
   - The secondary shear zone (tool-chip interface) is of constant thickness to simplify analysis.
3. Uniform Shear Strain:
   - Shear strain at shear plane is uniform and equal to half the strain in the primary shear zone.
4. Uniform Temperature and Strain:
   - Temperature and strain are uniform along shear plane.
5. Slip Line:
   - Line AB, referred to shear plane, is considered a straight slip line during chip formation, aligning with the shear plane in the Ernst and Merchant shear-plane model of chip formation.
6. Maximum Shear Stress and Strain-Rate:
   - Both shear plane AB and the tool-chip interface are directions of maximum shear stress and maximum shear strain-rate.
7. Strain-Rate Constants:
   - C_0 and δ are constant indicating strain rate at shear plane and tool-chip interface respectively.

In the original Oxley's model, the constants used in the power law equation ($\sigma = \sigma_1 \varepsilon^n$) were available just for carbon steel and for few aluminium alloys. To address this limitation, Lalwani et al. extended this model introducing a generalized term, n_{eq}, to replace the strain hardening exponent (n) of the Oxley's theory. In this way the model can be applied to different cases involving dissimilar materials and materials flow stress models beyond those initially considered [42].

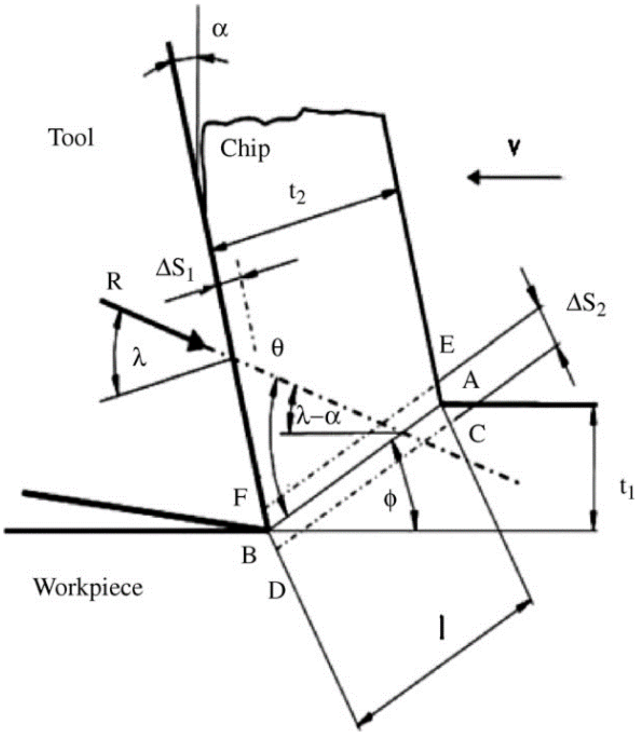

Figure 34: Parallel-sided shear zone model. [42]

The model exploits the J-C material model, which is nowadays commonly used as flow stress model of work material in modelling machining operations due to its simplicity and ease to use. This material model is given as:

$$\sigma = (A + B\,\varepsilon^{n})\left(1 + C\ln\frac{\dot{\varepsilon}}{\dot{\varepsilon}_0}\right)\left(1 - \left(\frac{T - T_w}{T_m - T_w}\right)^{m}\right) \quad (1)$$

where *A, B, C, n* and *m* are material constants that can be found either by material testing equipment or by machining tests, σ is the flow stress of material, ε is equivalent strain, $\dot{\varepsilon}$ is equivalent strain rate and $\dot{\varepsilon}_0$ is reference strain-rate, T is the material instantaneous temperature, T_w is initial workpiece temperature (i.e. room temperature) and T_m is melting point temperature of workpiece material. The first term in parenthesis in Johnson and Cook (JC) equation represents strain hardening. The parameter *A* in first term is yield stress of material and the parameter *B* is strain hardening modulus. Second term in parenthesis shows that flow stress increases when material is loaded with high strain-rate whereas, the third term represents the fact that as temperature increases the flow stress of material decreases. The term $\left(\frac{T - T_w}{T_m - T_w}\right)$ is known as normalized (homologous) temperature. The constant *m* controls the softening of material.

The orthogonal cutting model follows the work of [42], and starts by setting the uncut chip thickness t_1 to half of the feed of the drill bit:

$$t_1 = \frac{f}{2} \tag{2}$$

Analysis of the shear plane AB

The temperature at the shear plane can be expressed from the room/workpiece temperature, by an increase ΔT_{SZ}:

$$T_{AB} = T_w + \eta \Delta T_{SZ} \tag{3}$$

where:

- $\Delta T_{SZ} = \frac{(1-\beta) F_s V_s}{m_{chip}\, c_p}$ (Temperature rise on shear zone) (4)
- $\beta = 0.5 - 0.35\ log_{10}(R_T\ \tan\phi)$ $\quad for\ 0.04 \leq\ R_T\ \tan\phi \leq 10$ (5)
  $\beta = 0.3 - 0.15\ log_{10}\ (R_T\ \tan\phi)$ $\quad for\ R_T\ \tan\phi > 10$
  (heat partition going into the workpiece [42])
- $R_T = \frac{\rho c_p V_c t_1}{k}$ (non-dimensional thermal number) (6)
- η represents the efficiency with which the total shear deformation energy is converted into sensible heat in a machining process (90% in this work). The remaining energy, $(1-\eta)$, is stored in the deformed chip material as latent energy.

Since c_p and k are defined as functions of T_{AB}, Eq. 3 – 6 are a set of non-linear equations in T_{AB}.

The equivalent shear flow stress according to Von Mises yield criterion on the shear plane is:

$$k_{AB} = \frac{\sigma_{AB}}{\sqrt{3}} = \frac{1}{\sqrt{3}}(A + B\ \varepsilon_{AB}^n)\left(1 + C\ln\frac{\dot{\varepsilon}_{AB}}{\dot{\varepsilon}_0}\right)\left(1 - \left(\frac{T_{AB}-T_w}{T_m-T_w}\right)^m\right) \tag{7}$$

The equivalent strain hardening exponent related to the coefficient of JC model developed in the work of Lalwani et al. is approximated by the following relation:

$$n_{eq} \approx \frac{nB\varepsilon_{AB}^n}{(A+B\varepsilon_{AB}^n)} \tag{8}$$

The angle θ between the resultant force R and shear plane direction can be calculated in two ways:

$$\tan\theta = 1 + 2\left(\frac{\pi}{4} - \phi\right) - C_0\, n_{eq} \tag{9}$$

$$\theta = \phi + \lambda - \alpha_r \tag{10}$$

where:

- ϕ is the shear angle
- λ is the friction angle
- α_r is the rake angle
- C_0 is the ratio of shear plane length AB and thickness of the primary shear zone $\left(\frac{l}{\Delta s_2}\right)$
- n_{eq} is the generalized strain hardening exponent

Shear strain and equivalent shear strain according to Von Mises criterion become:

$$\gamma_{AB} = \frac{1}{2}\frac{\cos(\alpha_r)}{\sin\phi\cos(\phi-\alpha_r)} \quad ; \qquad \varepsilon_{AB} = \frac{\gamma_{AB}}{\sqrt{3}} \tag{11),(12}$$

While shear strain-rate and equivalent shear strain-rate, according to Von Mises criterion:

$$\dot{\gamma}_{AB} = \frac{C_0\, V_s}{l} \; ; \qquad \dot{\varepsilon}_{AB} = \frac{\dot{\gamma_{AB}}}{\sqrt{3}} \tag{13),(14}$$

The normal stress at point *B*, location of the tool cutting edge:

$$\sigma_N' = k_{AB}\left(1 + \frac{\pi}{2} - 2\alpha_r - 2C_0 n_{eq}\right) \tag{15}$$

Analysis of the tool chip interface

The average temperature at the tool–chip interface can be computed has the sum of room temperature, the increasing of temperature in the shear zone (computed in the previous equations) and the maximum increasing of temperature reached in the tool-chip interface:

$$T_{int} = T_w + \Delta T_{SZ} + \psi \Delta T_M \tag{16}$$

where:

- the maximum temperature rise in the chip, ΔT_M, assuming a rectangular heat source at the interface, can be found with [42]:

$$\log_{10}\left(\frac{\Delta T_M}{\Delta T_C}\right) = 0.06 - 0.195\,\delta\sqrt{\frac{R_T t_2}{t_1}} + 0.5\,\log_{10}\left(\frac{R_T t_2}{h}\right) \tag{17}$$

  and average temperature rise in the chip is defined as:

$$\Delta T_C = \frac{F V_{chip}}{m_{chip}\, c_p} \tag{18}$$

- ψ is a coefficient considering that T_{int} is an average value, 0.9 in this work.

An assumed rectangular plastic zone of average thickness $\Delta s_1 = \delta t_2$ has been considered equivalent to the triangular plastic zone on tool-chip interface (Fig. 34). The Equivalent maximum strain-rate at tool–chip interface can be calculated, using Von Mises criterion, as:

$$\dot{\varepsilon}_{int} = \frac{\dot{\gamma_{int}}}{\sqrt{3}} = \frac{1}{\sqrt{3}} \frac{V_c}{\delta\, t_2} \tag{19}$$

Considering the moments of the normal stresses on shear plane around point *B*, the tool–chip interface length, related to JC flow stress model, can be compute as:

$$h = \frac{t_1 \sin\theta}{\cos\lambda\, \sin\phi}\left(1 + \frac{C_0\, n_{eq}}{3\left(1+2\left(\frac{\pi}{4}-\phi\right)-C_0\, n_{eq}\right)}\right) \tag{20}$$

Normal stress at point *B* considering uniform normal stress at the tool-chip interface:

$$\sigma_N = \frac{N}{h\, w} \tag{21}$$

The maximum shear strain at the tool–chip interface:

$$\gamma_{int} = 2\gamma_{AB} + 0.5\gamma_M \tag{22}$$

where, γ_M represents the total maximum shear strain occurring at the tool–chip interface, computed as:

$$\gamma_M = \frac{h}{\delta t_2} \tag{23}$$

Equivalent strain at the tool–chip interface, using Von Mises criterion:

$$\varepsilon_{int} = \frac{\gamma_{int}}{\sqrt{3}} \tag{24}$$

And finally, the flow stress at the tool–chip interface can be computed as:

$$k_{chip} = \frac{\sigma_{int}}{\sqrt{3}} = \frac{1}{\sqrt{3}}(A + B\, \varepsilon_{int}^{n})\left(1 + C \ln\frac{\dot{\varepsilon}_{int}}{\dot{\varepsilon}_0}\right)\left(1 - \left(\frac{T_{int}-T_W}{T_m-T_W}\right)^m\right) \tag{25}$$

Forces, angles and other parameters used in the model are shown in Fig 34,35.

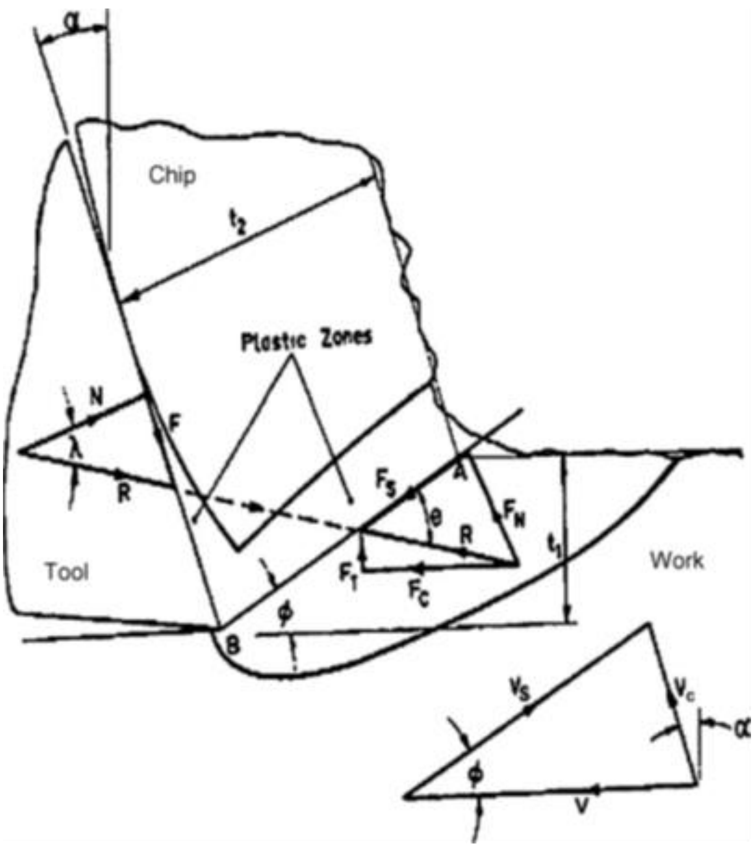

Figure 35: Chip formation model. [42]

The operative model is based on three nested iterative loops, suitable for running on a computer program, thanks to which three parameters can be fixed, the shear angle ϕ, the strain rate constant C_0 at the shear zone and the strain rate constant δ at the tool-chip interface, according to some mechanistic constrains. Precisely:

- the shear angle is selected when shear stress τ_{int} (calculated from resultant force in shear plane) equals the shear flow stress k_{chip} in the chip material on the interface;
- C_0 is selected when the normal stress at tool-chip interface, σ_n (calculated from resultant force in shear plane) equals σ_n', calculated using stress boundary condition at point coincident with tool bit; it represents the ratio of shear plane length AB and thickness of the primary shear zone $\left(\frac{l}{\Delta s_2}\right)$ (Fig. 34).
- δ is the ratio of the thickness of secondary shear zone to chip thickness $\left(\frac{\Delta s_1}{t_2}\right)$ (Fig. 34). It is selected for minimum cutting force criterion.

Indeed, the flow chart representing the algorithm developed in [42] has been reported.

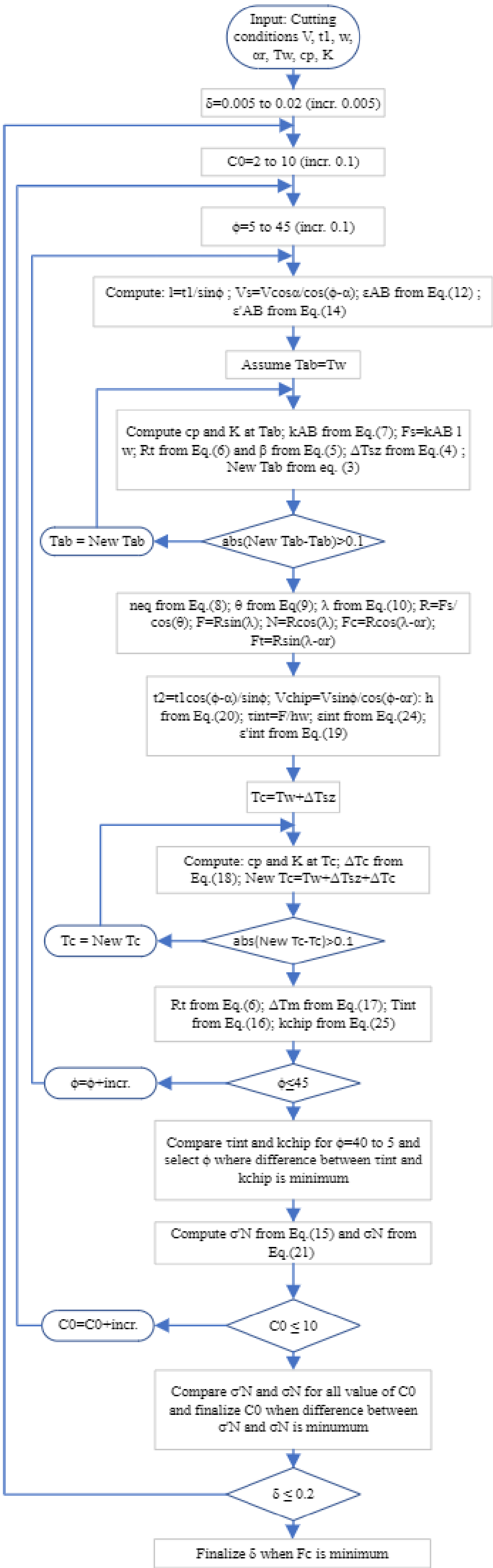

Figure 36: Flow chart for the Oxley's predictive theory applied to Johnson and Cook flow stress model. Adapted from [42]

2.2. Oblique cutting model

The drilling cutting process can be considered as an oblique cutting process, due to the particular direction of the cutting lip. It results not aligned with the radial direction of the tool and so it produces a cutting speed not orthogonal respect the cutting edge. Therefore, a model has been developed in this work modifying the orthogonal cutting model presented in the paragraph above, making it suitable for oblique cutting study. This mechanistic model is therefore able to compute all the forces, velocities and other dynamics parameters related to the drilling cutting action.

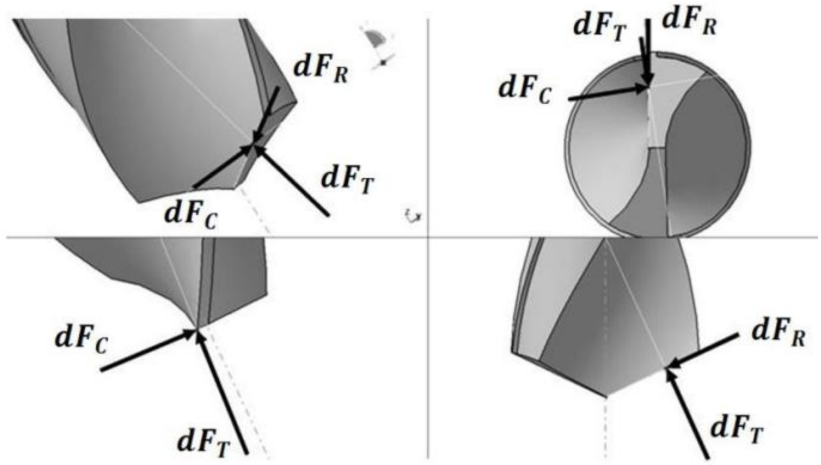

Figure 37: The projections of the elemental forces. [43]

The resulting forces in orthogonal cutting are two, cutting force and tangential force. Instead in oblique cutting we have a third force component, the radial force, due to the presence of the inclination angle *i* of the cutting edge (Fig. 38), not aligned with radial direction of tool.

Lin et.al [44] assessed that the cutting and tangential forces do not significantly depend on the inclination angle, performing some experimental measurement. For this reason, the cutting and tangential forces can be computed with the formulation of orthogonal cutting. Subsequently, the third component is computed as a function of these two forces and the inclination angle.

Minukhin's work [43] treats a complete review of the mathematical strategy to compute all the forces and angles dealing with oblique cutting and it supplies an improved strategy that has been used as basis in the present work to modify the orthogonal cutting model previously described.

In this work the cutting lip has been divided in 8 Elemental Cutting Tools (ECTS), number found as compromise between the needed of infinitesimal elemental cutting tools used in Minukhin's work and the finite width of ECT edge needed for the application of the model of the present work. The model has been applied to each ECT and then the results have been combined to find the total behaviour of cutting edge.

In the modified model, the oblique dynamic rake angle must be considered, replacing the normal rake angle of orthogonal cutting used in the model of Lawlani et al. Moreover, the inclination angle i, due to the cutting lip not being aligned with the radial direction of the drill bit, has to be computed. For the computation of oblique dynamic rake angle γ_d , inclination angle i (Fig.38), and reference angle ε (Fig.38), the formulations provided in the work of Minukhin have been used [43]:

$$\gamma_d = tan^{-1}\left(\frac{tan(\delta_r)}{sin(\kappa_t)}(cos(\omega) + sin(\omega) \cdot tan(\omega) \cdot cos^2(\kappa_t)) - tan\,\omega \cdot cos(\kappa_t)\right) \quad (26)$$

$$\text{with} \quad \delta_r = tan^{-1}\left(\frac{2r}{D} \cdot tan(\delta)\right) \quad (27)$$

$$i = sin^{-1}(\sin(\omega) \cdot sin\,(\kappa_t)) \quad (28)$$

$$\text{with} \quad \omega = sin^{-1}(\frac{t_p}{r}) \quad (29)$$

$$\varepsilon = \tan^{-1}(\tan(\omega) \cdot \cos(\kappa_t)) \quad (30)$$

This angle will be added to the input formulated by [42].

The formulas used to compute the uncut chip thickness related to oblique cutting, cutting force, transverse force, radial force are the following [43]

Uncut chip thickness t_1 has to consider the half taper angle κ_t and the reference angle ε, shown in Fig. 38:

$$t_1 = \frac{f\ \sin\kappa_t\ \cos\varepsilon}{2} \quad (31)$$

The radial force can be computed as combination of cutting and transversal forces as [43]:

$$F_r = \sqrt{F_c^2 + F_t^2}\sin\lambda\ \cos\gamma_d\ \tan i \quad (32)$$

The different forces must be composed to find the total elemental transversal, radial and cutting force of an infinitesimal element of the cutting edge according to the inclination angle i and the reference angle ε, (true view containing the cutting edge and the work velocity, Fig. 38):

$$\overline{dF_t} = dF_t \cos\varepsilon - dF_c \sin\varepsilon \tag{33}$$

$$\overline{dF_r} = dF_r \cos i - dF_c \sin i \tag{34}$$

$$\overline{dF_c} = dF_c \cos i + dF_r \sin i \tag{35}$$

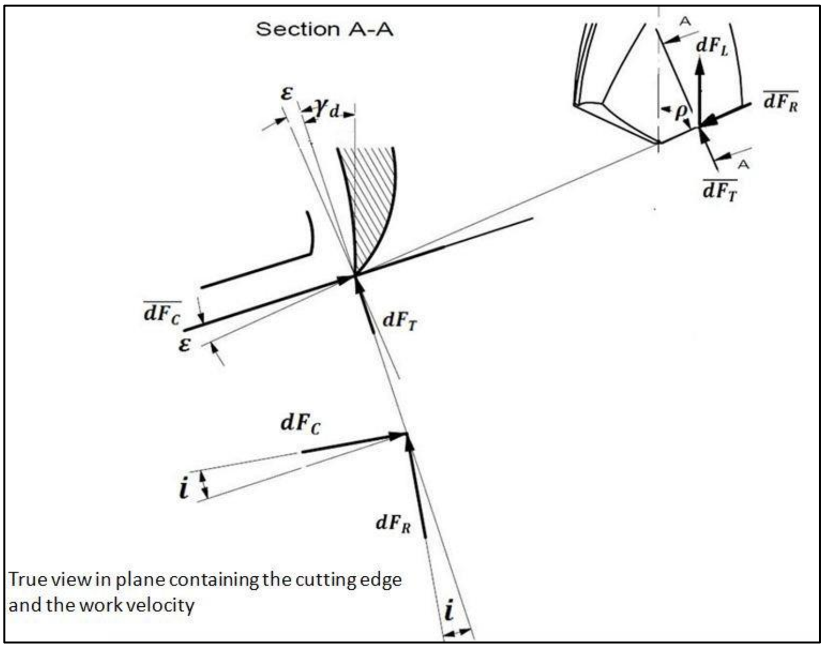

Figure 38: Representation of angles and forces on drilling oblique cutting [43].

Also, the friction force produced by the sliding of the chip on the rake face of the tool has been calculated, with the following formula [34]:

$$dF_f = \frac{dF_t \cdot cos\,\gamma_d \cdot cos\,i + dF_c \cdot sin\,\gamma_d}{cos^2\gamma_d \cdot \cos i \cdot cos\,\eta + sin\gamma_d\,(sin\,i \cdot sin\,\eta + sin\,\eta \cdot cos\,i\, \cdot cos\,\eta)} \tag{36}$$

In these formulations, it is assumed that chip flow angle η, can be considered equal to the inclination angle i, according to the Stabler's rule [38].

In the Minukhin's work the total forces acting on an edge element were integrated over the cutting lip length to find thrust forces and cutting torque formulations. The computation of the cutting torque has been performing summing the contribution of each ECT, multiplying the value of cutting force by the relative radial distance from drill axis. The value has been multiplied by 2 for considering the contribution of both the cutting lips.

The chisel only plays an important role in providing drill point strength to resist lateral bending moments due to vibration or unbalanced forces during drilling [41]. Therefore, the contribution of chisel in the computation of cutting torque has been neglected as suggested in [45]

$$M_{t,lip} = 2 \cdot \sum_{n=1}^{n^\circ ECTs} dF_{c,n} \cdot r_n \tag{37}$$

Finally, two contributions were considered to compute the thrust force, one related to the lips and one related to the action of chisel. The contribution related to the lips was computed with the following formula as a combination of tangential and radial forces computing their component in the vertical direction (by means of the half taper angle κ_t) [43]:

$$dF_{thrust}^{lip} = \sum_{n=1}^{n^\circ ECTs} (\overline{dF_{t,n}} \sin(\kappa_t) - \overline{dF_{r,n}} \cos(\kappa_t)) \tag{38}$$

The contribution related to the chisel's action was computed considering an indentation mechanism due to the approximately null cutting velocity and highly negative rake angle, since the chisel is the part closer to the axis of the drill [45]:

$$dF_{thrust,indent.}^{chisel} = A_{ch} \cdot H_b \tag{39}$$

$$\text{with} \quad A_{ch} = \frac{2\, t_p\, f}{\sin(\pi - \psi_c)\cos(\kappa_t)}; \qquad H_b = Brinell\ hardness\ of\ workpiece\ material \tag{40}$$

The flowchart of the oblique cutting model, with the modification conceived, is shown in the figure below.

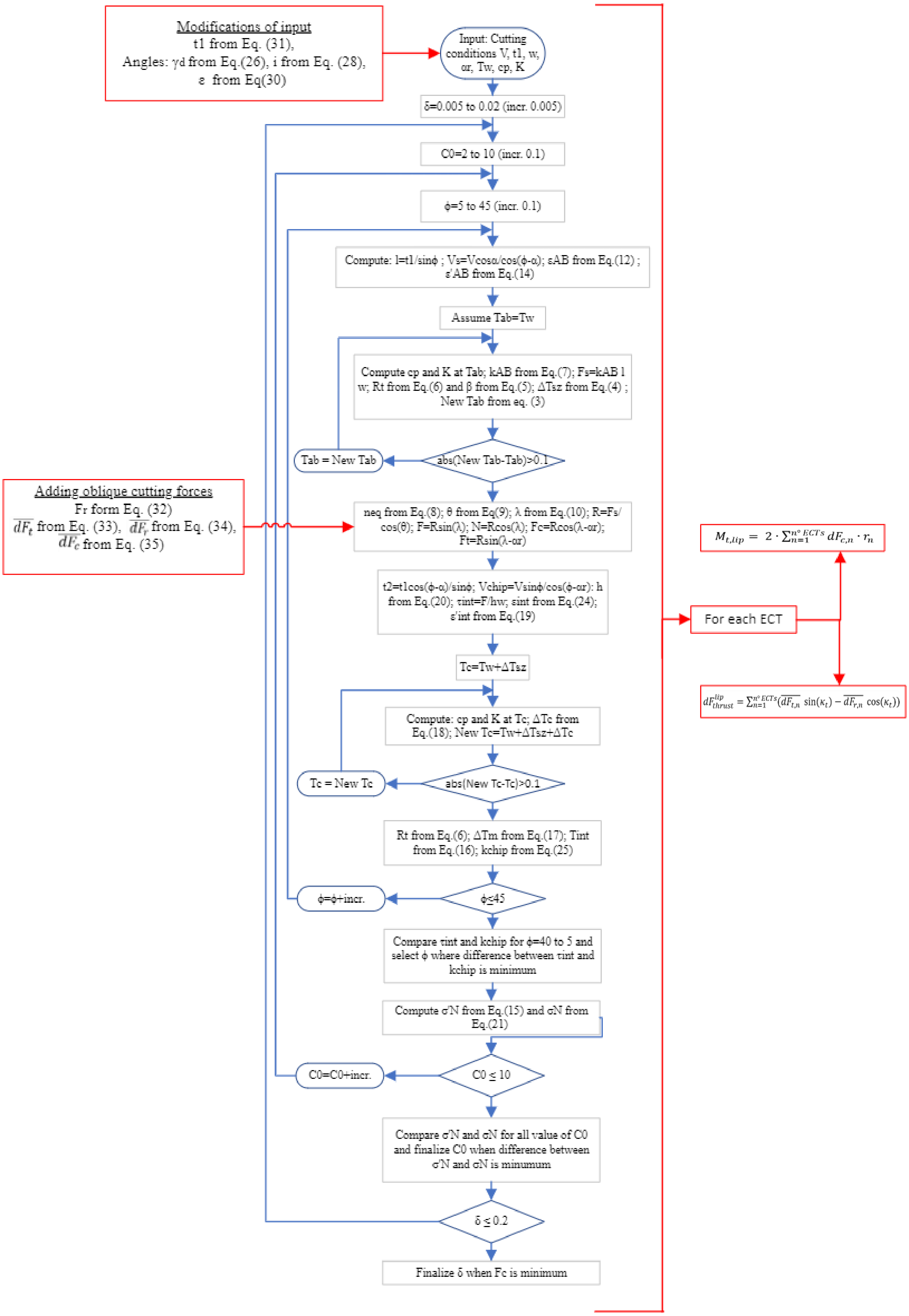

Figure 39: Modified flow chart for the Oblique cutting model.

3 Thermal models for peck drilling

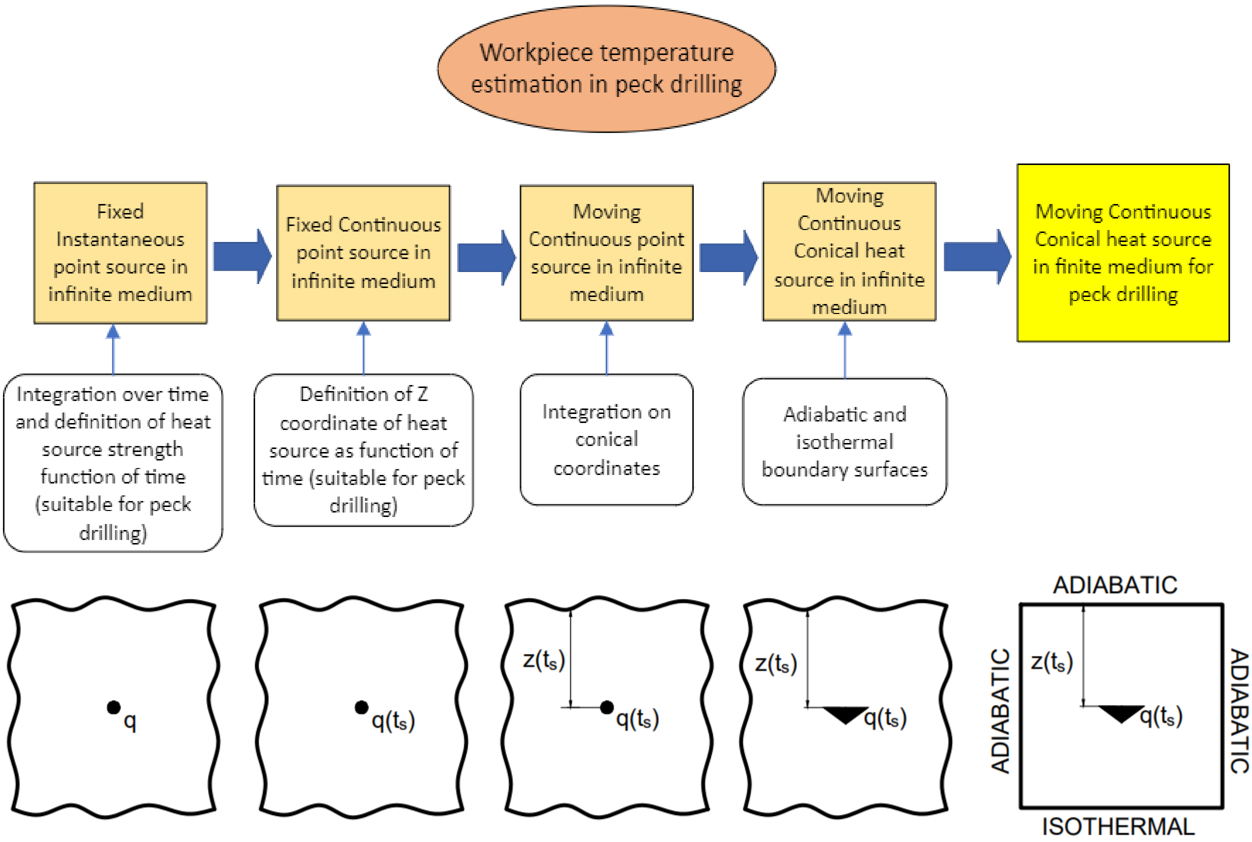

3.1. Conical moving heat source

In literature, most of the works dealing with the estimation of the temperature during drilling cutting, focused on the temperature of the tool in order to assess its wear behaviour. This is important to predict the remaining tool life of the tool and improving the quality of the workpiece surfaces. Moreover, some papers are present in literature dealing with the estimation of the temperature in the workpiece. Such temperature is influencing the material properties, when too high. Most of these works tried to estimate the temperature by means of the use of some FEM simulations, therefore requiring high computational cost and time and requiring a specific model for any specific problem to be examined. Furthermore, no research works in the estimation of temperature during peck drilling process were found, but just some paper tries to analyse the temperature as a help in understanding the complex surface roughness trends involved in different steps of peck drilling operations [46].

In this paper an analytical model for workpiece temperature estimation in peck drilling was developed in order to simplify this evaluation providing a closed formula to assess this important factor. The formulation developed by Shi et al. [47] has been revisited and adapted to the case studied. The work started considering the model developed in [48] dealing with a point source releasing heat instantaneously in an infinite medium as the solution of the conduction differential equation.

$$\frac{\partial T}{\partial t} = \alpha \left(\frac{\partial^2 T}{\partial^2 x} + \frac{\partial^2 T}{\partial^2 y} + \frac{\partial^2 T}{\partial^2 z} \right)$$

The temperature field at a point (x, y, z) at a specific time t due to an instantaneous point heat source located in (x_s, y_s, z_s) releasing heat at time $t = 0$ can be expressed as:

$$T(x, y, z, t) = \frac{Q}{(4\,\pi\,\alpha\,t)^{3/2}}\, e^{-\frac{[(x-x_S)^2+(y-y_S)^2+(z-z_S)^2]}{4\,\alpha\,t}} \quad (41)$$

where:

- α = diffusivity of workpiece material $\left[\frac{m^2}{s}\right]$
- t = time [s]
- Q = heat, considered as $\frac{E_{th}}{\rho c_p}$ $[Km^3]$ $(E_{th}\ thermal\ energy\ [J\,])$

In drilling operation, the heat source is continuously released in the material during the penetration of the drill bit inside the material. Therefore, the previous solution was modified to consider the continuous releasing of heat in the material. This is performed by integrating Eq. 41 with respect to time. To allow the integration, heat was considered as a function of time. Since this work aimed to describe the peck drilling process, the heat source strength $q(t_s)$ is defined by a piecewise function. This allows to represent the zone where the drill bit is cutting and when is retracted for chip evacuation and temperature mitigation. At this point, the solution refers to a point heat source located in (x_s, y_s, z_s) releasing heat at time t_s, from 0 to time t, and can be expressed as:

$$T(x, y, z, t) = \int_0^t \frac{q(t_S)}{\rho\,c_p\,[4\,\pi\,\alpha\,(t-t_S)]^{3/2}}\, e^{-\frac{[(x-x_S)^2+(y-y_S)^2+(z-z_S)^2]}{4\,\alpha\,(t-t_S)}}\, dt_s \quad (42)$$

where:

- ρ = density of workpiece material $[\frac{kg}{m^3}]$
- c_p = specific heat of workpiece material $[\frac{J}{kg\ K}]$
- $q(t_s)$ = heat power [W]

Eq. 42 represents the temperature field in the workpiece for a continuous but fixed point source. In order to represent a drilling operation, the model must consider also that the heat source is moving into the medium. A moving coordinate system has been set and centred in the axis of the drill bit and the Z-coordinate of the drill bit has been defined as a function of t_s:

$$z_s = f(t_s) \tag{43}$$

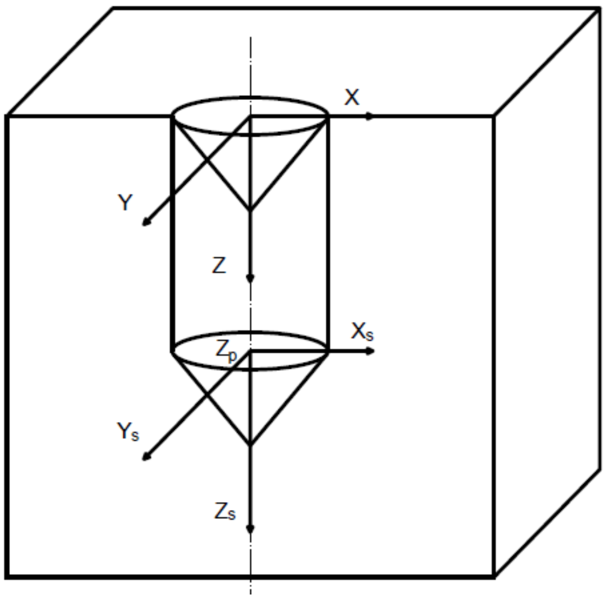

Figure 40: Fixed and moving coordinate system of conical heat source. Adapted from [47]

So, the solution of the temperature field at a point (x, y, z) at a specific time t due to a moving instantaneous point heat source located in $(x_s, y_s, z_s(t_s))$ releasing heat at time t_s can be expressed as:

$$T(x, y, z, t) = \int_0^t \frac{q(t_s)}{\rho\, c_p\ [4\,\pi\,\alpha\,(t-t_s)]^{3/2}}\, e^{-\frac{[(x-x_s)^2+(y-y_s)^2+(z-f(t_s))^2]}{4\,\alpha\,(t-t_s)}}\, dt_s \tag{44}$$

Moreover, the heat in drilling operation can be considered released through the conical surface generated by the drill bit during a complete revolution, as can be seen in the Fig. 41.

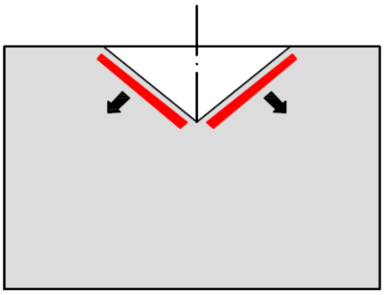

Figure 41: Conical heat sources in drilling process.

Therefore, the conical domain above which the heat is considered released was introduced in the analytical solution. Since the solution in Eq. 44 considers the heat source as a point, the conical area can be thought as the sum of infinitesimal point sources. Thus, each point source releases at an infinitesimal surface dA:

$$dA = \frac{dz_i}{\cos(\kappa_t)} \cdot R \cdot d\beta \tag{45}$$

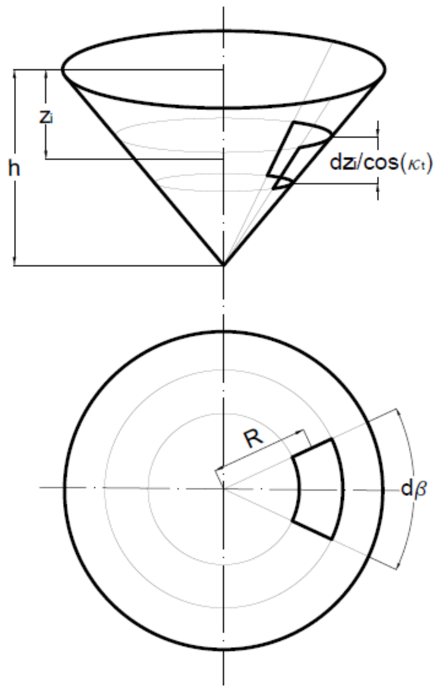

Figure 42: Heat source infinitesimal area. Adapted from [47]

The Z-coordinate of the heat source can be expressed as a general piecewise function of (t_s), allowing to apply this model for both continuous and peck drilling:

$$z_s = f(t_s) = z_p(t_s) + z_i \tag{46}$$

The final solution was defined by integrating the previous solution along the angle β and the length z_i considering the formulation of z-coordinate of heat source (Eq. 46) and the infinitesimal area expression (Eq. 45). At this point the solution refers to the temperature field at a specific time t due to a moving conical heat source with origin in $(x_s, y_s, z_p(t_s) + z_i)$, releasing heat from time 0 to time $t_s = t$ and can be expressed as:

$$T(x_t, y_t, z_t, t) = \int_0^t \int_0^h \int_0^{2\pi} \frac{q(t_s)\, R}{\cos(\kappa_t)\, \rho\, c_p\, S\, (4\,\pi\,\alpha\,(t-t_s))^{3/2}}\, e^{-\frac{((x-x_s)^2+(y-y_s)^2+(z-z_p(t_s)-zi)^2)}{(4\,\alpha\,(t-t_s))}}\, d\beta\, dz_i\, dt_s \tag{47}$$

where:

- $q(t_s)$ Heat power [W]
- $R = (h - z_i) \tan(\kappa_t)$ Radial coordinate of infinitesimal area (48)
- $x_s = R \cos(\beta)$ X coordinate of infinitesimal area (49)
- $y_s = R\, \mathrm{sen}(\beta)$ Y coordinate of infinitesimal area (50)
- $S = \pi\, r_c$ a Lateral area of cone (r_c = *cone radius*, *a* = *apothem*) (51)

3.2. Semi-infinite medium

The analytical solution of Eq. 47 deals with the temperature field of a point in the workpiece considering it as an infinite medium. In the case studied in this work the drilled holes performed are in the neighbouring of the lateral surface of the workpiece, due to the presence of the hole where the thermocouple has been inserted. Moreover, the surface where the holes start to be performed, in not considered in this solution. So, the hypothesis of infinite medium cannot be applied to the studied case.

In order to consider the medium as semi-infinite, it is necessary to introduce mirror heat sources. Mirroring is performed with respect to the boundary surface to be introduced in the model. In Fig. 43, an illustration of the application of adiabatic and isothermal boundary conditions on different faces is shown, as well as the heat source combinations required to achieve these conditions.

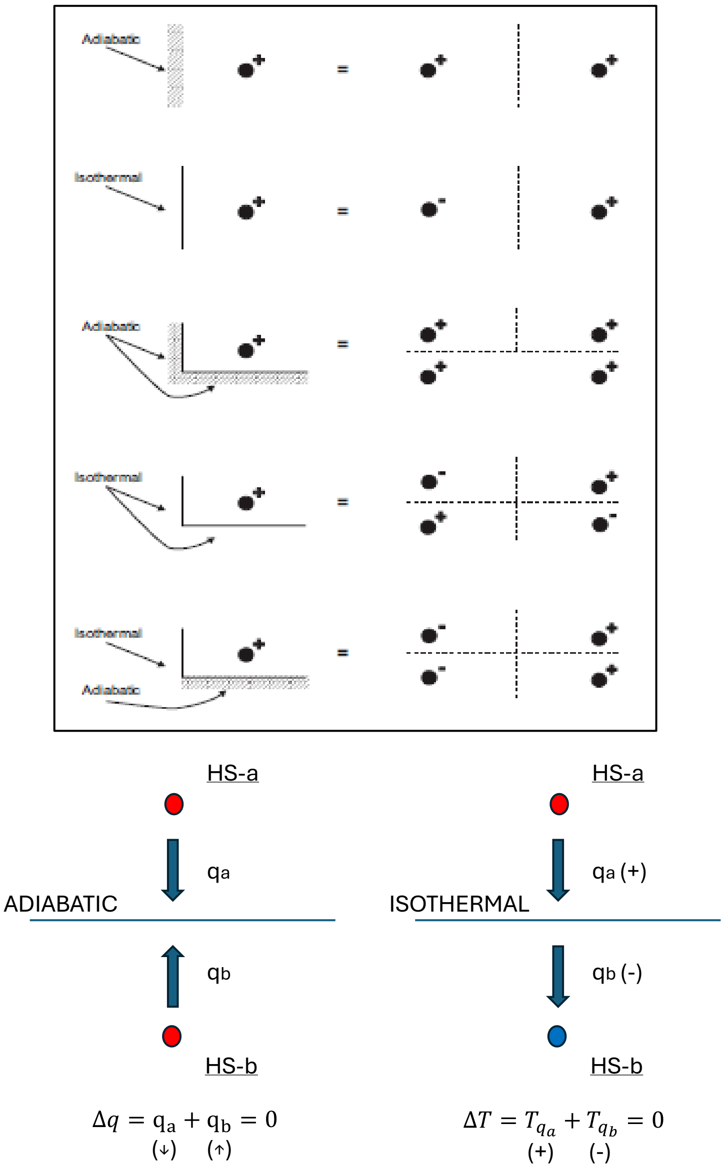

Figure 43: Adiabatic and isothermal boundary conditions and relative heat source to consider [49].

In the case of the workpiece used in this work we can considered the workpiece upper surface as adiabatic as well as the two lateral surfaces, whereas the bottom surface can be considered isothermal because it is in contact with the dynamometric table and consequently with the pallet, that can be considered having an infinite thermal inertia, leading to a constant temperature on this surface. In the Fig. 44, a representation of the full set of heat sources considered in this work is presented. The triangles represent the conical heat source considered. HS-1 is the real heat source, instead the others are all the heat sources to be considered to implement surface boundary conditions. The red ones are positive heat source, whereas the blue ones must be considered negative (heat sinks).

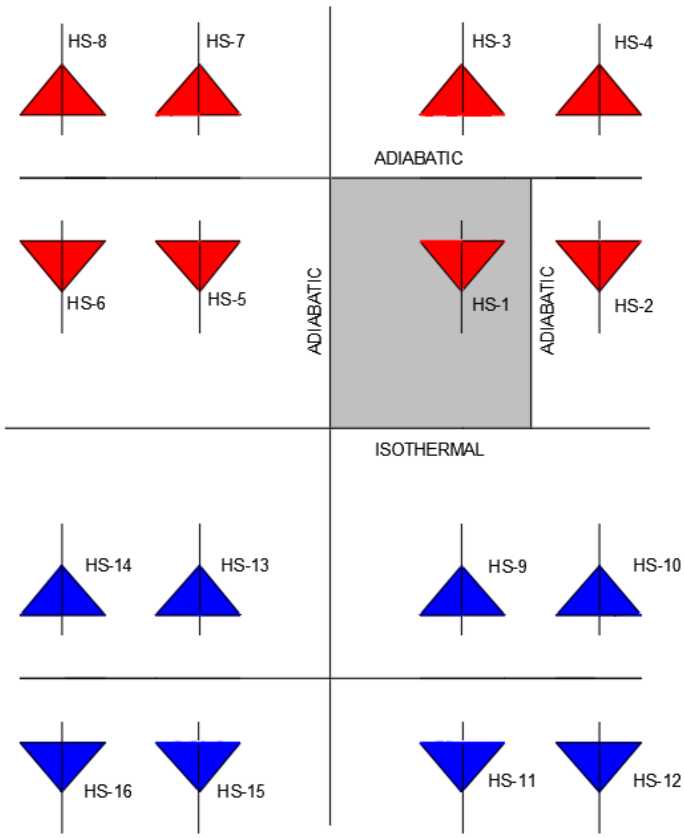

Figure 44: Schematic representation of the heat source considered to implement the adiabatic and isothermal boundary surfaces. The grey part is the section of the workpiece. The blue sources are negative sources (heat sinks), the red ones are positive sources.

As can be visible in the scheme of Fig. 43, when the symmetry plane considered is related to an isothermal boundary surface, the imaginary heat source must be considered negative (heat sink), because the net flux moves from the heat source to the heat sink. In this way, the two sources changed the temperature of the point analysed but since the two contributions are equal in magnitude but of opposite sign, the net temperature increasing on the boundary surfaces is equal to zero. Whereas, when an adiabatic boundary surface is considered, the two fluxes across the plane, generated by the equal heat sources, provoke the effect of having net flux equal to zero, because they are in opposite direction. Therefore, in the case analysed in the present work, the temperature field is due to the sum of the solution for each heat source of Fig. 44, where the different equations for each heat source can be defined as:

HS-1

$$T(x_t, y_t, z_t, t) = \int_0^t \int_0^h \int_0^{2\pi} \frac{q(t_s)\, R}{\cos(\kappa_t)\, \rho\, c_p\, S(4\,\pi\,\alpha\,(t-t_s))^{3/2}}\, e^{-\frac{((x-x_s)^2+(y-y_s)^2+(z-z_p(t_s)-zi)^2)}{(4\,\alpha\,(t-t_s))}} d\beta\, dz_i\, dt_s \tag{52}$$

HS-2

$$T(x_t, y_t, z_t, t) = \int_0^t \int_0^h \int_0^{2\pi} \frac{q(t_s)\, R}{\cos(\kappa_t)\, \rho\, c_p\, S(4\,\pi\,\alpha\,(t-t_s))^{3/2}}\, e^{-\frac{(((-x+2x_0)-x_s)^2+(y-y_s)^2+\left(z-z_p(t_s)-zi\right)^2)}{(4\,\alpha\,(t-t_s))}} d\beta\, dz_i\, dt_s \tag{53}$$

HS-3

$$T(x_t, y_t, z_t, t) = \int_0^t \int_0^h \int_0^{2\pi} \frac{q(t_s)\, R}{\cos(\kappa_t)\, \rho\, c_p\, S(4\,\pi\,\alpha\,(t-t_s))^{3/2}}\, e^{-\frac{((x-x_s)^2+(y-y_s)^2+\left((-z+2z_0)-z_p(t_s)-zi\right)^2)}{(4\,\alpha\,(t-t_s))}} d\beta\, dz_i\, dt_s \tag{54}$$

HS-4

$$T(x_t, y_t, z_t, t) = \int_0^t \int_0^h \int_0^{2\pi} \frac{q(t_s)\, R}{\cos(\kappa_t)\, \rho\, c_p\, S(4\,\pi\,\alpha\,(t-t_s))^{3/2}}\, e^{-\frac{(((-x+2x_0)-x_s)^2+(y_t-y_s)^2+\left((-z+2z_0)-z_p(t_s)-zi\right)^2)}{(4\,\alpha\,(t-t_s))}} d\beta\, dz_i\, dt_s \tag{55}$$

HS-5

$$T(x_t, y_t, z_t, t) = \int_0^t \int_0^h \int_0^{2\pi} \frac{q(t_s)\, R}{\cos(\kappa_t)\, \rho\, c_p\, S(4\,\pi\,\alpha\,(t-t_s))^{3/2}}\, e^{-\frac{(((-x+2x_1)-x_s)^2+(y-y_s)^2+\left(z-z_p(t_s)-zi\right)^2)}{(4\,\alpha\,(t-t_s))}} d\beta\, dz_i\, dt_s \tag{56}$$

HS-6

$$T(x_t, y_t, z_t, t) = \int_0^t \int_0^h \int_0^{2\pi} \frac{q(t_s)\, R}{\cos(\kappa_t)\, \rho\, c_p\, S(4\,\pi\,\alpha\,(t-t_s))^{3/2}}\, e^{-\frac{(((x-2(x_1-x_0))-x_s)^2+(y-y_s)^2+\left(z-z_p(t_s)-zi\right)^2)}{(4\,\alpha\,(t-t_s))}} d\beta\, dz_i\, dt_s \tag{57}$$

HS-7

$$T(x_t, y_t, z_t, t) = \int_0^t \int_0^h \int_0^{2\pi} \frac{q(t_s)\, R}{\cos(\kappa_t)\, \rho\, c_p\, S(4\,\pi\,\alpha\,(t-t_s))^{3/2}}\, e^{-\frac{(((-x+2x_1)-x_s)^2+(y_t-y_s)^2+\left((-z+2z_0)-z_p(t_s)-zi\right)^2)}{(4\,\alpha\,(t-t_s))}} d\beta\, dz_i\, dt_s \tag{58}$$

HS-8

$$T(x_t, y_t, z_t, t) = \int_0^t \int_0^h \int_0^{2\pi} \frac{q(t_s)\, R}{\cos(\kappa_t)\, \rho\, c_p\, S(4\,\pi\,\alpha\,(t-t_s))^{3/2}}\, e^{-\frac{(((x-2(x_1-x_0)-x_s)^2+(y_t-y_s)^2+\left((-z+2z_0)-z_p(t_s)-zi\right)^2)}{(4\,\alpha\,(t-t_s))}} d\beta\, dz_i\, dt_s \tag{59}$$

HS-9

$$T(x_t, y_t, z_t, t) = \int_0^t \int_0^h \int_0^{2\pi} \frac{-q(t_s)\, R}{\cos(\kappa_t)\, \rho\, c_p\, S(4\, \pi\, \alpha\, (t - t_s))^{3/2}} e^{-\frac{(((x-2(x_1-x_0)-x_s)^2+(y_t-y_s)^2+\left((-z+2z_1)-z_p(t_s)-zi\right)^2)}{(4\, \alpha\, (t-t_s))}} d\beta\, dz_i\, dt_s \tag{60}$$

HS-10

$$T(x_t, y_t, z_t, t) = \int_0^t \int_0^h \int_0^{2\pi} \frac{-q(t_s)\, R}{\cos(\kappa_t)\, \rho\, c_p\, S(4\, \pi\, \alpha\, (t - t_s))^{3/2}} e^{-\frac{(((-x+2x_0)-x_s)^2+(y_t-y_s)^2+\left((-z+2z_1)-z_p(t_s)-zi\right)^2)}{(4\, \alpha\, (t-t_s))}} d\beta\, dz_i\, dt_s \tag{61}$$

HS-11

$$T(x_t, y_t, z_t, t) = \int_0^t \int_0^h \int_0^{2\pi} \frac{-q(t_s)\, R}{\cos(\kappa_t)\, \rho\, c_p\, S(4\, \pi\, \alpha\, (t - t_s))^{3/2}} e^{-\frac{(((x-x_s)^2+(y_t-y_s)^2+\left((z-2(z_1-z_0))-z_p(t_s)-zi\right)^2)}{(4\, \alpha\, (t-t_s))}} d\beta\, dz_i\, dt_s \tag{62}$$

HS-12

$$T(x_t, y_t, z_t, t) = \int_0^t \int_0^h \int_0^{2\pi} \frac{-q(t_s)\, R}{\cos(\kappa_t)\, \rho\, c_p\, S(4\, \pi\, \alpha\, (t - t_s))^{3/2}} e^{-\frac{(((-x+2x_0)-x_s)^2+(y_t-y_s)^2+\left((z-2(z_1-z_0))-z_p(t_s)-zi\right)^2)}{(4\, \alpha\, (t-t_s))}} d\beta\, dz_i\, dt_s \tag{63}$$

HS-13

$$T(x_t, y_t, z_t, t) = \int_0^t \int_0^h \int_0^{2\pi} \frac{-q(t_s)\, R}{\cos(\kappa_t)\, \rho\, c_p\, S(4\, \pi\, \alpha\, (t - t_s))^{3/2}} e^{-\frac{(((-x+2x_1)-x_s)^2+(y_t-y_s)^2+\left((-z+2z_1)-z_p(t_s)-zi\right)^2)}{(4\, \alpha\, (t-t_s))}} d\beta\, dz_i\, dt_s \tag{64}$$

HS-14

$$T(x_t, y_t, z_t, t) = \int_0^t \int_0^h \int_0^{2\pi} \frac{-q(t_s)\, R}{\cos(\kappa_t)\, \rho\, c_p\, S(4\, \pi\, \alpha\, (t - t_s))^{3/2}} e^{-\frac{(((x-2(x_1-x_0))-x_s)^2+(y_t-y_s)^2+\left((-z+2z_1)-z_p(t_s)-zi\right)^2)}{(4\, \alpha\, (t-t_s))}} d\beta\, dz_i\, dt_s \tag{65}$$

HS-15

$$T(x_t, y_t, z_t, t) = \int_0^t \int_0^h \int_0^{2\pi} \frac{-q(t_s)\, R}{\cos(\kappa_t)\, \rho\, c_p\, S\left(4\, \pi\, \alpha\, (t - t_s)\right)^{\frac{3}{2}}} e^{-\frac{\left(\left((-x+2x_1)-x_s\right)^2+(y_t-y_s)^2+\left(\left(z-2(z_1-z_0)\right)-z_p(t_s)-zi\right)^2\right)}{(4\, \alpha\, (t-t_s))}} d\beta\, dz_i\, dt_s$$

(66)

HS-16

$$T(x_t, y_t, z_t, t) = \int_0^t \int_0^h \int_0^{2\pi} \frac{-q(t_s)\, R}{\cos(\kappa_t)\, \rho\, c_p\, S(4\, \pi\, \alpha\, (t - t_s))^{3/2}}\, e^{-\frac{(((x-2(x_1-x_0))-x_s)^2+(y_t-y_s)^2+\left((z-2(z_1-z_0))-z_p(t_s)-zi\right)^2)}{(4\,\alpha\,(t-t_s))}}\, d\beta\, dz_i\, dt_s$$

(67)

The coordinate $x_0, x_1, z_{0,}, z_1$ refers to the distance of the boundary surface imposed to the problem and the fixed coordinate system, as can be seen in the picture below.

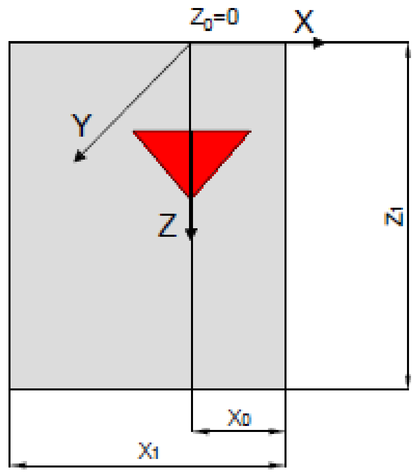

Figure 45: Representation of the coordinate $x_0, x_1, z_{0,}, z_1$ related to the distances of the boundary surface to the reference system.

4 Experimental Campaign

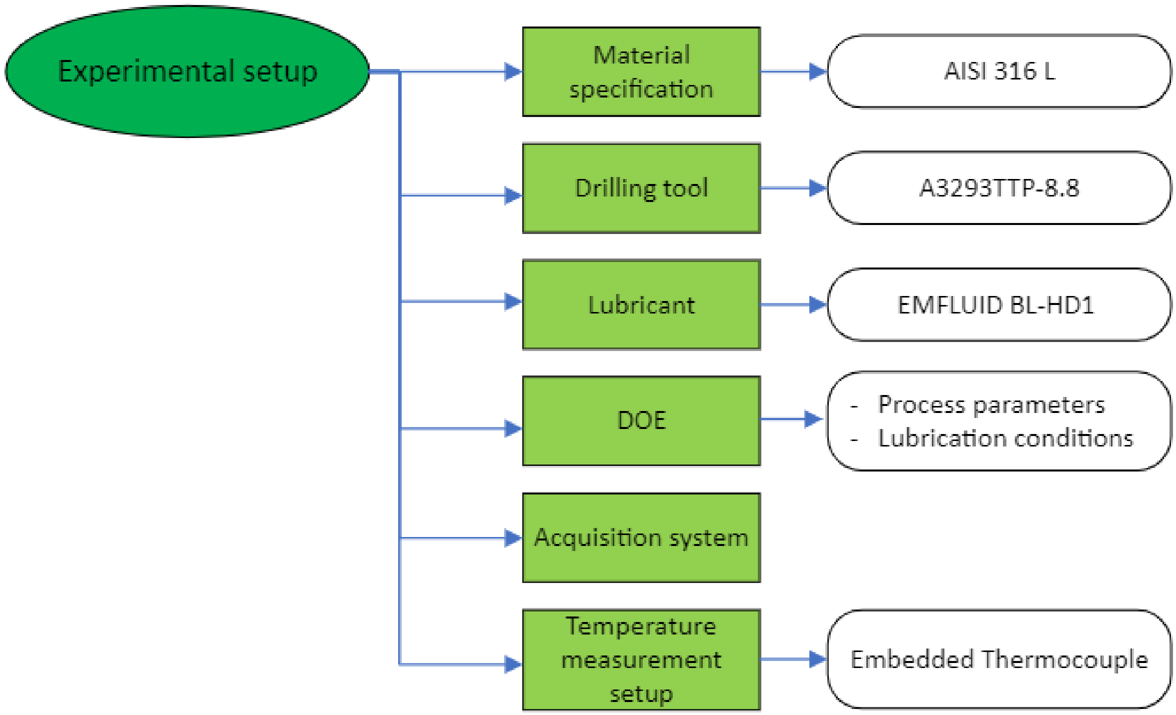

4.1. Experimental setup

To validate the process and, thus, to compare the results obtained in the model previously reported, an experimental campaign was led with drilling processes on an austenitic stainless steel (AISI 316L) plate of dimensions 210mmX38mmX28mm, whose material properties are listed in Table 3. The machine used for the drilling tests is a Mandelli M5 machine tool, a CNC horizontal milling machine (max speed 7000rpm).

Workpiece material AISI 316L		
Chemical Composition, %	Carbon, C	<= 0.030 %
	Chromium, Cr	16-18%
	Iron, Fe	61.9-72%
	Manganese, Mn	<=2.0%
	Molybdenum, Mo	2.0-3.0%
	Nickel, Ni	10-14%
	Phosphorus, P	<=0.045%
	Silicon, Si	<=1.0%
	Sulphur, S	<=0.030%
Density (ρ)		8 [g/cm3]
Specific Heat Capacity (c)		0.5 [$J/g°C$]
Thermal diffusivity (α_w)		3.98x10-6 [$m2/s$]
Hardness, Brinel (HB)		165
Tensile Strength, Yield		290 MPa

Table 3: AISI 316L specifications.

The holes were machined with the peck drilling process, in order not to overheat the drill tool and enabling the chip evacuation, with 4 steps of 3 mm each, for a total length of the hole of 12 mm. 18 holes were machined on a surface of the workpiece. The workpiece was machine on both the sides, by releasing the clamps and turning it upside down. The setup of the position of the series of holes is shown in Fig. 46.

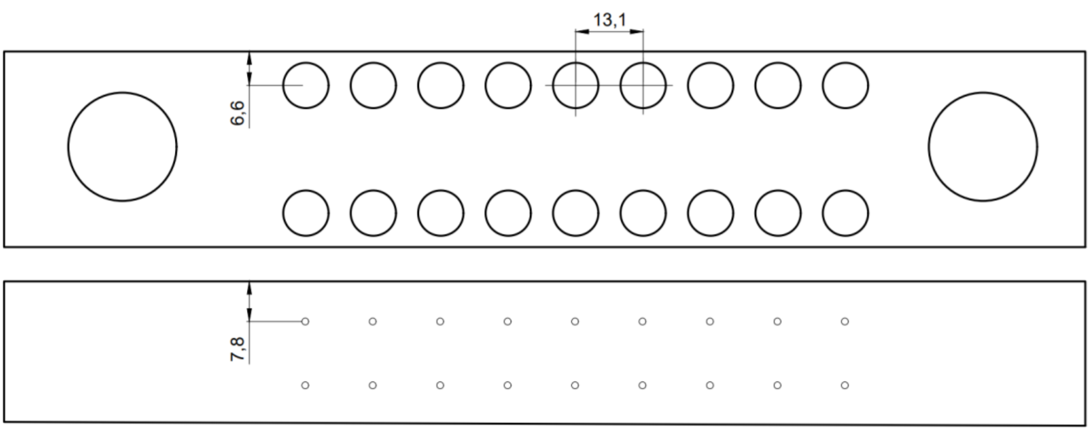

Figure 46: Setup of series of holes for experimental campaign. The two lateral holes were present to enable the fixing of the workpiece on the machine tool.

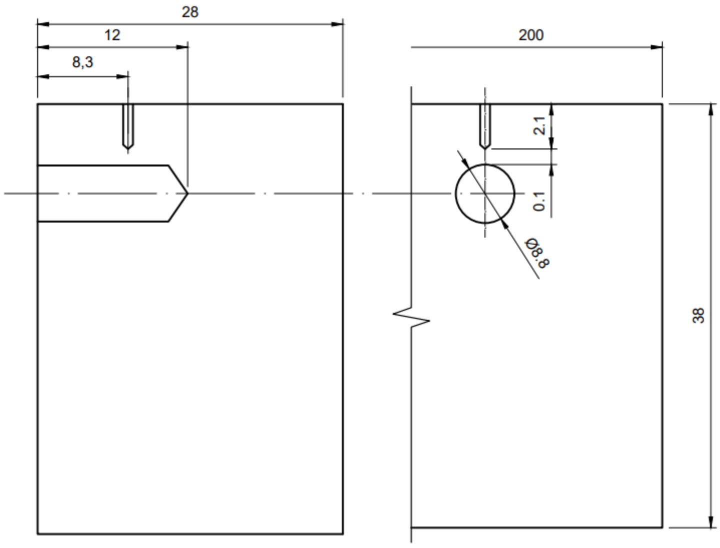

Figure 47: Thermocouple setup.

A particular tool holder offered by Gühring was employed to reduce the impact of tool run-out and the condensation of the oil mist. The HSK-A80 tool-holder employed in the experimental campaign was specifically made for single-channel MQL applications, allowing for the hydraulic system to clamp the tool while minimizing the tool run-out impact. Solid carbide drills with coolant-through provided by Walter were used for the experimental tests (Drill code: A3293TTP-8.8).

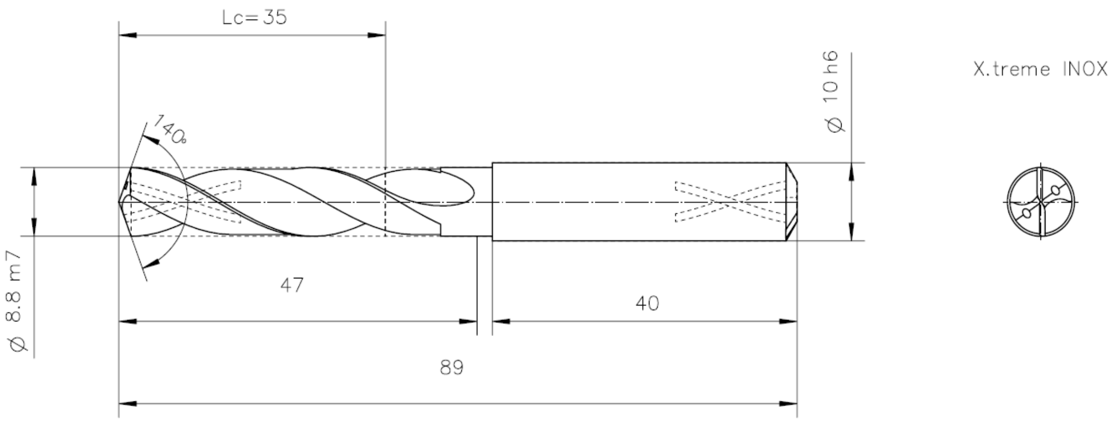

Figure 48: Twist drill.

Parameter	Symbol	Value
Cutting edge diameter	D	8.8 [mm]
Cutting edge length	Lc	35 [mm]
Overall length	l1	89 [mm]
Projection length	l2	47 [mm]
Shank diameter (h6)	d1	10 [mm]
Taper angle	2kr	140 °

Table 4: Twist drill parameters.

The rake angle can be calculated with the formula of Eq. 26 for general twist drilling tool. The drilling tool was analysed with a digital microscope Keyence VHX7000 to determine its correct shape. The drill bit presented a milled surface near to the chisel, leading to different values of the rake angle, with respect to literature formulations.

Since determining this angle is complex, the analysis performed with the digital microscope and the values coming from the Eq. 26 were combined to consider a more reliable rake angle profile along the radial coordinate.

The trend of the value of the rake angle along the lip of the drilling tool is shown in Fig.49.

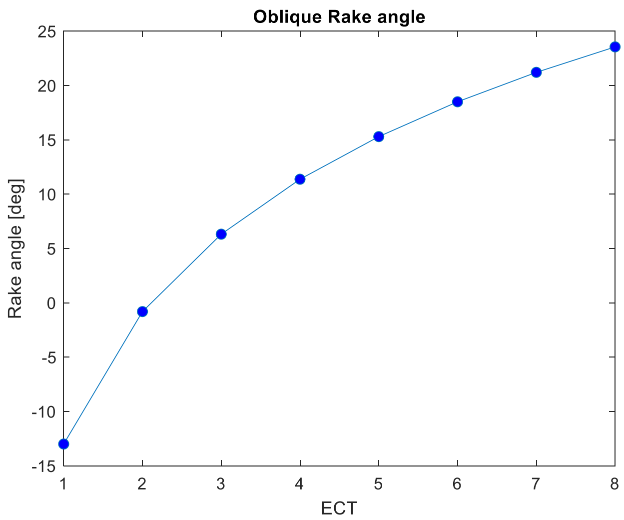

Figure 49: Rake angle of the drill lip used in oblique cutting model

Whereas inclination and reference angles have been computed with the formula in Eq.28,30.

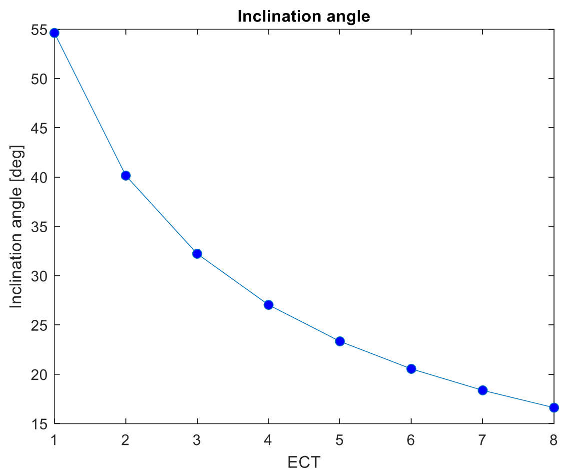

Figure 50: Inclination angle

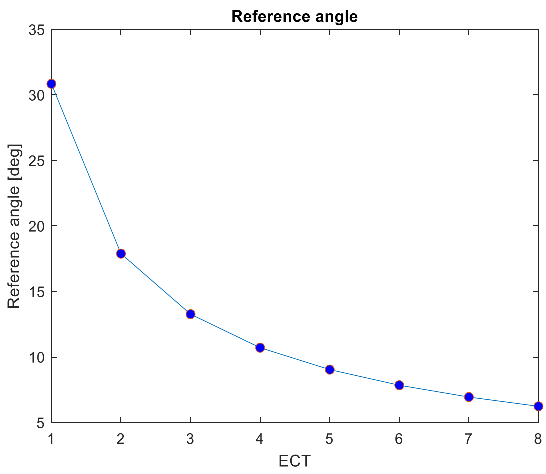

Figure 51: Reference angle

In the application of the model of oblique cutting (see section 2.1.2), the lip has been divided into 8 ECTs, so the dots present in the curves of Fig. 49, 50, 51, represent the different value of the angles for each ECT considered in the algorithm implementation.

Experiments were conducted at different MQL conditions and different process parameters (cutting speed and cutting feed-rate). The MQL is supplied internally through the spindle and provided by MWM Schmieranlagen Srl, LS35 with a single channel system.

The lubricant used for the tests was the EMFLUID BL-HD1 oil, which is a mixture of synthetic esters with strong EP additivities, containing sulphur, but free from chlorine. The physical properties of lubricant are reported in the Table 5.

Lubricant EMFLUID BL-HD1	
Viscosity at 40°C	40 mm2/s
Density at 20°C	1 g/cm3
Flash Point	200°C

Table 5: Lubricant specifications.

The acquisition system, see Sec. 3.2, reported the Spindle power, Torque, Feed force and Temperature for each test conducted.

4.2. Acquisition system

Machine tool parameters such as electrical spindle power, cutting thrust forces, air and oil flow rates required for the calculation purpose in this study were measured using the NI cDAQ9174 installed on the machine tool. The parameters are acquired at a sampling frequency of 19560 Hz and the samples were saved at a frequency of 20 Hz to minimize the aliasing effect in electrical power measurements.

Four NI modules were in a NI cDAQ9174 acquisition system for the measurements, Fig. 52.

• MOD1 (NI 9219): Relative Air flow and Oil flow measurement.

• MOD2 (NI 9215): Fx, Fy and Fz (NB: the cutting forces are acquired on the piece in the table reference system)

• MOD3 (NI 9205): General power and spindle power

• MOD4 (NI 9214): Thermocouple

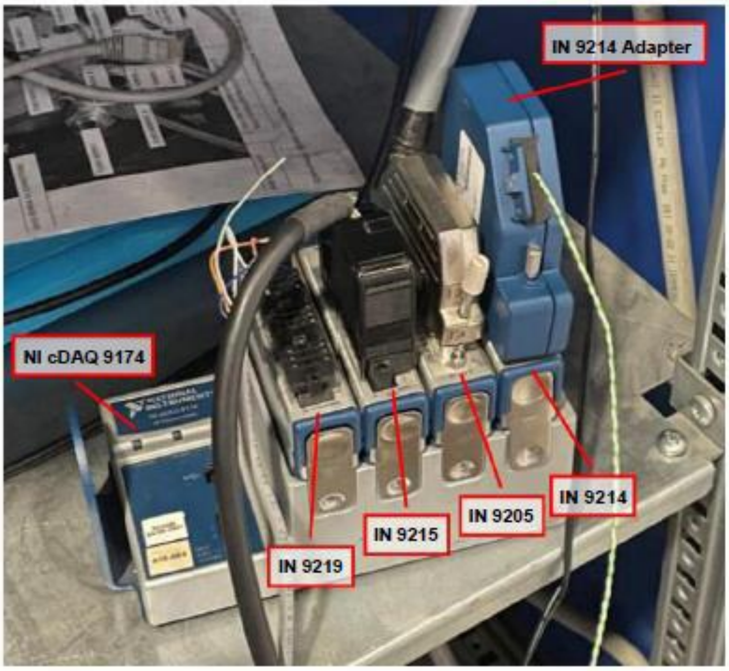

Figure 52: Acquisition board

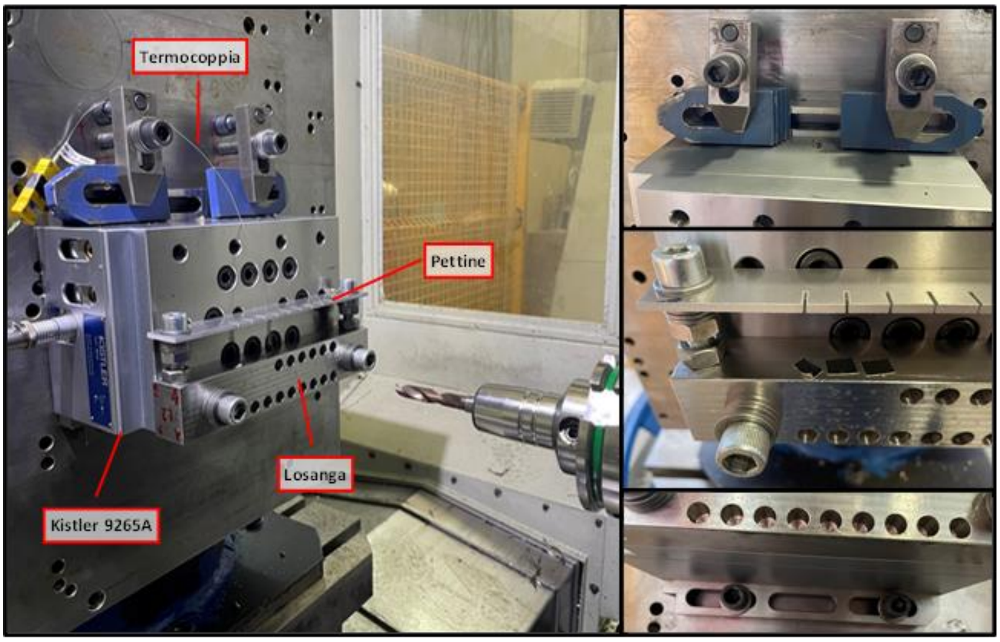

Figure 53: Setup of experiment components and dynamometric table.

The machining setup entails the use of the Kistler 9265A dynamometric plate, on which the workpiece with the comb was fixed to support the thermocouple on the faces with the micro-holes (2.1 mm deep) where the thermocouples are placed (see Sec. 4.1).

Another acquisition system, directly connected to the CN of machine tool, was used. The information related to position and velocity of each linear axis and the spindle were acquired. This acquisition system, SINUCOM (Siemens), acquired the signal with a frequency of 250 Hz. The signal related to the position of the axis has been used to the description of the movement of the drill bit inside the material (peck drilling).

4.3. Temperature Measurement

The measurement of temperature was carried out by means of a workpiece embedded thermocouple with isolated junction, covered with an Inconel made sheath and insulation with magnesium oxides. The thermocouple was placed in a pre-drilled micro hole with a depth of 2.1 mm as shown in the Fig. 47.

The distance between the end of the micro hole and the drilling test hole was maintained at h = 0.1mm. The thermocouple was away from the upper surface of the workpiece of 8.3 mm.

The holes were performed with 4 passes, to not overheat the drill bit and workpiece, as can be seen in the example of a temperature measurement shown below, where different peaks are present due to this cutting strategy.

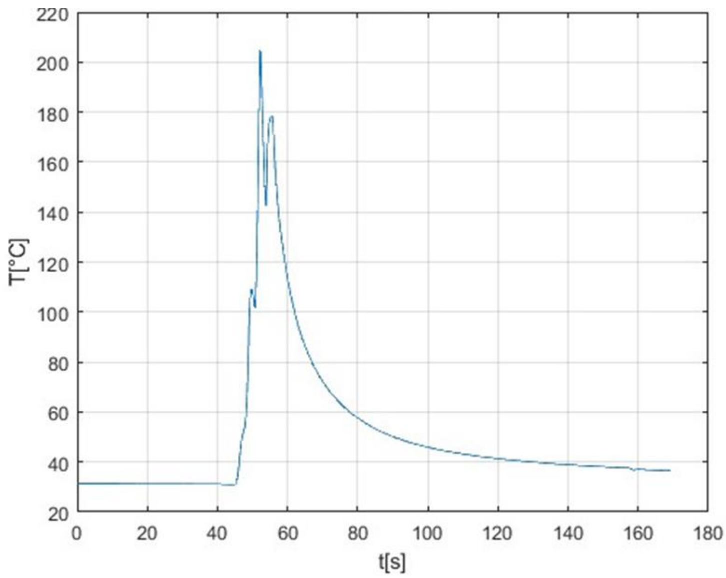

Figure 54: Example of temperature measurement during an experimental test.

4.4. Design of experiment

The experimental tests conducted aimed at studying the MQL system's impact on the cutting tests parameters as well as the effect of MQL on the temperature of the workpiece. With this in mind, the tests have been conducted with different combination of process parameters: feed rate, cutting velocity, air and oil volumetric flow rates.

The different process parameters and lubrication conditions used in the tests are reported in Table 6.

Process parameters			
Parameter	Low level	Medium level	High level
$\dot{m}_{oil}$ $[mL/h]$	0	5	10
$\dot{m}_{air}$ $[L/min]$	60	80	100
f_{rev} $[mm/rev]$	0.048	0.08	0.112
V_c $[m/min]$	40	50	60

Table 6: DOE parameters.

The different combinations of lubrication condition tested are:

- LC-1 $\dot{m}_{air} = 60\ L/min$ $\dot{m}_{oil} = 0\ mL/h$
- LC-2 $\dot{m}_{air} = 60\ L/min$ $\dot{m}_{oil} = 10\ mL/h$
- LC-3 $\dot{m}_{air} = 80\ L/min$ $\dot{m}_{oil} = 5\ mL/h$
- LC-4 $\dot{m}_{air} = 100\ L/min$ $\dot{m}_{oil} = 0\ mL/h$
- LC-5 $\dot{m}_{air} = 100\ L/min$ $\dot{m}_{oil} = 10\ mL/h$

The different combinations of process parameters tested are:

- PP-1 $V_c = 40\ m/min$ $f = 0.048\ mm/rev$
- PP-2 $V_c = 40\ m/min$ $f = 0.112\ mm/rev$
- PP-3 $V_c = 50\ m/min$ $f = 0.08\ mm/rev$
- PP-4 $V_c = 60\ m/min$ $f = 0.048\ mm/rev$
- PP-5 $V_c = 60\ m/min$ $f = 0.112\ mm/rev$
- PP-6 $V_c = 50\ m/min$ $f = 0.048\ mm/rev$
- PP-7 $V_c = 50\ m/min$ $f = 0.08\ mm/rev$
- PP-8 $V_c = 50\ m/min$ $f = 0.112\ mm/rev$

All the tests have been performed with two repetitions, precisely with two drilling tools of the same type.

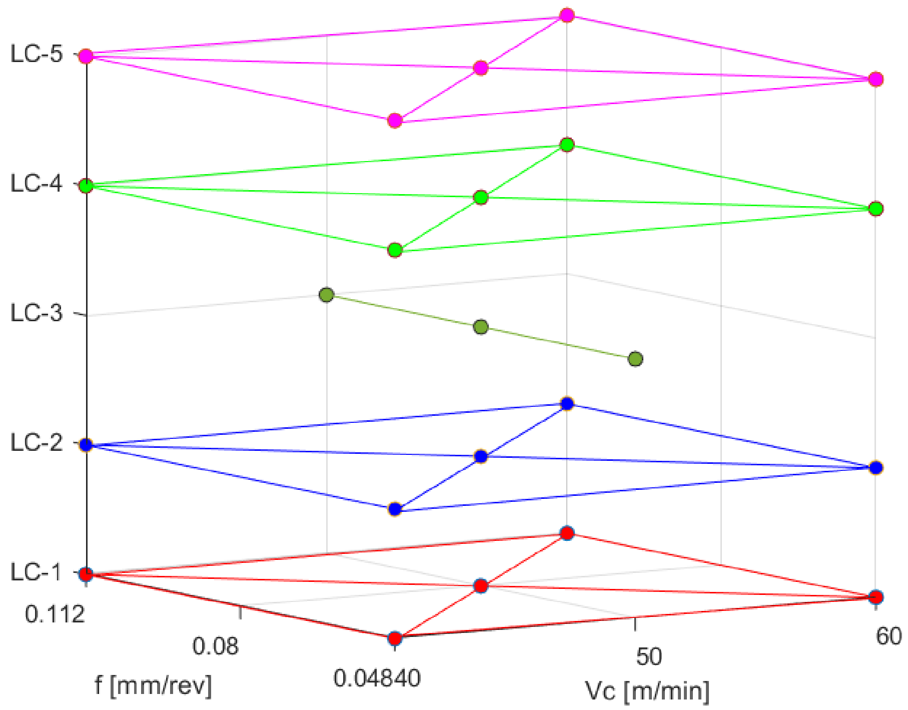

Figure 55: Combination of the parameters of experiment.

In the following table the complete list of tests performed is provided.

Test no.	Order	Drill bit	$\dot{m}_{oil}$ $[mL/h]$		$\dot{m}_{air}$ $[L/min]$		f $[mm/rev]$		V_c $[m/min]$	
1	20	1	low	0	low	60	low	0.048	low	40
2	2	1	high	10	low	60	low	0.048	low	40
3	19	1	low	0	high	100	low	0.048	low	40
4	29	1	high	10	high	100	low	0.048	low	40
5	1	1	low	0	low	60	high	0.112	low	40
6	25	1	high	10	low	60	high	0.112	low	40
7	7	1	low	0	high	100	high	0.112	low	40
8	22	1	high	10	high	100	high	0.112	low	40
9	28	1	low	0	low	60	low	0.048	high	60
10	5	1	high	10	low	60	low	0.048	high	60
11	10	1	low	0	high	100	low	0.048	high	60
12	8	1	high	10	high	100	low	0.048	high	60
13	18	1	low	0	low	60	high	0.112	high	60
14	21	1	high	10	low	60	high	0.112	high	60
15	24	1	low	0	high	100	high	0.112	high	60
16	12	1	high	10	high	100	high	0.112	high	60
17	16	1	medium	5	medium	80	medium	0.08	medium	50
18	11	1	medium	5	medium	80	medium	0.08	medium	50
19	52	2	low	0	low	60	low	0.048	low	40
20	51	2	high	10	low	60	low	0.048	low	40
21	45	2	low	0	high	100	low	0.048	low	40
22	50	2	high	10	high	100	low	0.048	low	40
23	31	2	low	0	low	60	high	0.112	low	40
24	41	2	high	10	low	60	high	0.112	low	40
25	34	2	low	0	high	100	high	0.112	low	40
26	42	2	high	10	high	100	high	0.112	low	40

27	30	2	low	0	low	60	low	0.048	high	60
28	53	2	high	10	low	60	low	0.048	high	60
29	37	2	low	0	high	100	low	0.048	high	60
30	33	2	high	10	high	100	low	0.048	high	60
31	44	2	low	0	low	60	high	0.112	high	60
32	35	2	high	10	low	60	high	0.112	high	60
33	36	2	low	0	high	100	high	0.112	high	60
34	48	2	high	10	high	100	high	0.112	high	60
35	49	2	medium	5	medium	80	medium	0.08	medium	50
36	38	2	medium	5	medium	80	medium	0.08	medium	50
37	4	1	low	0	low	60	medium	0.08	medium	50
38	15	1	high	10	low	60	medium	0.08	medium	50
39	3	1	low	0	high	100	medium	0.08	medium	50
40	26	1	high	10	high	100	medium	0.08	medium	50
41	13	1	medium	5	medium	80	low	0.048	medium	50
42	6	1	medium	5	medium	80	high	0.112	medium	50
43	17	1	low	0	low	60	validation	0.096	validation	55
44	27	1	high	10	low	60	validation	0.096	validation	55
45	14	1	low	0	high	100	validation	0.096	validation	55
46	23	1	high	10	high	100	validation	0.096	validation	55
47	9	1	medium	5	medium	80	validation	0.096	validation	55
48	46	2	low	0	low	60	medium	0.08	medium	50
49	43	2	high	10	low	60	medium	0.08	medium	50
50	32	2	low	0	high	100	medium	0.08	medium	50
51	40	2	high	10	high	100	medium	0.08	medium	50
52	47	2	medium	5	medium	80	low	0.048	medium	50
53	39	2	medium	5	medium	80	high	0.112	medium	50

Table 7: List of experiment campaign tests.

5 Results

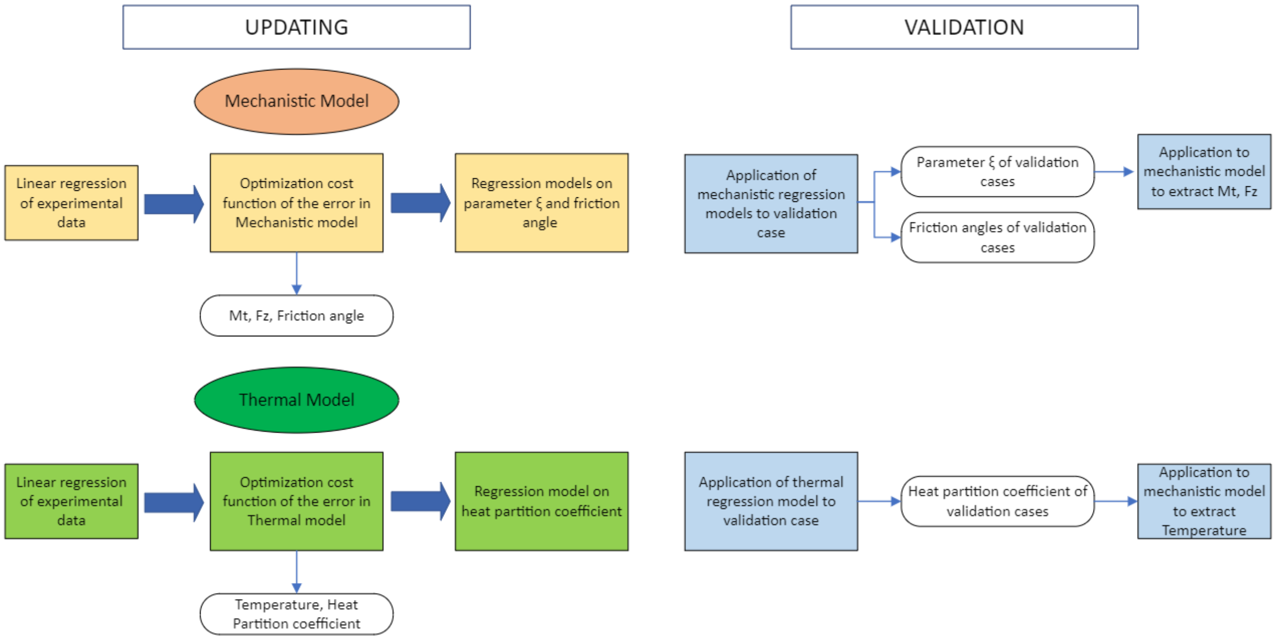

The updating part was performed for each of the test except the ones of order #17, #27, #14, #23, #9, used instead for the validation part.

5.1. Experimental Torque and Thrust Force

The results of the following section aim at understanding the effect of MQL on the chip formation mechanism. Indeed, a set of statistical analysis was performed both on mechanical quantities and model parameters.

Initially a linear regression was performed on the value of the torque and the thrust force measured. The aim was to assess the relations between these values and the cutting and lubrication conditions. The input for the linear regression model was the cutting velocity V_c, the feed-rate f, the quantity of lubrication component (oil and air), and the torque and thrust force measured. The analysis was performed through a multivariate regression approach following [50].

The results on torque and thrust force, obtained with the linear model described, were then validated comparing the results coming from the application of the oblique cutting model with the ones obtained experimentally. The experimental cutting torque was computed from the power measured during the experimental campaign for each test performed. In particular the mean of the cutting power measured on the different 4 passes due to peck drilling was considered. The cutting torque was instead computed with the following formula, as the ratio of cutting power P and angular velocity ω_{ang}:

$$M_t = \frac{P}{\omega_{ang}} \tag{68}$$

```
Linear regression model:
    Cutting torque ~ 1 + Vc + f + oil + air

Estimated Coefficients:
                    Estimate         SE         tStat       pValue
                   __________    _________    _______    __________

    (Intercept)        3.3847      0.36532     9.2651    8.3065e-12
    Vc              -0.040219    0.0054566    -7.3706     3.755e-09
    f                  44.297       1.6077     27.553    5.9122e-29
    oil              -0.04365    0.0097611    -4.4718    5.5877e-05
    air            -0.0027125    0.0024403    -1.1116       0.27251


Number of observations: 48, Error degrees of freedom: 43
Root Mean Squared Error: 0.309
R-squared: 0.951,  Adjusted R-Squared: 0.946
F-statistic vs. constant model: 209, p-value = 1.47e-27
```

```
Linear regression model:
    Thrust force ~ 1 + Vc + f + olio + aria

Estimated Coefficients:
                   Estimate      SE        tStat        pValue
                   ________    _______    ________    __________

    (Intercept)     720.29      146.17      4.9276    1.2827e-05
    Vc             -4.2594      2.1834     -1.9508      0.057613
    f                12857      643.28      19.986    2.1742e-23
    olio             -2.39      3.9057    -0.61192       0.54381
    aria           -0.2075     0.97643    -0.21251       0.83271


Number of observations: 48, Error degrees of freedom: 43
Root Mean Squared Error: 124
R-squared: 0.904,  Adjusted R-Squared: 0.895
F-statistic vs. constant model: 101, p-value = 2.85e-21
```

Figure 56: Linear regression models on the experimental data for cutting torque and thrust force

Analysing the Adjusted R-Squared indicator, the regression models present a good capability of describing the dependency among the variables (values close to unity). The same can be stated looking at the p-Values of the two regression models (values well below 5%). From the results of the ANOVA test on cutting torque of Fig. 56 (left), it can be seen how the cutting torque depends on the cutting speed, with a negative trend, whereas it increases if the feed-rate increases too. For what concerned the relations with the parameters of MQL, it can be noticed that the cutting torque is negative correlated to the flowrate of oil. It is interesting to notice that cutting torque is independent from air flowrate. In fact, the p-Value in correspondence of the air flowrate analysis is high. These relations may be explained with the increase of effectiveness of cutting (decrease of cutting power required) considering a higher cutting speed. Moreover, increasing feed-rate the chip section increased too, requiring higher effort to the cutting process.

On the other hand (Fig. 56 (right)), the ANOVA on thrust force shows independence from all the parameters but feed-rate. The same trend on cutting torque can be notices for the values of cutting speed and feed-rate. Nevertheless, the p-Value for the cutting velocity is slightly over 5%, indicating a weak influence of this cutting parameter on the thrust force. From the following results the same conclusions on cutting torque, about the relations with respect to the cutting velocity and feed-rate, seem reasonable for the thrust force, too. It's interesting to notice how the oil and air flowrate does not influence the thrust force at all.

The results obtained from experimental analysis are in accordance with the results found in the work of Daturi [11]: cutting speed influences torque but not significantly the thrust force, feed-rate influences both the considered quantities, oil flow rate affects considerably the cutting torque and slightly the thrust force, air flow rate does not influence at all none of the two measured quantities.

5.2. Mechanistic model results

The mechanistic model for oblique cutting was applied to all the cutting parameter condition cases. An optimization was applied in order to predict the right forces according to the change on friction due to MQL. An assessment on the influences of cutting and lubrication parameters was performed conceiving an ANOVA analysis of linear regression model of the results of optimization model.

As described in Sec. 2.2, the principal cutting edge of the tool was divided in 8 ECTSs, and the model was applied to each of the section of the cutting edge.

The mechanistic model needs the parameters of Johnson Cook model as input to impose the mechanical material behaviour. In this work the values of these parameters were not calibrated but chosen according to different JC parameters related to AISI 316L founded in literature. The values of JC parameters giving the best results for the case studied in this analysis were chosen. Specifically, the ones of the research of Amor [51] presented in the following table were used:

Johnson Cook parameters for AISI 316L		
A	412	[MPa]
B	761	[MPa]
C	0.038	**-**
n	0.510	**-**
m	0.520	**-**

Table 8: JC parameters used in the model. [51]

For the implementation of the mechanistic model, the dependency of c_p and k from the temperature is need. The values used in this work were:

AISI 316L	
Specific heat $\boldsymbol{c_p}$ $[\frac{J}{kg\,K}]$	Conductivity $\boldsymbol{k}$ $[\frac{W}{m\,K}]$
$459.32 + 0.1328 \cdot \mathrm{T[K]}$	$9.2848 + 0.0157 \cdot T[\mathrm{K}]$

Table 9: Dependency of c_p and k from temperature. [52]

According to Daturi [11], during the drilling process with the use of MQL, the friction decreases increasing the amount of MQL oil parameters. Whereas the contribution of air flowrate can be completely neglected. To validate this statement, the model was optimized for each experimental test setting a combined error between cutting torque and thrust force. The aim of the code implemented in Matlab 2024a was to minimize a cost function defined as:

$$J_m = \left(\frac{M_{t,calc} - M_{t,meas}}{M_{t,meas}}\right)^2 + \left(\frac{F_{z,calc} - F_{z,meas}}{F_{z,meas}}\right)^2 \quad (69)$$

acting on the value of ξ. The ξ value is a coefficient introduced in Eq. 17, allowing to act on the temperature ΔT_m of the mechanistic cutting model. T_m is defined as the temperature reached in the interface between the tool and the chip.

$$\Delta T_m = \xi \cdot \Delta T_c \cdot 10^{0.06-0.195\,\delta\sqrt{\frac{R_T t_2}{t_1}}+0.5\,\log_{10}\left(\frac{R_T t_2}{h}\right)} \quad (70)$$

Then, after the implementation of the optimization model for each of the cases tested in the experiment, the friction angle λ derived from the iterative oblique cutting model has been extracted. As can be seen from Fig. 35, the angle λ is formed by the resultant force R and the force normal to rake face N. R, N, and frictional force F are the forces involved in the Merchant's theory. From Fig. 35, the angle λ can be calculated as the ratio between the frictional force F and the normal force N (see Fig. 35):

$$\tan\lambda = \frac{F}{N} \quad (71)$$

Therefore, if the frictional force is decreased, also the friction angle λ should decrease. The results of cutting torque and thrust force obtained from the application of the optimization model for each of the lubricating condition tested are summarized below.

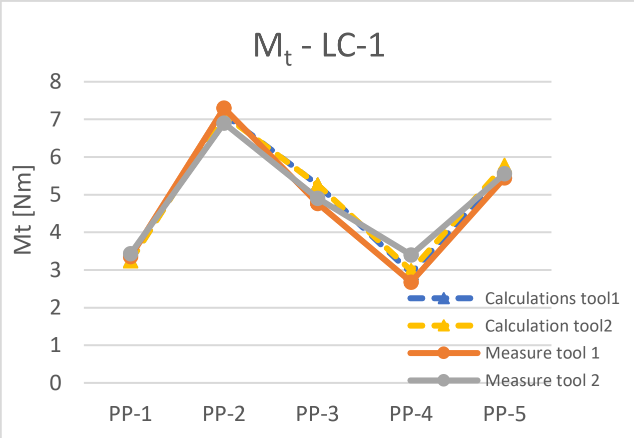

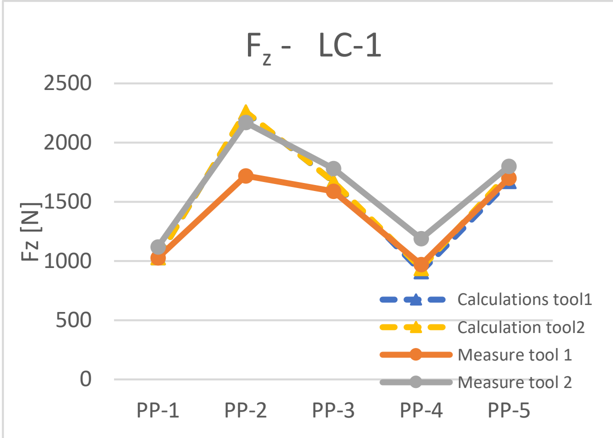

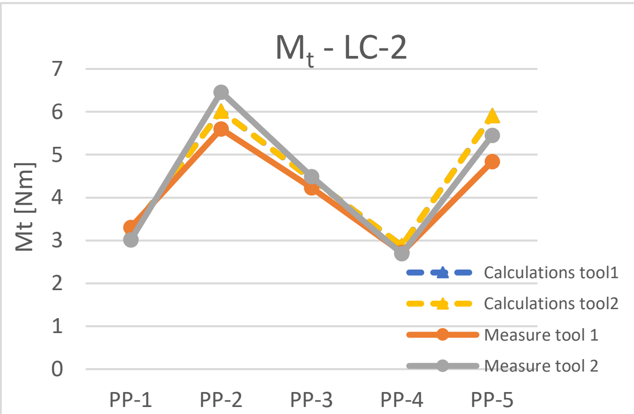

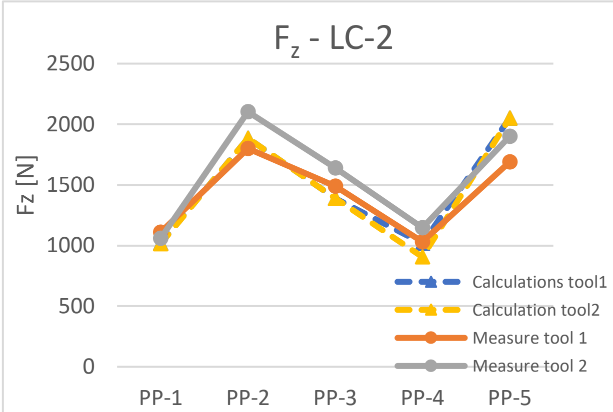

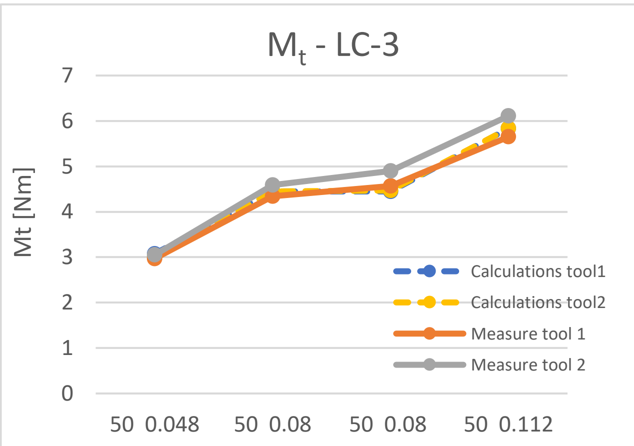

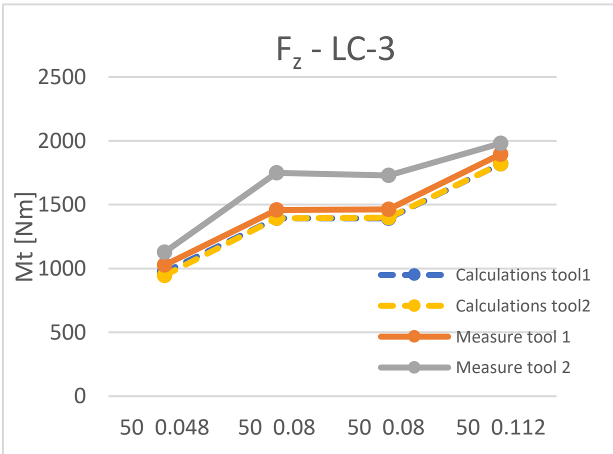

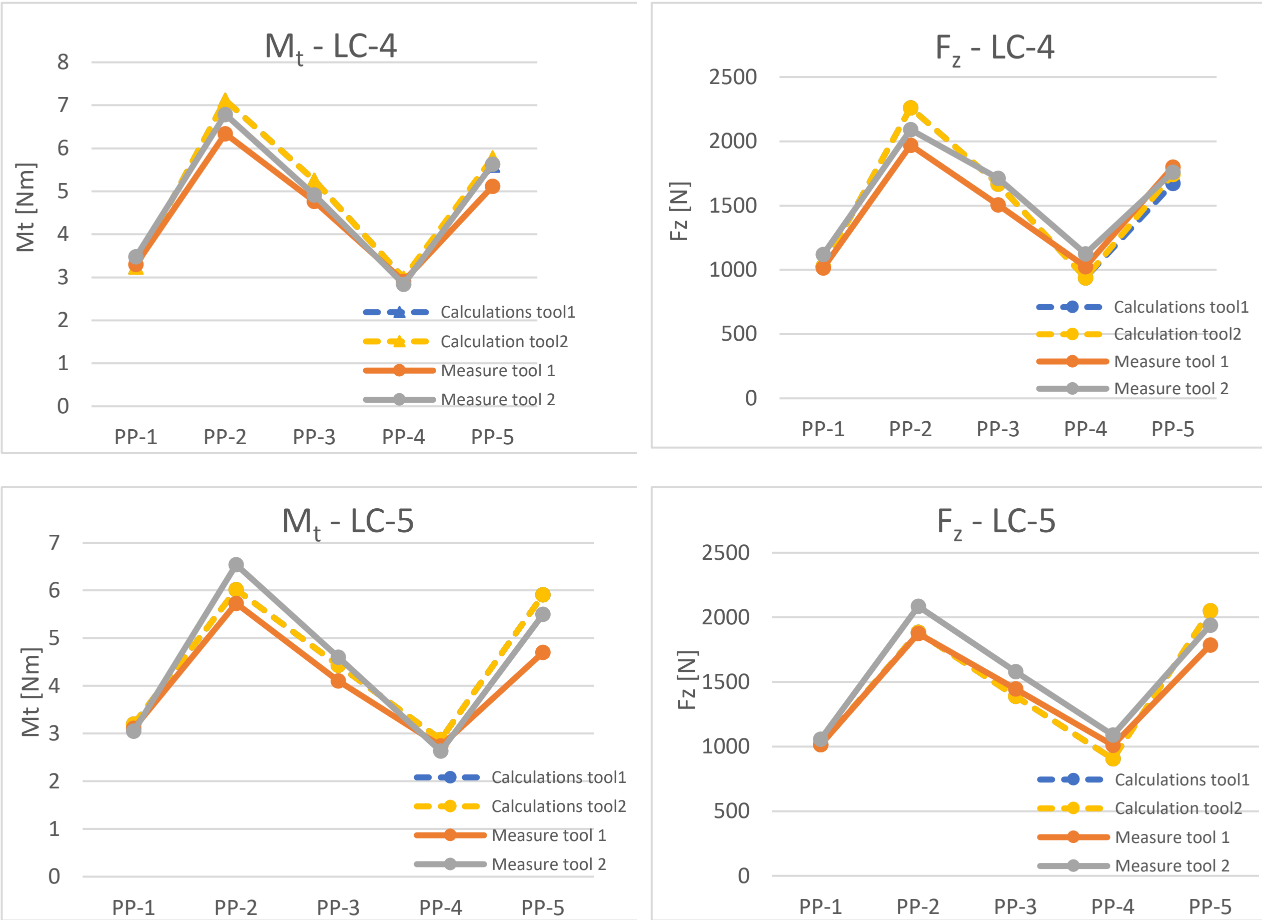

- LC-1 $\dot{m}_{air} = 60\ L/min$ $\dot{m}_{oil} = 0\ mL/h$
- LC-2 $\dot{m}_{air} = 60\ L/min$ $\dot{m}_{oil} = 10\ mL/h$
- LC-3 $\dot{m}_{air} = 80\ L/min$ $\dot{m}_{oil} = 5\ mL/h$
- LC-4 $\dot{m}_{air} = 100\ L/min$ $\dot{m}_{oil} = 0\ mL/h$
- LC-5 $\dot{m}_{air} = 100\ L/min$ $\dot{m}_{oil} = 10\ mL/h$

- PP-1 V_c=40 m/min f = 0.048 mm/rev
- PP-2 V_c=40 m/min f = 0.112 mm/rev
- PP-3 V_c=50 m/min f = 0.08 mm/rev
- PP-4 V_c=60 m/min f = 0.048 mm/rev
- PP-5 V_c=60 m/min f = 0.112 mm/rev
- PP-6 V_c=50 m/min f = 0.048 mm/rev
- PP-7 V_c=50 m/min f = 0.08 mm/rev
- PP-8 V_c=50 m/min f = 0.112 mm/rev

Figure 57: Results on cutting torque and Thrust force from optimization of mechanistic model

The relative errors computed with respect to the measured value are reported below.

Lubrication conditions	**Max Relative Error [%]**		**Mean Relative Error [%]**	
	Mt	Fz	Mt	Fz
LC-1	8.63	16.16	1.04	1.14
LC-2	8.63	11.33	4.52	-1.06
LC-3	14.88	21.27	4.89	-2.28
LC-4	14.9	-13.74	5.37	-3.76
LC-5	0.79	-13.20	-0.69	-10.74

Table 10: Error resulting from optimization model of cutting torque and thrust force

As visible in Table 10, the prediction of the model presents a very good matching with the experimental measured torque and thrust force. A different behavior was noticed between the tool drill bit used, despite they were of the same type. From Fig. 57 is visible how the tool 1 present curves always below the ones of the other tool, both for cutting torque and thrust force. This can be attributed to the unavoidable slightly different geometry and the different level of wear among the represented tests. The wear can affect the cuttability of the tool requiring more effort to perform the cutting action, increasing torque and thrust force.

A primary evaluation of the dependency of the friction angle λ from the cutting process parameters and lubrication conditions after the application of the model optimization, is shown in the following graphs. Here, λ is fitted versus a parameter per time. The continuous line represents the fitted curve on the data and the dotted line represent the curve mean simultaneous 95% confidence interval

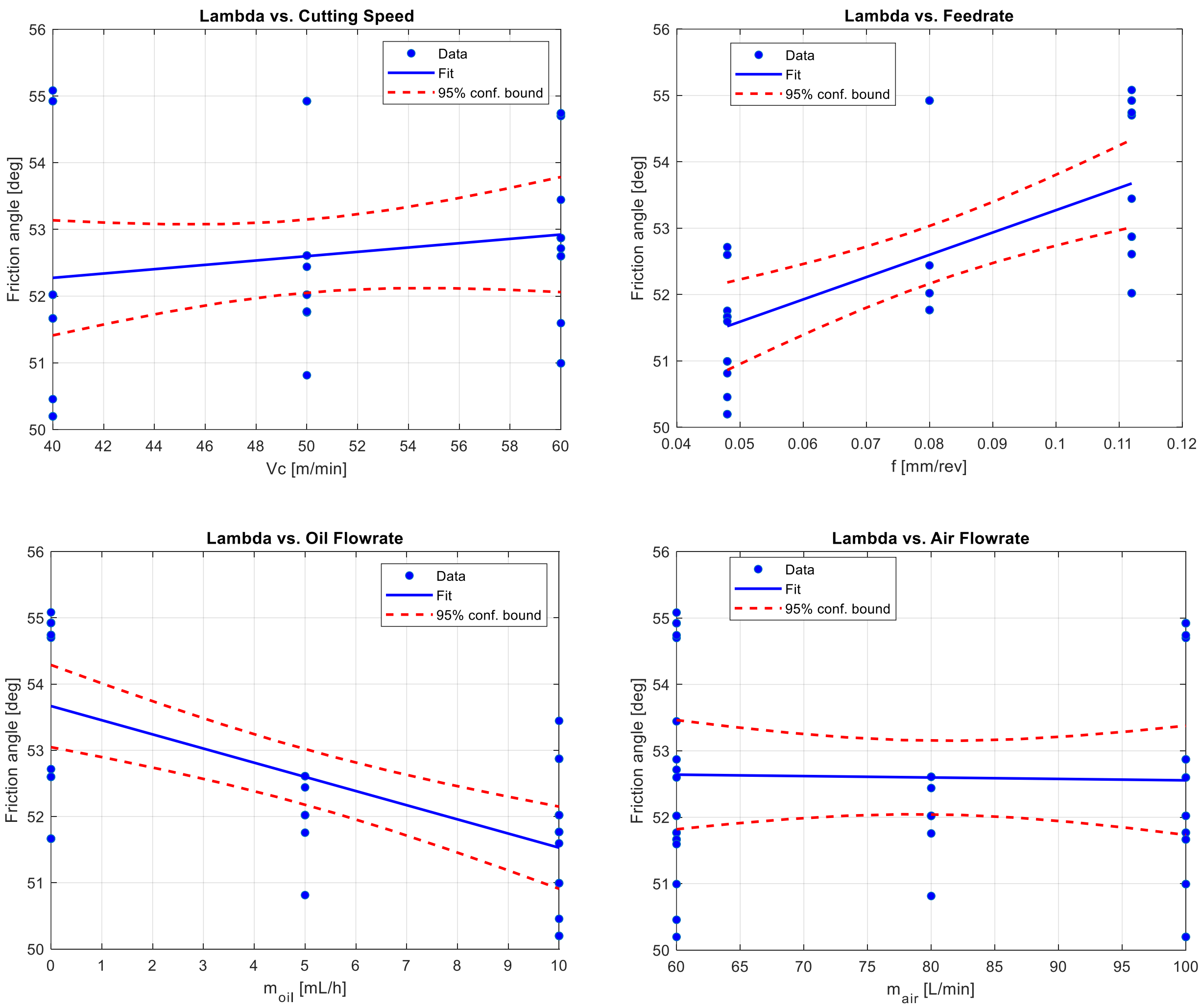

Figure 58: Dependency of friction angle lambda on cutting parameters (Vc and f) and lubrication conditions (m_{oil} and m_{air}) after model optimization.

As can be noticed the friction coefficient depends on cutting velocity and feed-rate. By increasing these two parameters, the friction coefficient increases too. For what concerned the flowrate of oil and air of the MQL, two different trends were visible: friction angle is negative correlated to oil flowrate because the friction force decreases too; whereas it is interesting to notice how the friction angle seems not to depend on the air flow rate of MQL. All these relationships will be confirmed in the next section where an ANOVA analysis on a multivariate linear regression is performed.

5.2.1. Regression on friction angle

From the analysis performed above, a primary evaluation of the effects of process parameters and lubrication condition on the friction angle was highlighted. Moreover, the effectiveness of the model to predict the mechanistic behaviour of the process was analysed and confirmed.

Subsequently, a linear regression on the friction angle was computed with the optimization model. The aim of the linear regression model was to predict the behaviour of any case under study, considering any process parameter and lubrication conditions.

The linear regression model was performed considering as variables the cutting velocity, the feed-rate and the flowrate of oil and air of MQL and the friction angle as the predicted object. In Fig. 59, the fitted regression model was reported.

```
Linear regression model:
    lambda ~ 1 + Vc + f + oil + air

Estimated Coefficients:
                    Estimate        SE        tStat       pValue
                   __________    _________    _______    __________

    (Intercept)        49.527      0.70489     70.262    5.1773e-46
    Vc               0.032452     0.010529     3.0823     0.0035788
    f                  33.616        3.102     10.837    7.1192e-14
    oil              -0.21382     0.018834    -11.353    1.5984e-14
    air            -0.0021358    0.0047086    -0.4536       0.65239


Number of observations: 48, Error degrees of freedom: 43
Root Mean Squared Error: 0.596
R-squared: 0.856,  Adjusted R-Squared: 0.843
F-statistic vs. constant model: 64, p-value = 1.51e-17
```

Figure 59: Linear regression models on the friction angle values from optimization model

Analysing the Adjusted R-Squared indicator, the regression models present a good capability of describing the dependency among the variables (values close to unity). The same can be stated looking at the p-Values of the regression model (values well below 5%). The results coming from this regression model confirmed the primary evaluation done, highlighting the increasing trend of friction coefficient as process parameters increase. The decreasing trend associated to the oil flowrate and the independency of the friction angle from the air flowrate were confirmed, too.

In the graphs below the relations of the lambda angle from cutting parameters obtained from linear regression was shown with the confidence interval of prediction with 95% of probability computed on simultaneous mean curve.

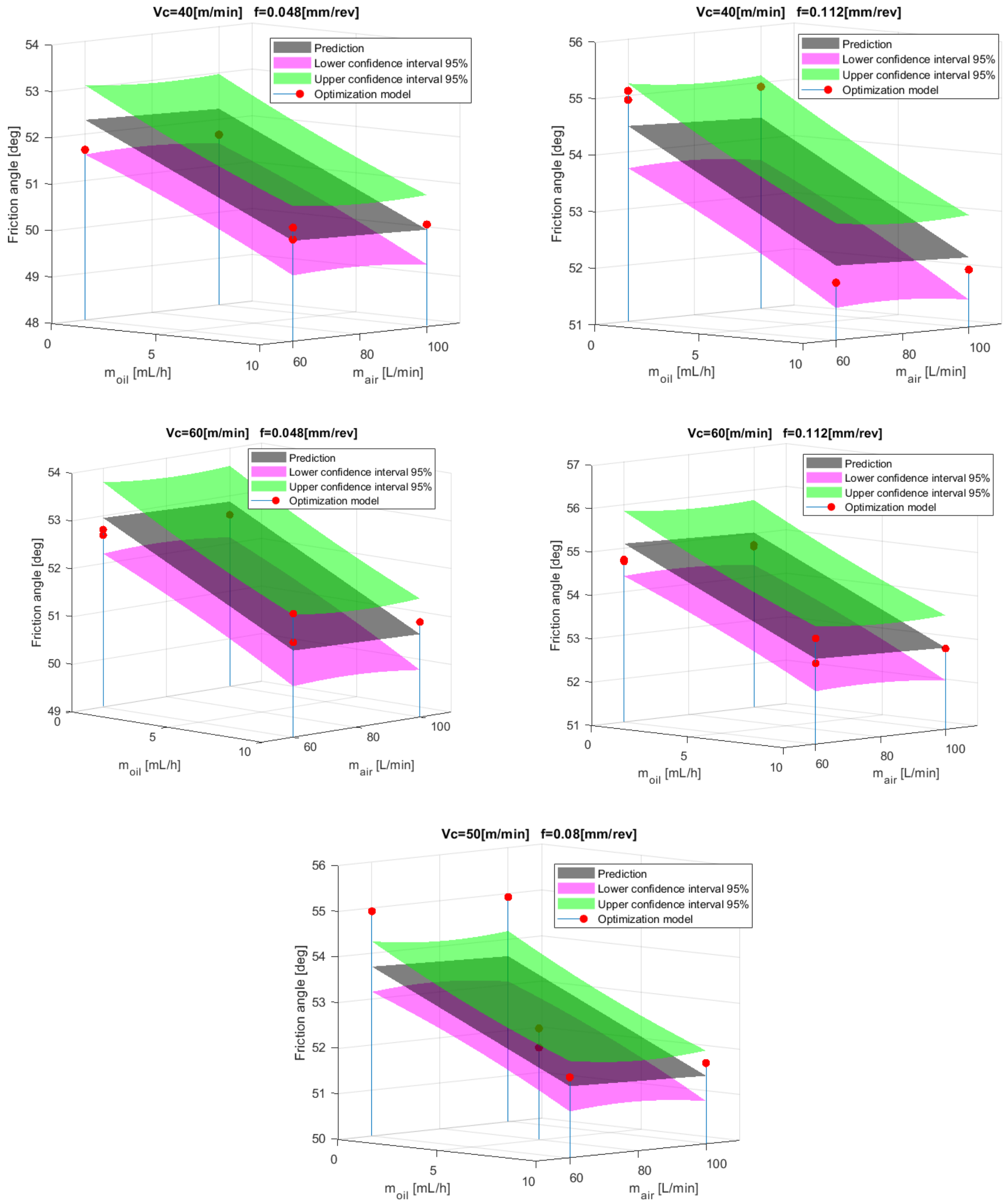

Figure 60: Graphs on prediction model of friction angle for different cutting parameters (V_c and f) with indication of confidence interval at 95%

In the graphs below the relations of the lambda friction angle with the lubrication conditions obtained from linear regression has been shown, comprending the curve mean simultaneous 95% confidence interval.

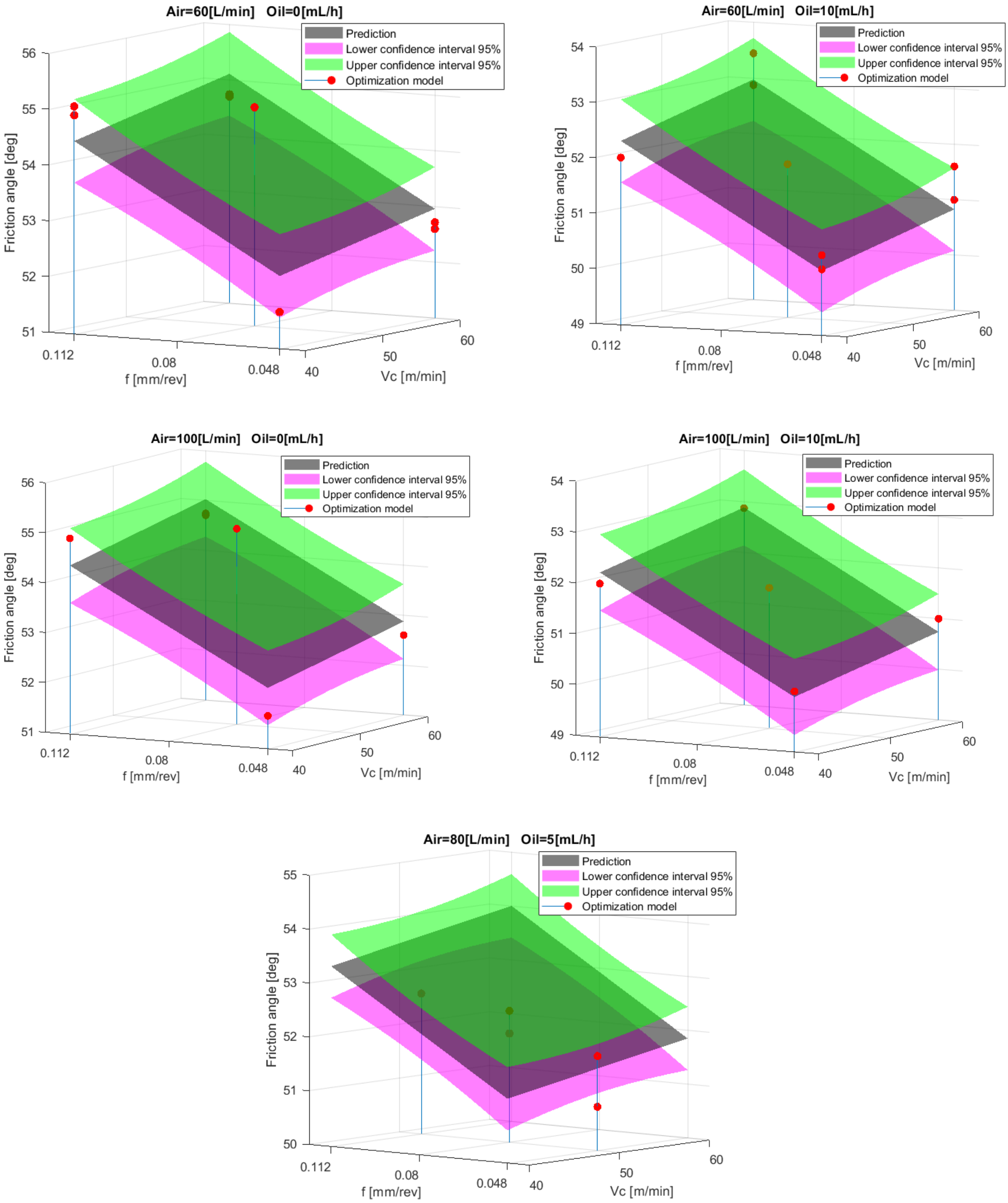

Figure 61: Graphs on prediction model of friction angle for different lubrication conditions (m_{air} and m_{oil}) with indication of confidence interval at 95%

From Fig. 60 and 61 the good capability on prediction of the regression model was confirmed. Just in the case of $V_c = 50\,[\frac{m}{min}]$ and $f = 0.08\,[\frac{mm}{rev}]$ and $\dot{m}_{oil} = 0\,[ml/h]$ the prediction of friction angle λ performed by the regression model results underestimated. This is due to the unavoidable uncertanty for the experimental nature of result values. Moreover, this can suggests that a relationship among the variables is not purely linear.

5.3. Experimental Workpiece Temperature

The thermal model for temperature analysis on peck drilling was applied to all the cutting parameter condition cases. An optimization was applied in order to predict the right workpiece temperature according to the change on heat partition. An assessment on the influences on temperature of cutting and lubrication parameters was performed conceiving an ANOVA analysis of linear regression model of the results of optimization model.

Initially a linear regression was performed on the value of temperature measured, to assess the parameters affecting the temperature. The input for the linear regression model was the cutting velocity, the feed-rate, the quantity of lubrication components (oil and air), and the temperature of the workpiece. For temperature the third peak was chosen, since it was recorded when the drill bit was nearest to the thermos couple.

```
Linear regression model:
    Temperature ~ 1 + Vc + f + oil + air

Estimated Coefficients:
                   Estimate       SE        tStat       pValue
                   ________    _______    _______    __________

    (Intercept)      295.92     16.729      17.69     4.457e-21
    Vc              -1.3424    0.24959    -5.3784    3.0921e-06
    f               -448.59     73.535    -6.1003    2.8491e-07
    oil             -1.4657    0.45244    -3.2395     0.0023435
    air            -0.44096    0.11311    -3.8985    0.00034254


Number of observations: 47, Error degrees of freedom: 42
Root Mean Squared Error: 14.1
R-squared: 0.688,  Adjusted R-Squared: 0.658
F-statistic vs. constant model: 23.1, p-value = 3.74e-10
```

Figure 62: Linear regression model on the experimental data for temperature of the third peak.

Analysing the Adjusted R-Squared indicator, the regression models present a worse capability of describing the dependency among the variables respect to the models developed for friction angle (0.658 against 0.895 and 0.946). The same can be stated comparing the p-Values of the two regression models, even if the value is well below 5%, indicating good reliability of results. The result of the ANOVA test on the figure above (Fig. 62) suggests the negative dependency of the temperature on all the cutting and lubricating conditions. The negative correlation of the temperature with respect to cutting velocity and feed-rate can be explained with the lower time available for the heat to diffuse into the material and the higher capability of the tool to cutting the material and create the chip by plastic deformation.

The explanation for the negative correlation between the temperature and the amount of oil and air, is the reduction of friction. In fact, friction generates heat during cutting action, reduced by the presence of oil. The increase of the convective coefficient due to the presence of the air, represents another factor for the reduction of temperature generated. From this evidence, it can be interesting to understand if the MQL presence affects the splitting of the heat generated during the process among workpiece, tool and chip or directly the total amount of the heat generated.

5.4. Thermal model results

As done for the mechanics of cutting, in order to describe what happens during the drilling process with the use of MQL and understanding why the temperature decreases, the model described in the Sec. 3 was applied for all the cases tested during the experiment. First of all, the motion of the drilling tool $z_p(t)$ inside the material with respect to the fixed coordinate system was imposed in the Eq. 43, creating a piecewise function, due to peck drilling, as a function of time. The function was created thanks to the measurement of Z axis position of the machine tool used for the drilling experiment.

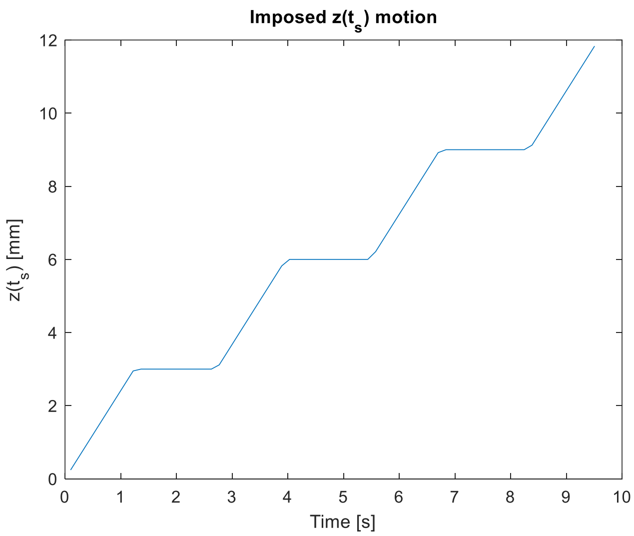

Figure 63: Imposed motion of the drilling tool inside the material during peck drilling process

A similar procedure was applied to the heat input of the model $q(t_s)$. The cutting power generated during the process was considered totally transformed in heat generation during cutting, neglecting the power losses for inefficiencies.

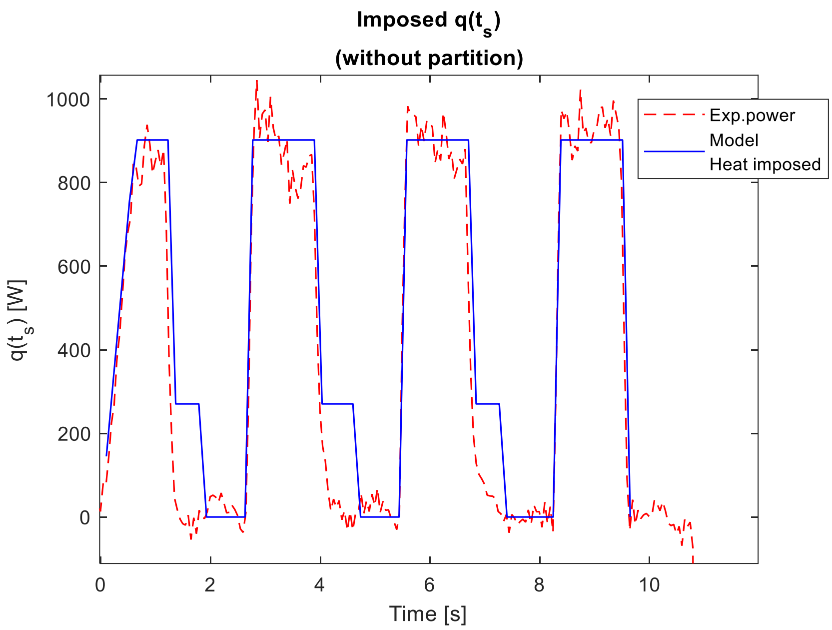

Figure 64: Imposed total heat power generated during peck drilling process

The power piecewise function is composed from a first portion where the power increases with a linear trend due to the gradual engagement of the drill bit into the material. Then the power remains constant to the steady maximum value for the time of cutting of the first pass. The portion with a constant power equal to 30% of the steady value, was introduced to represent a phenomenon observed during the analysis of the experiment. In this zone the drilling tool remains fixed at the position reached after the cutting pass, continuing to turn at the same rotational speed of the cutting phase. Thus, in this portion a certain quantity of power is generated due to friction between tool and workpiece. After this part, the tool goes up to a position far from the workpiece surface set on the drilling cycle, to allow the chip evacuation. The cycle starts again the process of cutting for the other 3 passes. After the last pass the tool does not remain fixed at the position reached but goes up far from workpiece surface immediately after the end of cutting.

The maximum heat power of Fig. 64 was computed summing the measured power related to the spindle absorption and the feed contribution.

$$q(t_s) = P + F_z \cdot V_f \tag{72}$$

Since the model was developed for the computation of the temperature field of the material, not all the power generated during the process was considered has the input of the model. The power splits among the tool, the workpiece and the chip, so a heat partition coefficient *B*, taking into consideration the portion of heat going into the tool, was included in the equation of the model heat input.

$$q(t_s) = \mathrm{B} \cdot (P + F_z \cdot V_f) \tag{73}$$

An optimization model was generated into Matlab 2024a with the aim of reducing the error on the temperature measured on the third peak of the temperature measurement curve. Thus, the code minimized the following cost function:

$$J_T = \left(\frac{T_{calc} - T_{meas}}{T_{meas}}\right)^2 \tag{74}$$

Acting on the value of the heat partition coefficient *B*, it changed the heat partition toward the workpiece in the different case studies.

During the implementation of the model, it was noticed that only some of the heat sources in Sec. 3.2 provided a relevant contribution to the temperature field. Indeed, only heat sources HS-1, HS-2, HS-3, HS-4, were considered in the calculation (the increased of temperature due to the other heat sources can be neglected for the process studied in this work, as visible in Fig. 65).

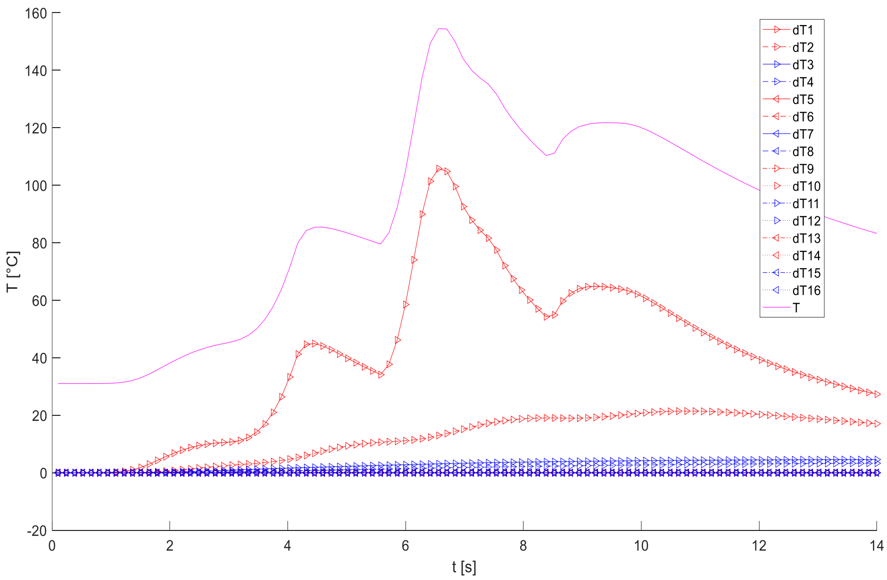

Figure 65: Curve of the temperature value for each of the heat source implemented in Section. 3.2

The comparison among the measured temperatures and the ones calculated from the model for the test orders #04, #28, #01 (PP-3,LC-1; PP-4,LC-1; PP-2,LC-1) and #43, #05, #25 (PP-3,LC-2; PP-4,LC-2; PP-2,LC-1) from Table 7, was shown in Fig. 66,67. The model predicts very well the temperature measured, with heat partition coefficients of 0.235, 0.285, 0.235 and 0.285, 0.265, 0.22, respectively. The temperature associated to the fourth peak was not accurate instead. After the third peak the drill bit overcome the position of thermocouple in Z direction, so the surface of the machined hole happened to be in contact with the chip produced by the drill bit. Being the chip at very high temperature, the Thermocouple sensed its influence. Nevertheless, this component of heat has a stochastic nature. Therefore, in this work, it was chosen to neglect the curve of temperature after the third peck, because the extra source of heat due to the chip friction and conduction on the wall was not considered.

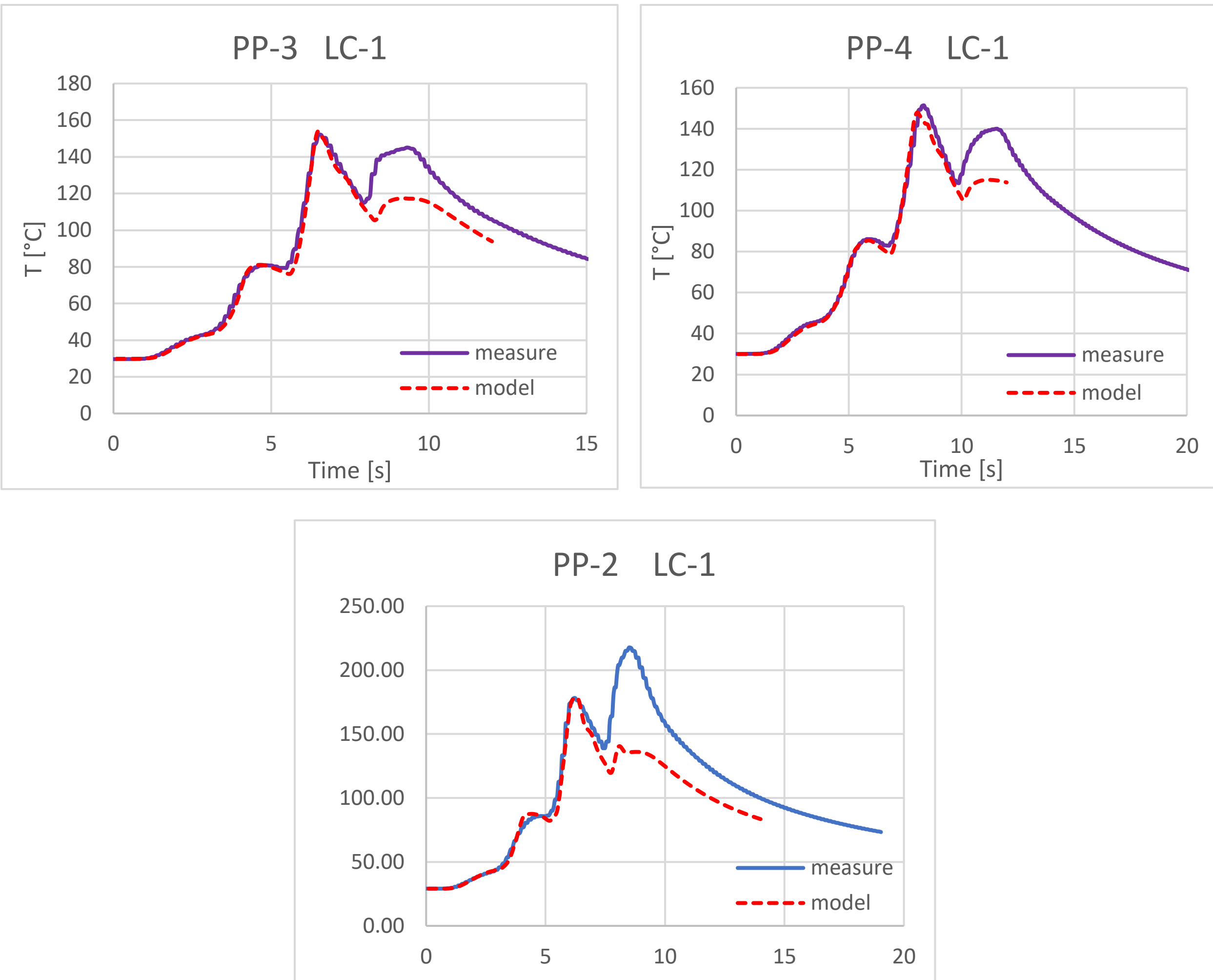

- LC-1 $\dot{m}_{air} = 60\ L/min$ $\dot{m}_{oil} = 0\ mL/h$
- LC-2 $\dot{m}_{air} = 60\ L/min$ $\dot{m}_{oil} = 10\ mL/h$

- PP-2 V_c=40 m/min f = 0.112 mm/rev
- PP-3 V_c=50 m/min f = 0.08 mm/rev
- PP-4 V_c=60 m/min f = 0.048 mm/rev

Figure 66: Comparison measured and modelled temperature for three cases of process parameters (PP-2, PP-3, PP-4) without oil flowrate (LC-1)

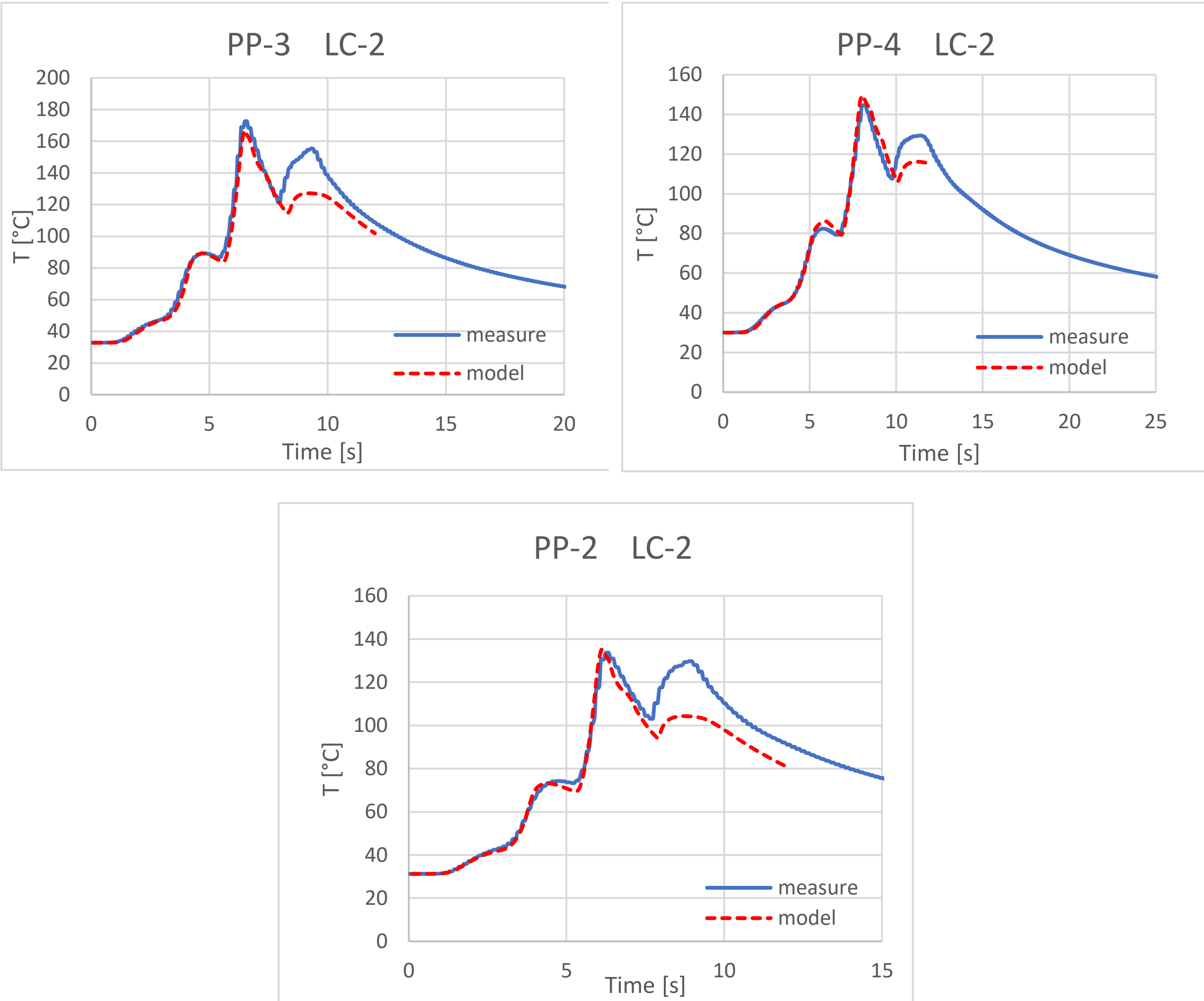

- LC-1 $\dot{m}_{air} = 60\ L/min$ $\dot{m}_{oil} = 0\ mL/h$
- LC-2 $\dot{m}_{air} = 60\ L/min$ $\dot{m}_{oil} = 10\ mL/h$

- PP-2 V_c=40 m/min f = 0.112 mm/rev
- PP-3 V_c=50 m/min f = 0.08 mm/rev
- PP-4 V_c=60 m/min f = 0.048 mm/rev

Figure 67: Comparison measured and modelled temperature for three cases of process parameters (PP-2, PP-3, PP-4) with maximum oil flowrate (LC-2)

From the results of Fig. 67 the relative errors respect to the measured values on the third peak were computed and shown below.

Experimental test	Relative error
#04 PP-3,LC-1	0.0012%
#28 PP-4,LC-1	0.0045%
#01 PP-2,LC-1	-0.0058%
#43 PP-3,LC-2	0.0072%
#05 PP-4,LC-2	-0.0057%
#25 PP-2,LC-1	0.0017%

Table 11: Relative error on prediction of temperature of third peak

After the optimization process, aimed to find the optimum heat partition coefficient allowing to match the measured temperature curve, the analysis of the data leads to the following results, shown in the Fig.68. Here, univariate linear regression model was fitted against process and lubrication parameters. The continuous line represents the fitted curve of the data, and the dotted line represents the curve mean simultaneous 95% confidence interval.

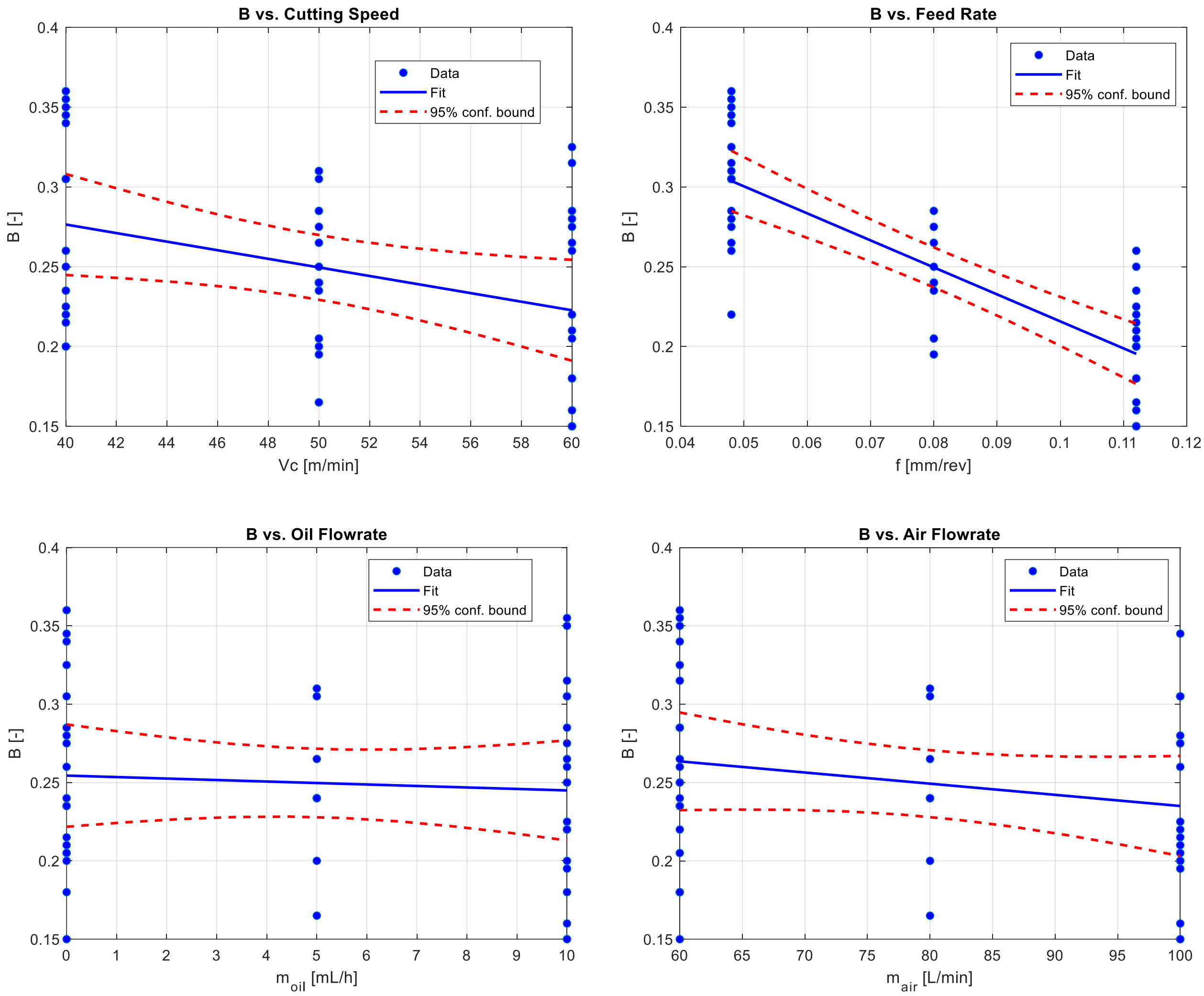

Figure 68: Dependency of heat partition B on cutting parameters (Vc and f) and lubrication conditions (m_{oil} and m_{air})

The obtained graphs indicated that the heat partition coefficient inside the material is affected by the cutting velocity and the feed-rate, increasing the cutting parameters the heat partition coefficient decreases, with an higher negative trend for the feedrate. Whereas it seems that the heat partition coefficient does not depend on the quantity of oil flow -rate of MQL. A sligthly dependence on the air flow rate is visible.

This interesting result suggests that the lubricating oil of MQL do not decrease the temperature by changing the fraction of input heat going into the material. Oil changes the total amount of power (heat) generated during the process, by reducing friction, leading to a decreased temperature at the workpiece. The increase of convection due to air presence, is translated in a reduction of heat partition coefficient, since this work consider just the conduction phenomenon.

The results will be confirmed on the next section where ANOVA analysis on a multivariate linear regression on these results was performed.

5.4.1. Regression of workpiece heat partition coefficient

As done for the friction coefficient, the same procedure was applied to the values of heat partition coefficient obtained from the results of optimization model. Cutting velocity, feed-rate and flowrate of oil and air of MQL were considered as regressor to predict the heat partition coefficient behaviour.

```
Linear regression model:
    B ~ 1 + Vc + f + oil + air

Estimated Coefficients:
                     Estimate         SE         tStat       pValue
                    ___________    __________    _______    __________

    (Intercept)         0.58006      0.025496     22.751    3.0634e-25
    Vc               -0.0026875    0.00038039    -7.0651    1.1733e-08
    f                   -1.6927       0.11207    -15.104     1.407e-18
    oil             -0.00087298    0.00068956     -1.266       0.21249
    air             -0.00070675    0.00017239    -4.0998    0.00018526


Number of observations: 47, Error degrees of freedom: 42
Root Mean Squared Error: 0.0215
R-squared: 0.876,  Adjusted R-Squared: 0.864
F-statistic vs. constant model: 74.2, p-value = 1.77e-18
```

Figure 69: Linear regression models on the heat partition coefficients from optimization model

Analysing the Adjusted R-Squared indicator, the regression model presents a good reliability on describing the dependency among the variables (value close to unity). The same can be stated looking at the p-Values of the regression model (value well below 5%).

All the hypothesis done to explain the relationship between heat partition coefficient and cutting and lubricating parameters have been confirmed. In the graphs below the relations of the heat partition coefficient to the workpiece with the cutting process parameters obtained from linear regression has been shown, comprending the curve mean simultaneous 95% confidence interval.

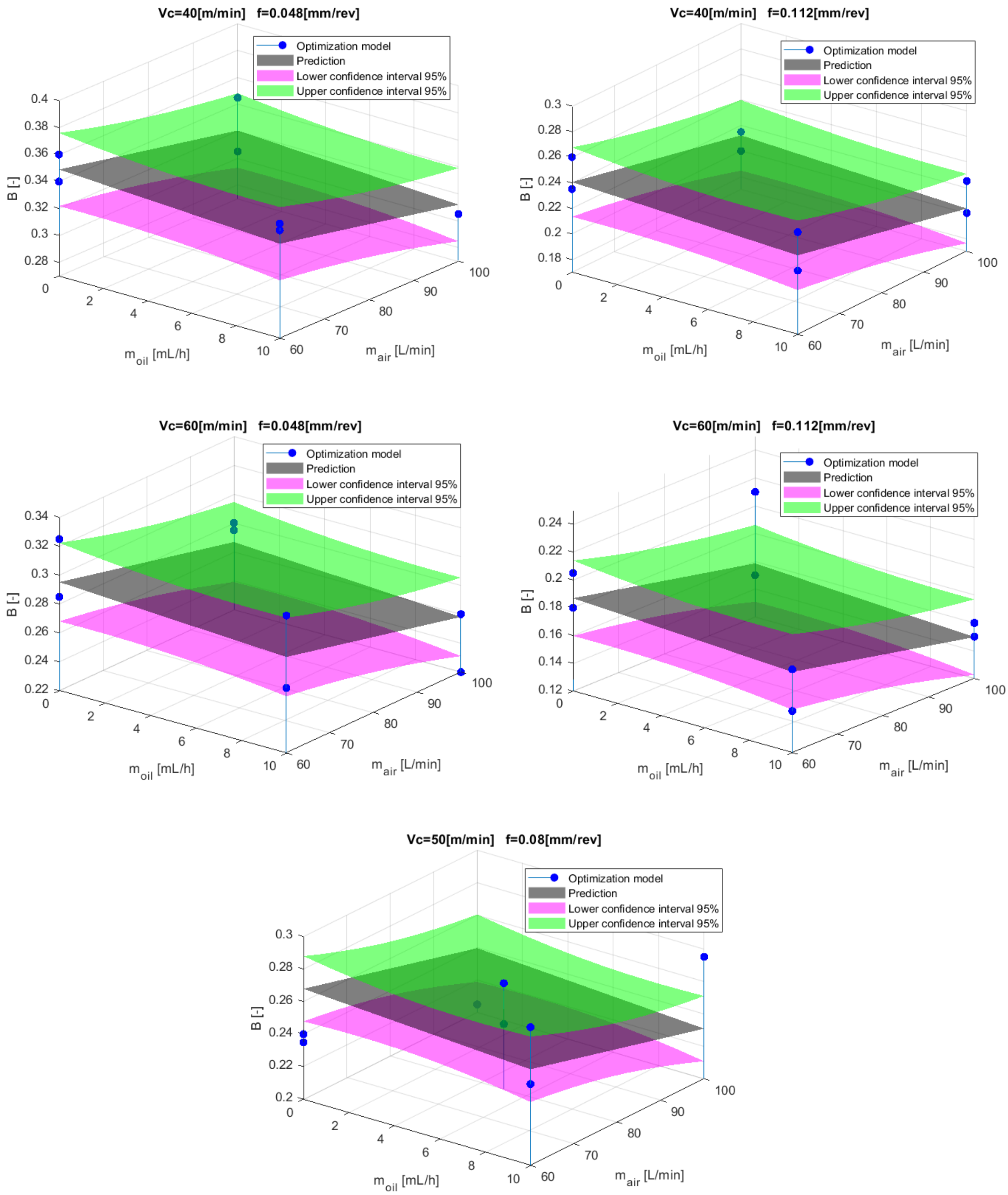

Figure 70: Graphs on prediction model of heat partition coefficient for different cutting parameters (V_c and f) with indication of confidence interval at 95%

In the graphs below the relations of the heat partition coefficient to the workpiece with the lubrication conditions obtained from linear regression has been shown, comprending the curve mean simultaneous 95% confidence interval.

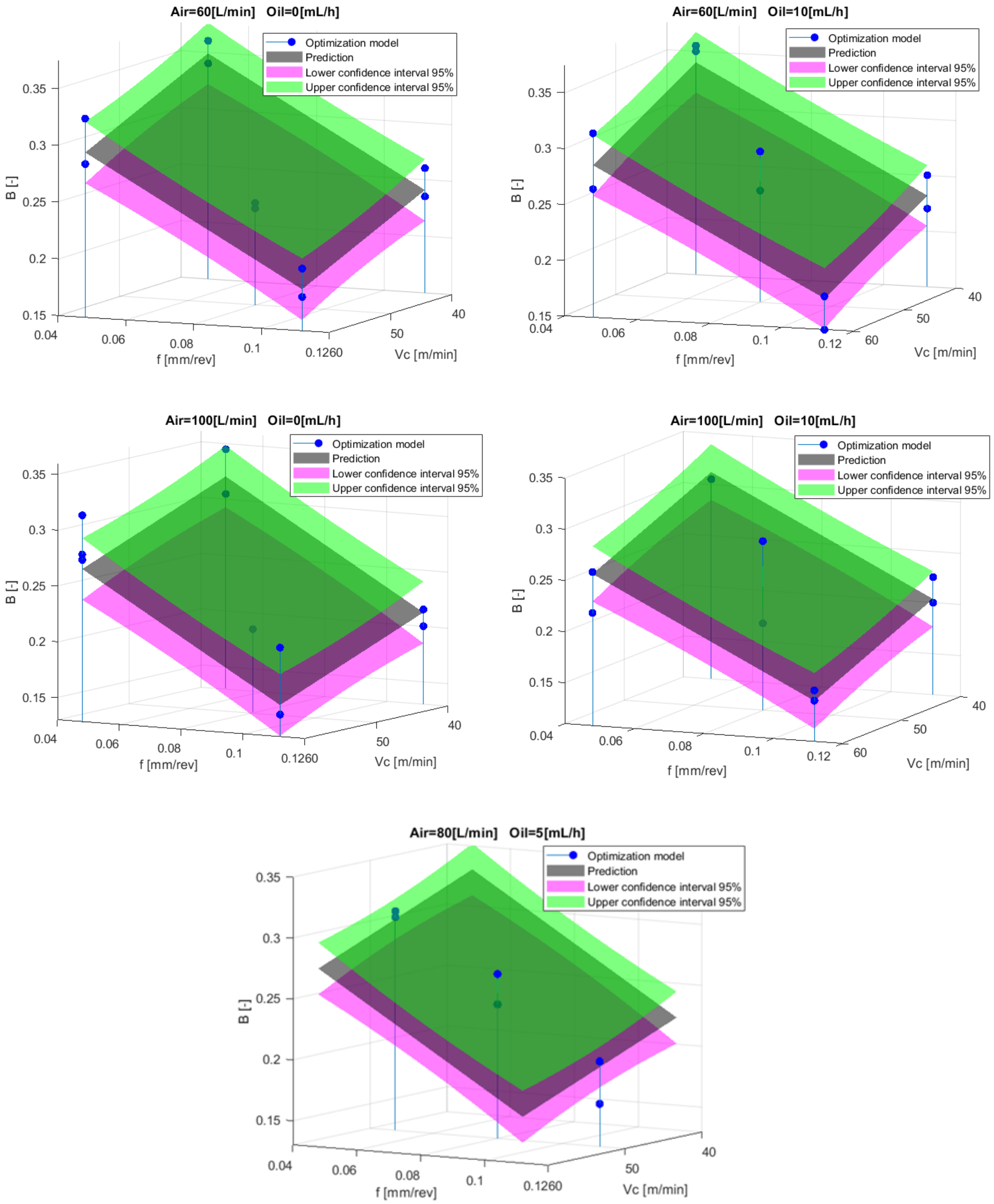

Figure 71: Graphs on prediction model of heat partition coefficient for different lubrication conditions (m_{air} and m_{oil}) with indication of confidence interval at 95%.

From Fig. 70 and 71 the good capability on prediction of the regression model was confirmed. Just in the case of $V_c = 50\ [\frac{m}{min}]$ and $f = 0.08\ [\frac{mm}{rev}]$ and $\dot{m}_{oil} = 0\ [ml/h]$, exactly as for the prediction of friction angle λ, the prediction of heat partition coeffcient B, results not internal to the confidence bounds. This is probably due to the unavoidable uncertanty for the experimental nature of result values. Moreover, this can suggests that a relationship among the variables is not purely linear.

5.5. Validation

A validation scenario to set the prediction ability of the model was conceived. Specific experimental tests were conceived for this reason. Validation was performed at cutting velocity $V_c = 55\ \frac{m}{min}$ and feed-rate of $f = 0.096\ \frac{mm}{rev}$, thus different from the ones used for training the regression models. 5 validation tests were obtained changing the lubrication conditions (tests order #17, #27, #14, #23, #9, of Table 7).

For the mechanics of cutting, the linear regression model on ξ is evaluated at the validation cutting conditions. The linear regression model used was:

$$\hat{\xi}_{val} = 1.017 + 0.00111 \cdot V_c - 0.09645 \cdot f - 0.03533 \cdot \dot{m}_{oil} - 0.00022 \cdot \dot{m}_{air}$$

The true counterpart is instead obtained through the optimization process shown in Sec. 5.2. The predicted values of the optimization parameter have been computed from the regression model and used in the application of the mechanistic model to extract torque, thrust force and friction angles for the validation case. The comparison between the friction angle lambda computed with the optimization of the oblique cutting model and the one computed with the regression model is shown in the figure below.

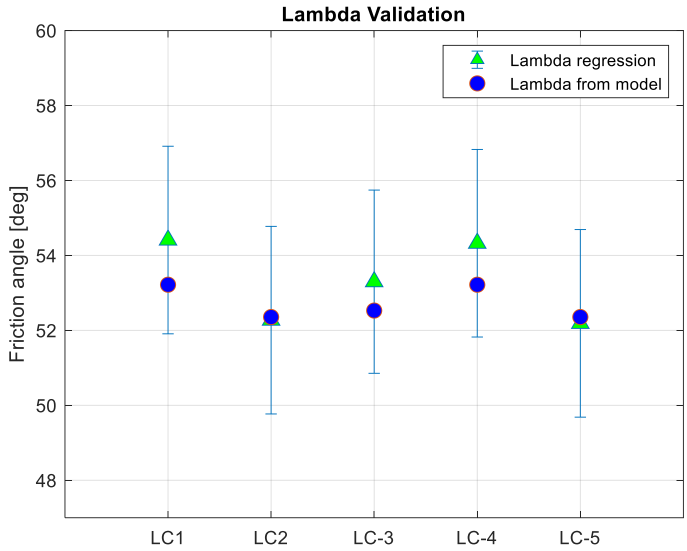

- LC-1 $m_{air} = 60\ L/min$ $m_{oil} = 0\ mL/h$
- LC-2 $m_{air} = 60\ L/min$ $m_{oil} = 10\ mL/h$
- LC-3 $m_{air} = 80\ L/min$ $m_{oil} = 5\ mL/h$
- LC-4 $m_{air} = 100\ L/min$ $m_{oil} = 0\ mL/h$
- LC-5 $m_{air} = 100\ L/min$ $m_{oil} = 10\ mL/h$

Figure 72: Comparison from the friction angle computed with optimization model and regression model. Error bars represent 95% prediction intervals for a single observation.

The mean relative error, on the different lubrication conditions, respect to the measured value in prediction of the friction angle λ is 1.06%. All the prediction intervals included the true λ obtained by optimization, suggesting excellent prediction capabilities for the conceived model.

Secondly, the results on the cutting torque and thrust force predicted from the mechanistic model for the validation case were shown in Fig. 73:

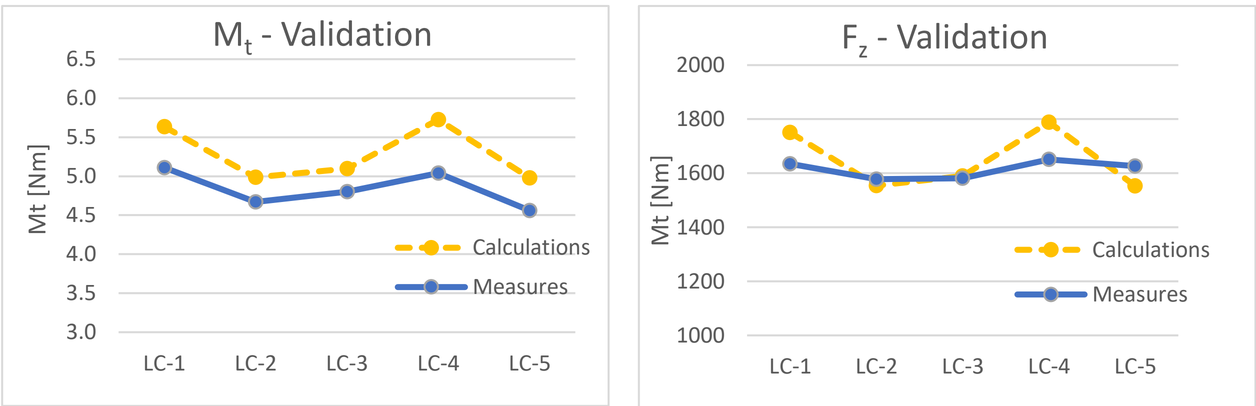

- LC-1 $m_{air} = 60\ L/min$ $m_{oil} = 0\ mL/h$
- LC-2 $m_{air} = 60\ L/min$ $m_{oil} = 10\ mL/h$
- LC-3 $m_{air} = 80\ L/min$ $m_{oil} = 5\ mL/h$
- LC-4 $m_{air} = 100\ L/min$ $m_{oil} = 0\ mL/h$
- LC-5 $m_{air} = 100\ L/min$ $m_{oil} = 10\ mL/h$

Figure 73: Values of cutting torque and thrust force for the validation case.

The mean relative prediction error, on the different lubrication conditions, with respect to the measured values of the torque is 9.17%, whereas the mean error on the thrust force is 1.98%.

The same procedure was adopted for the validation of the heat partition coefficient. The comparison between the heat partition coefficient B computed with the optimization of the thermal model and the one computed with the regression model is shown in the figure below.

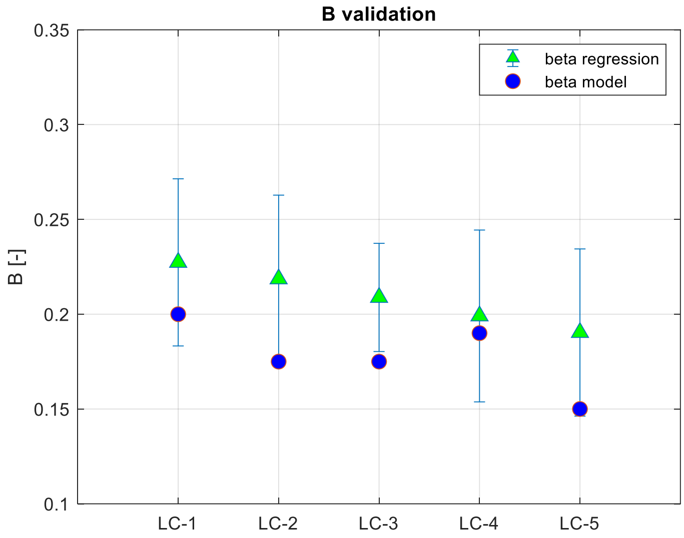

- LC-1 $m_{air} = 60\ L/min$ $m_{oil} = 0\ mL/h$
- LC-2 $m_{air} = 60\ L/min$ $m_{oil} = 10\ mL/h$
- LC-3 $m_{air} = 80\ L/min$ $m_{oil} = 5\ mL/h$
- LC-4 $m_{air} = 100\ L/min$ $m_{oil} = 0\ mL/h$
- LC-5 $m_{air} = 100\ L/min$ $m_{oil} = 10\ mL/h$

Figure 74: Comparison from the friction angle computed with optimization model and regression model

The mean relative error, on the different lubrication conditions, respect to the measured value in prediction of the heat partition coefficient B is 17.89%. The values of the heat partition coefficient B predicted from the regression model have been used as the input of the thermal model developed in Sec. 3 to compute the temperature at the position of thermocouple for the case of validation.

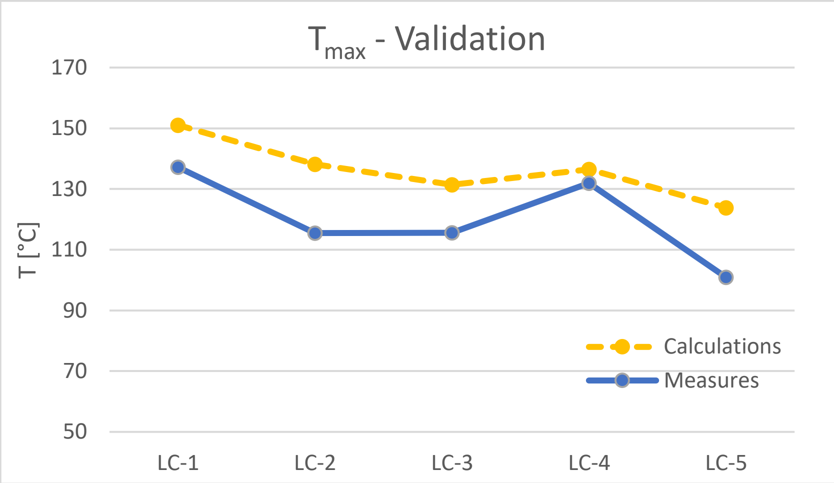

- LC-1 $\boldsymbol{m}_{air} = 60\ L/min$ $\boldsymbol{m}_{oil} = 0\ mL/h$
- LC-2 $\boldsymbol{m}_{air} = 60\ L/min$ $\boldsymbol{m}_{oil} = 10\ mL/h$
- LC-3 $\boldsymbol{m}_{air} = 80\ L/min$ $\boldsymbol{m}_{oil} = 5\ mL/h$
- LC-4 $\boldsymbol{m}_{air} = 100\ L/min$ $\boldsymbol{m}_{oil} = 0\ mL/h$
- LC-5 $\boldsymbol{m}_{air} = 100\ L/min$ $\boldsymbol{m}_{oil} = 10\ mL/h$

Figure 75: Values of cutting torque and thrust force for the validation case.

The mean relative error, on the different lubrication conditions, with respect to the measured values in prediction of the temperature of the third peak is 13.91%. The ANOVA on regression model of experimental results of third peak temperature, Fig. 62, indicates the uncertainty on the thermal experimental results. In fact, the Adjust R-squared value is 0.658, thus not so close to unity. This seems to be reflected on the error found in comparison of temperature measure and predicted in validation. Moreover, the cutting and lubrication parameters of validation was close to the centre of the surface plotted in Fig. 71, where the higher discrepancy between regressor and prediction were found.

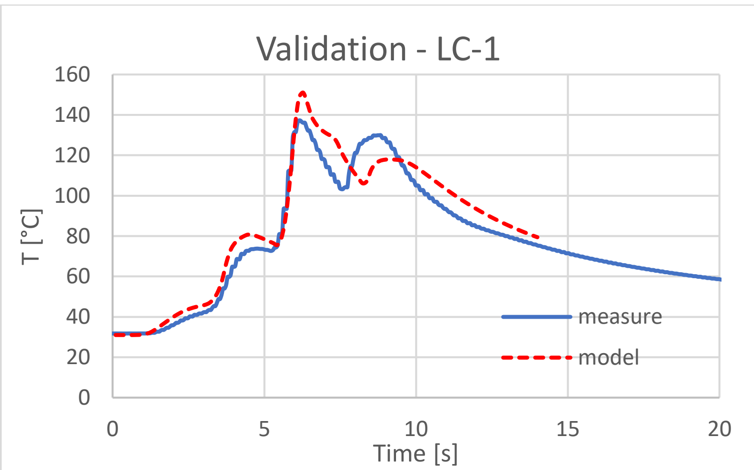

Figure 76: Predicted temperature curve for validation case with lubricating condition LC-1

6 Conclusion and future developments

In this work an analytical mechanistic model for the prediction of the dynamic behaviour of the oblique cutting process was developed. It was applied to the analysis of the peck drilling process and from the results described in Section 5 the model was able to predict the cutting torque and the thrust force in the different lubrication condition analysed.

From the analysis of the mechanistic results the capability of the oil in MQL to reduce the friction action in the cutting process was highlighted. Indeed, MQL usage can reduce the total cutting torque and thrust force, by reducing the friction angle. Moreover, it has been proved that the air flowrate present in the MQL does not affect the dynamic behaviour of the process.

A linear regression model on the results of friction angle predicted by the optimization of the mechanistic oblique cutting model was conceived. The predicted values of coefficient ξ has been used to apply the mechanistic model on the validation case. It confirmed the cutting torque and thrust force prediction ability with a mean relative error of 9.17% and 1.98% for thrust force.

Furthermore, an analytical model to predict the temperature reached during peck drilling process was developed. Also in this case, the validity of the application of this model to the experimental campaign produced very good results, being able to predict the temperature at a location of the workpiece, in the different lubrication condition analysed.

From the analysis of the thermal results the capability of the MQL to reduce the temperature reached in the cutting process was confirmed. MQL oil was found to reduce the temperature in the workpiece by reducing the friction coefficient and thus, the total power generated in the process. The independence of the heat partition coefficient into the workpiece with the oil flowrate of MQL was proved. Moreover, the results evidenced that the air flowrate present in the MQL affects the thermal behaviour of the cutting process by increasing the convective coefficient. Indeed, the air flow reduced the heat partition coefficient. This effect can be related to an increase of the heat flow removed from the workpiece by convection.

Thanks to the optimization process of the thermal model, the heat partition into the workpiece was computed and the percentage of the total power generated during the cutting process conducting into the workpiece varied as a function of cutting speed and feed-rate. By increasing these cutting parameters, the heat partition coefficient decreases strongly, as can be seen in Section 5.4.1. The heat partition coefficient varied in range between 15-36% for the cutting speed and feed-rate considered in the present analysis.

A linear regression model produced on the temperature results of thermal model has been applied to a validation case confirming a good prediction on temperature for the various lubrication condition analysed, detecting a mean relative error of prediction of 17.89%.

As future development it would be interesting to include in the thermal model the characterization of the heat produced by the chip during the movement inside the hole. This will further confirm the validity of the developed model being able to predict also the part of the process where the drilling tool is moving under the position of the thermal sensor (fourth peak).

Moreover, it would be interesting to include the analysis of the heat partition coefficient describing the division of the other part of the heat, towards tool and chip. This would complete the thermal characterization of the cutting process by considering also the unmodelled components involved in the process. To describe the thermal behaviour of the tool, the Green's function could be used to predict the temperature field of the rake surface of the tool and therefore the heat flow according to the heat partition coefficient for the tool. An example of such approach can be found in the work by Karaguzel et al. [53]. In this work the authors developed a model for cutting temperature prediction in face milling using Green's function and identified a heat partition of heat flowing into the tool in relation to the measured cutting force of about 10%. Another example could be the research of Augspurger et al. [54] where force and temperature measurements were used in the Green's function models to calculate mechanical process power, heat flows and the heat partitioning in the milling process.

Bibliography

[1] K. Weinert, I. Inasaki, J. W. Sutherland, and T. Wakabayashi, "Dry Machining and Minimum Quantity Lubrication," *CIRP Annals*, vol. 53, no. 2, pp. 511–537, Jan. 2004, doi: 10.1016/S0007-8506(07)60027-4.

[2] T. He *et al.*, "Progress and trend of minimum quantity lubrication (MQL): A comprehensive review," *J Clean Prod*, vol. 386, p. 135809, 2023, doi: https://doi.org/10.1016/j.jclepro.2022.135809.

[3] V. Vasu and G. Pradeep Kumar Reddy, "Effect of minimum quantity lubrication with Al2O3 nanoparticles on surface roughness, tool wear and temperature dissipation in machining Inconel 600 alloy," *Proceedings of the Institution of Mechanical Engineers, Part N: Journal of Nanoengineering and Nanosystems*, vol. 225, no. 1, pp. 3–16, Mar. 2011, doi: 10.1177/1740349911427520.

[4] N. Balki and B. Nelge, *EXPERIMENTAL INVESTIGATION OF COOLING METHODS FOR DIFFERENT MACHINING CONDITIONS*. 2015.

[5] A. S. Siju, K. K. Gajrani, and S. S. Joshi, "Dual textured carbide tools for dry machining of titanium alloys," *Int J Refract Metals Hard Mater*, vol. 94, p. 105403, 2021, doi: https://doi.org/10.1016/j.ijrmhm.2020.105403.

[6] S. Debnath, M. M. Reddy, and Q. S. Yi, "Environmental friendly cutting fluids and cooling techniques in machining: a review," *J Clean Prod*, vol. 83, pp. 33–47, 2014, doi: https://doi.org/10.1016/j.jclepro.2014.07.071.

[7] K. E, B. Ozcelik, Prof. E. Demirbas, and E. Şık, "Effects of the Cutting Fluid Types and Cutting Parameters on Surface Roughness and Thrust Force," *Lecture Notes in Engineering and Computer Science*, vol. 2, Jun. 2010.

[8] Y. M. Shashidhara and S. R. Jayaram, "Vegetable oils as a potential cutting fluid—An evolution," *Tribol Int*, vol. 43, no. 5–6, pp. 1073–1081, May 2010, doi: 10.1016/J.TRIBOINT.2009.12.065.

[9] H. S. Abdalla, W. Baines, G. McIntyre, and C. Slade, "Development of novel sustainable neat-oil metal working fluids for stainless steel and titanium alloy machining. Part 1. Formulation development," *The International Journal of Advanced Manufacturing Technology*, vol. 34, no. 1, pp. 21–33, 2007, doi: 10.1007/s00170-006-0585-4.

[10] J. Kundrak and G. Varga, "Use of coolants and lubricants in hard machining," *Tehnicki Vjesnik-Technical Gazette*, vol. 20, pp. 1081–1086, Dec. 2013.

[11] A. Daturi, "Study of the effects of Minimum Quantity Lubrication in AISI 316 L drilling," Politecnico di Milano, Milan, 2021.

[12] M. Sayuti, A. A. D. Sarhan, and F. Salem, "Novel uses of SiO2 nano-lubrication system in hard turning process of hardened steel AISI4140 for less tool wear, surface roughness and oil consumption," *J Clean Prod*, vol. 67, pp. 265–276, Mar. 2014, doi: 10.1016/J.JCLEPRO.2013.12.052.

[13] V. S. Sharma, G. Singh, and K. Sørby, "A Review on Minimum Quantity Lubrication for Machining Processes," *Materials and Manufacturing Processes*, vol. 30, no. 8, pp. 935–953, Aug. 2015, doi: 10.1080/10426914.2014.994759.

[14] V. S. Sharma, G. Singh, and K. Sørby, "A Review on Minimum Quantity Lubrication for Machining Processes," *Materials and Manufacturing Processes*, vol. 30, no. 8, pp. 935–953, Aug. 2015, doi: 10.1080/10426914.2014.994759.

[15] V. S. Sharma, M. Dogra, and N. M. Suri, "Cooling techniques for improved productivity in turning," *Int J Mach Tools Manuf*, vol. 49, no. 6, pp. 435–453, 2009, doi: https://doi.org/10.1016/j.ijmachtools.2008.12.010.

[16] B. Boswell, N. Islam, I. Davies, Y. Ginting, and A. Ong, "A review identifying the effectiveness of minimum quantity lubrication (MQL) during conventional machining," *The International Journal of Advanced Manufacturing Technology*, vol. 92, pp. 321–340, Sep. 2017, doi: 10.1007/s00170-017-0142-3.

[17] N. R. Dhar, M. T. Ahmed, and S. Islam, "An experimental investigation on effect of minimum quantity lubrication in machining AISI 1040 steel," *Int J Mach Tools Manuf*, vol. 47, no. 5, pp. 748–753, 2007, doi: https://doi.org/10.1016/j.ijmachtools.2006.09.017.

[18] D. Thakur, B. Ramamoorthy, and L. Vijayaraghavan, "Optimization of minimum quantity lubrication parameters in high speed turning

of superalloy Inconel 718 for sustainable development," *World Acad Sci Eng Technol*, vol. 54, pp. 224–226, Jan. 2009.

[19] S. M. Ali, N. Dhar, and D. SK, "Effect of minimum quantity lubrication (MQL) on cutting performance in turning medium carbon steel by uncoated carbide insert at different speed-feed combinations," *Advances in Production and Management*, vol. 6, pp. 185–196, Jan. 2011.

[20] M. Gupta *et al.*, "Machinability investigations of hardened steel with biodegradable oil-based MQL spray system," *The International Journal of Advanced Manufacturing Technology*, vol. 108, May 2020, doi: 10.1007/s00170-020-05477-6.

[21] Z. Liu, X. Cai, M. Chen, and Q. An, "Investigation of cutting force and temperature of end-milling Ti-6Al-4V with different minimum quantity lubrication (MQL) parameters," *Proc Inst Mech Eng B J Eng Manuf*, vol. 225, pp. 1273–1279, Oct. 2011, doi: 10.1177/2041297510393793.

[22] L. Yan, S. Yuan, and Q. Liu, "Influence of minimum quantity lubrication parameters on tool wear and surface roughness in milling of forged steel," *Chinese Journal of Mechanical Engineering*, vol. 25, no. 3, pp. 419–429, 2012, doi: 10.3901/CJME.2012.03.419.

[23] R. P. Zeilmann and W. L. Weingaertner, "Analysis of temperature during drilling of Ti6Al4V with minimal quantity of lubricant," *J Mater Process Technol*, vol. 179, no. 1, pp. 124–127, 2006, doi: https://doi.org/10.1016/j.jmatprotec.2006.03.077.

[24] E. Rahim and H. Sasahara, "Investigation of tool wear and surface integrity on MQL machining of Ti-6AL-4V using biodegradable oil," *Proc Inst Mech Eng B J Eng Manuf*, vol. 225, pp. 1505–1511, Oct. 2011, doi: 10.1177/0954405411402554.

[25] C. S. Akhil, M. H. Ananthavishnu, C. K. Akhil, P. M. Afeez, R. Akhilesh, and R. Rahul, "Measurement of cutting temperature during machining," *IOSR Journal of Mechanical and Civil Engineering*, vol. 13, no. 2, pp. 108–122, 2016.

[26] B. M. Pereira Guimarães, C. M. da Silva Fernandes, D. Amaral de Figueiredo, F. S. Correia Pereira da Silva, and M. G. Macedo Miranda, "Cutting temperature measurement and prediction in machining processes: comprehensive review and future perspectives," *The International Journal of Advanced Manufacturing Technology*, vol. 120, no. 5, pp. 2849–2878, 2022, doi: 10.1007/s00170-022-08957-z.

[27] R. Komanduri and Z. B. Hou, "A review of the experimental techniques for the measurement of heat and temperatures generated in some manufacturing processes and tribology," *Tribol Int*, vol. 34, no. 10, pp. 653–682, 2001, doi: https://doi.org/10.1016/S0301-679X(01)00068-8.

[28] H. Elmoussami, "A METHOD TO ESTIMATE THE AVERAGE TEMPERATURE ON THE CUTTING EDGE OF TOOLS: APPLICATION ON THE MILLING PROCESS," *Experimental Heat Transfer*, vol. 16, no. 2, pp. 139–158, Jan. 2003, doi: 10.1080/08916150390126513.

[29] A. F. V Campidelli, H. V Lima, A. M. Abrão, and A. A. T. Maia, "Development of a wireless system for milling temperature monitoring," *The International Journal of Advanced Manufacturing Technology*, vol. 104, no. 1, pp. 1551–1560, 2019, doi: 10.1007/s00170-019-04088-0.

[30] G. Arndt and R. H. Brown, "On the temperature distribution in orthogonal machining," *International Journal of Machine Tool Design and Research*, vol. 7, no. 1, pp. 39–53, 1967, doi: https://doi.org/10.1016/0020-7357(67)90024-8.

[31] M. Hirao, "Determining temperature distribution on flank face of cutting tool," *Journal of Materials Shaping Technology*, vol. 6, no. 3, pp. 143–148, 1989, doi: 10.1007/BF02833765.

[32] E. Leonidas, S. Ayvar-Soberanis, H. Laalej, S. Fitzpatrick, and J. R. Willmott, "A Comparative Review of Thermocouple and Infrared Radiation Temperature Measurement Methods during the Machining of Metals," *Sensors*, vol. 22, no. 13, 2022, doi: 10.3390/s22134693.

[33] B. M. Pereira Guimarães, C. M. da Silva Fernandes, D. Amaral de Figueiredo, F. S. Correia Pereira da Silva, and M. G. Macedo Miranda, "Cutting temperature measurement and prediction in machining processes: comprehensive review and future perspectives," *The International Journal of Advanced Manufacturing Technology*, vol. 120, no. 5, pp. 2849–2878, 2022, doi: 10.1007/s00170-022-08957-z.

[34] H. S. Patne, A. Kumar, S. Karagadde, and S. S. Joshi, "Modeling of temperature distribution in drilling of titanium," *Int J Mech Sci*, vol. 133, pp. 598–610, 2017, doi: https://doi.org/10.1016/j.ijmecsci.2017.09.024.

[35] R. Li and A. Shih, "Tool Temperature in Titanium Drilling," *Journal of Manufacturing Science and Engineering-transactions of The Asme - J MANUF SCI ENG*, vol. 129, Aug. 2007, doi: 10.1115/1.2738120.

[36] U. Segurajauregui and P. J. Arrazola, "Heat-flow determination through inverse identification in drilling of aluminium workpieces with MQL," *Production Engineering*, vol. 9, no. 4, pp. 517–526, 2015, doi: 10.1007/s11740-015-0631-x.

[37] J. Fleischer, R. Pabst, and S. Kelemen, "Heat Flow Simulation for Dry Machining of Power Train Castings," *CIRP Annals*, vol. 56, no. 1, pp. 117–122, 2007, doi: https://doi.org/10.1016/j.cirp.2007.05.030.

[38] Oxley p., *The mechanics of machining: an analytical approach to assessing machinability.* Ellis Horwood Publisher, 1989.

[39] J. R. Flachs, M. Salahshoor, and S. N. Melkote, "Mechanistic models of thrust force and torque in step-drilling of Al7075-T651," *Production Engineering*, vol. 8, no. 3, pp. 319–333, 2014, doi: 10.1007/s11740-014-0531-5.

[40] V. Chandrasekharan, S. G. Kapoor, and R. E. DeVor, "A Mechanistic Approach to Predicting the Cutting Forces in Drilling: With Application to Fiber-Reinforced Composite Materials," *Journal of Engineering for Industry*, vol. 117, no. 4, pp. 559–570, Nov. 1995, doi: 10.1115/1.2803534.

[41] J. S. Strenkowski, C. C. Hsieh, and A. J. Shih, "An analytical finite element technique for predicting thrust force and torque in drilling," *Int J Mach Tools Manuf*, vol. 44, no. 12, pp. 1413–1421, 2004, doi: https://doi.org/10.1016/j.ijmachtools.2004.01.005.

[42] D. I. Lalwani, N. K. Mehta, and P. K. Jain, "Extension of Oxley's predictive machining theory for Johnson and Cook flow stress model," *J Mater Process Technol*, vol. 209, no. 12, pp. 5305–5312, 2009, doi: https://doi.org/10.1016/j.jmatprotec.2009.03.020.

[43] I. Minukhin, "An Improved Method of Cutting Forces Prediction for the Primary Cutting Edges of Twist Drills," 2013. [Online]. Available: https://api.semanticscholar.org/CorpusID:56208383

[44] G. C. I. Lin, P. Mathew, P. L. B. Oxley, and A. R. Watson, "Predicting Cutting Forces for Oblique Machining Conditions," *Proceedings of the Institution of Mechanical Engineers*, vol. 196, no. 1, pp. 141–148, Jun. 1982, doi: 10.1243/PIME_PROC_1982_196_015_02.

[45] Altintas Y Author and Ber AA Reviewer, "Manufacturing Automation: Metal Cutting Mechanics, Machine Tool Vibrations,

and CNC Design," *Appl Mech Rev*, vol. 54, no. 5, pp. B84–B84, Sep. 2001, doi: 10.1115/1.1399383.

[46] S. Pervaiz, I. Deiab, and H. A. Kishawy, "Experimental study of conventional and peck drilling operations," *Transactions of the North American Manufacturing Research Institute of SME*, vol. 40, p. 423-431, Jun. 2012.

[47] H. Shi, Z. Chen, X. Lin, and T. Zhu, "Accurate temperature characterization and experimental verification in the PCB drilling process," *The International Journal of Advanced Manufacturing Technology*, vol. 120, no. 5, pp. 3507–3518, 2022, doi: 10.1007/s00170-022-08808-x.

[48] H. S. Carslaw and J. C. Jaeger, *Conduction of heat in solids*, Second Edition. 1959.

[49] "https://docs.itascacg.com/3dec700/3dec/docproject/source/options/thermal/thermal_analytical.html."

[50] C. St, *Design and Analysis of Experiments*. 2022.

[51] B. Amor, "Experimental Investigation and Numerical Prediction of the Effects of Cutting Tool Geometry During Turning of AISI 316L Steel," *Periodica Polytechnica Mechanical Engineering*, vol. 65, Sep. 2021, doi: 10.3311/PPme.16844.

[52] C. S. Kim, "Thermophysical properties of stainless steels," United States, 1975. doi: 10.2172/4152287.

[53] U. Karaguzel, M. Bakkal, and E. Budak, "Modeling and Measurement of Cutting Temperatures in Milling," *Procedia CIRP*, vol. 46, pp. 173–176, 2016, doi: https://doi.org/10.1016/j.procir.2016.03.182.

[54] T. Augspurger, M. Koch, T. Lakner, A. De Bartolomeis, A. Shokrani, and T. Bergs, "Development of a virtual sensor for the comparison of heat partitions in milling under cryogenic cooling lubrication and high-pressure cutting fluid supply," *CIRP J Manuf Sci Technol*, vol. 35, pp. 118–131, 2021, doi: https://doi.org/10.1016/j.cirpj.2021.05.004.